LSU Doctoral Dissertations

Graduate School

2009

Polymer-Based Microfluidic Devices for High Throughput Single Molecule Detection: Applications in Biological and Drug Discovery

Paul Ichide Okagbare
Louisiana State University and Agricultural and Mechanical College, pokagb1@tigers.lsu.edu

POLYMER-BASED MICROFLUIDIC DEVICES FOR HIGH THROUGHPUT SINGLE MOLECULE DETECTION: APPLICATIONS IN BIOLOGICAL AND DRUG DISCOVERY

A Dissertation

Submitted to the Graduate Faculty of the
Louisiana State University and
Agricultural and Mechanical College
in partial fulfillment of the
requirements for the degree of
Doctor of Philosophy

in

The Department of Chemistry

by
Paul I. Okagbare
B.S., Delta State University, Nigeria, 1997
M.S., University of Ibadan, Nigeria, 2000
May, 2009

DEDICATION

To my late Parents: Jackson Okagbare Ichide and Rhoda Esiekpe Okagbare; with special appreciation to my mother, Esiekpe, although, you have departed to the great beyond, I perceived the smile on your face as you watch from heaven to see that your investment of love and care, came to fruition.

To my wife, Jennifer, for your continuous love, support and encouragement. Your unperturbed patience gave me confidence to remain focus.

To my son, Daniel, for understanding that your Dad is somewhere working hard for the future and can keep in touch with him on the telephone. Those smiles of yours were encouragements that kept my focus. You are a great son!

ACKNOWLEDGEMENTS

TABLE OF CONTENTS

LIST OF TABLES

LIST OF FIGURES

ABREVIATIONS AND ACRONYMS

AFM………………………………………………………….Atomic Force Microscopy

ADC……………………………………………………………Analog-to-digital converter

APE1………………………………………………………………….AP-Endonuclease

AP………………………………………………………………………………..Apurinic

A……………………………………………………………………………….Adenine

ATP………………………………………………………....Adenosine Tri-Phosphate

A/D…………………………………………………………………….Analog digital

AC………………………………………………………………….Alternating Current

bp………………………………………………………………………..base pair

BHQ-3…………………………………………………….Black-Hole-Quencher-3

BM………………………………………………………………….Bone Marrow

CCD…………………………………………………………….Charge-Coupled Device

Cb………………………………………………………………….Molecular concentration

COC……………………………………………………………….Cyclic Olefin Copolymer

C……………………………………………………………………………….Cytosine

CTCs……………………………………………………………….Circulating Tumor Cells

Cp………………………………………………………………….parasitic capacitance

DNA……………………………………………………….. Deoxyribonucleic acid

DE………………………………………………………………..Detection Efficiency

dsDNA……………………………………………..double stranded Deoxyribonucleic acid

DR………………………………………………………………..Delivery rate

DC………………………………………………………………..Duty Cycle

dB………………………………………………………………...Decibels

IR…………………………………………………………………....Infra-red

ISC……………………………………………………....Intersystem crossing

K$^+$…………………………………………………….Potassium ion

KCL………………………………………………....Potassium Chloride

LiGA……………………………………………Lithography, Electroplating, Molding

LI-EN…………………………………………………..L1-Endonuclease

LIF…………………………………………………..Laser-Induced Fluorescence

LOC…………………………………………………..Lab-on-a-chip

MLC…………………………………………..Maximum-likelihood criterion

MgCL$_2$…………………………………………….Magnesium Chloride

MCF-7 …………………………………………….Breast Cancer cell line

MSU……………………………………………Microsampling Unit

NA…………………………………………………...Numerical Aperture

NSOM……………………………………………...Near-field scanning microscopy

NIR……………………………………………………..Near infra-red

Ni…………………………………………………………Nickel

N$_{ev}$……………………………………………...Number of molecular events

Na$^+$ ………………………………………………Sodium ion

OD………………………………………………..Outside Diameter

OFC………………………………………………Optical Fiber Coupled

PCR………………………………………………Polymerase Chain Reaction

PMMA……………………………………………Poly (methyl methacrylate)

PMTs……………………………………………..Photomultiplier tubes

POC………………………………………………...Point of care

SEMs………………………………………………………………Scanning electron micrographs

T_1…………………………………………………………………..Lowest triplet state

TIR…………………………………………………………………..Total Internal Reflection

T_g…………………………………………………………………....Glass Transition Temperature

TDI…………………………………………………………………Time-Delayed Integration

TTE…………………………………………………………………...Tris-Taps-EDTA

T_m…………………………………………………………………...melting temperature

T_d…………………………………………………………………..detection time

T……………………………………………………………………Thymine

µ-TAS………………………………………………………………...Micro-total analysis system

UV…………………………………………………………………..Ultra-violet

µ-EIS………………………………………………………micro-Electrical Impedance Spectroscopy

λ-DNA……………………………………………………………Lambda- Deoxyribonucleic acid

WQS………………………………………………………………Weighted Quadratic Sum

WBC …………………………………………………………………..White Blood Cells

ABSTRACT

The realization of high throughput sample processing has become a primary ambition in many research applications with an example being high throughput screening (HTS), which represents the first step in the drug discovery pipeline. Microfluidics is a viable platform for parallel processing of biochemical reactions to increase data production rates due to its ability to generate fluidic networks with a high number of processors over small footprints suitable for optical imaging. Single-molecule detection (SMD) is another technology which has emerged to facilitate the realization of high throughput data processing afforded by its ability to eliminate sample processing steps and generate results with high statistical accuracy. A combination of microfluidics and SMD with wide-field fluorescence detection provides the ability to monitor biochemical reactions in a high throughput format with single-molecule sensitivity. In this dissertation, the integration of these techniques was presented for HTS applications in drug discovery.

An ultra-sensitive fluorescence detection system with a wide field-of-view (FoV) was constructed to transduce fluorescence signatures from single chromophores that were electrokinetically transported through a series of tightly packed fluidic channels poised on poly(methylmethacrylate), PMMA and contained within the FoV of a laser detection system. The system was used to monitor biochemical reactions at the single-molecule level in a continuous-flow format. Enhancement in sampling-throughput was demonstrated by constructing a high density fluidic network for parallel analysis of multiple biochemical assays. In another development, the ability to enhance single-molecule sensitivity in a flow-based biochemical assay was investigated using a novel cyclic olefin copolymer (COC) planar waveguide embedded in PMMA and situated

orthogonal to multiple fluidic channels. This design allowed for fluorescence detection from multiple fluidic channels using evanescent excitation and a wide FoV fluorescence detection system for parallel readout. Results from these technologies were presented as well as their applications in drug discovery for increasing data production rates and quality.

An approach toward monitoring the efficacy of therapeutic agents, which is important in clinical evaluation of drug potency in the drug discovery process, was also considered, by designing a microfluidic system with integrated conductivity sensor for label-free enumeration of isolated tumor cells from clinical samples.

INTRODUCTION

I.1 Overview of the Drug Discovery Process

Drug discovery research is an interdisciplinary endeavor, which has been increasingly propelled by chemistry and guided by pharmacology and the clinical sciences with deep impact from molecular biology and the genome sciences. The latter, combined with bioinformatics' tools, allows us to clearly understand the genetic basis of diseases and to determine the most suitable sites of attack for future therapeutic agents. Thus, novel chemical structures with drug-like properties are generated through a discourse between biologists and chemists, with adequate understanding of biological structures and functions that define the biological mechanism of action.[1,2] The advent of combinatorial chemistry has led to the generation of diverse sets of novel organic compounds (structure-based synthesis) to form large libraries of small molecules (combinatorial libraries),[3-6] with each generated molecule being subjected to a series of purification and characterization processes followed by screening the entire library against a particular target to register potential drug candidates that can enter clinical trials.[7] An overview of the drug discovery process is represented in Figure I.1. It takes 10–15 years or more with an enormous financial investment (in excess of $500 million) to bring a new drug to the market.[8] With advancements in scientific research, a number of new technologies that focus on improving the chances of discovering a new drug, which could also reduce the time line (discovery cycle) to 5–7 years, have been introduced. One key technology is centered on improving the efficiency of drug screening processes using high throughput assays and hardware.
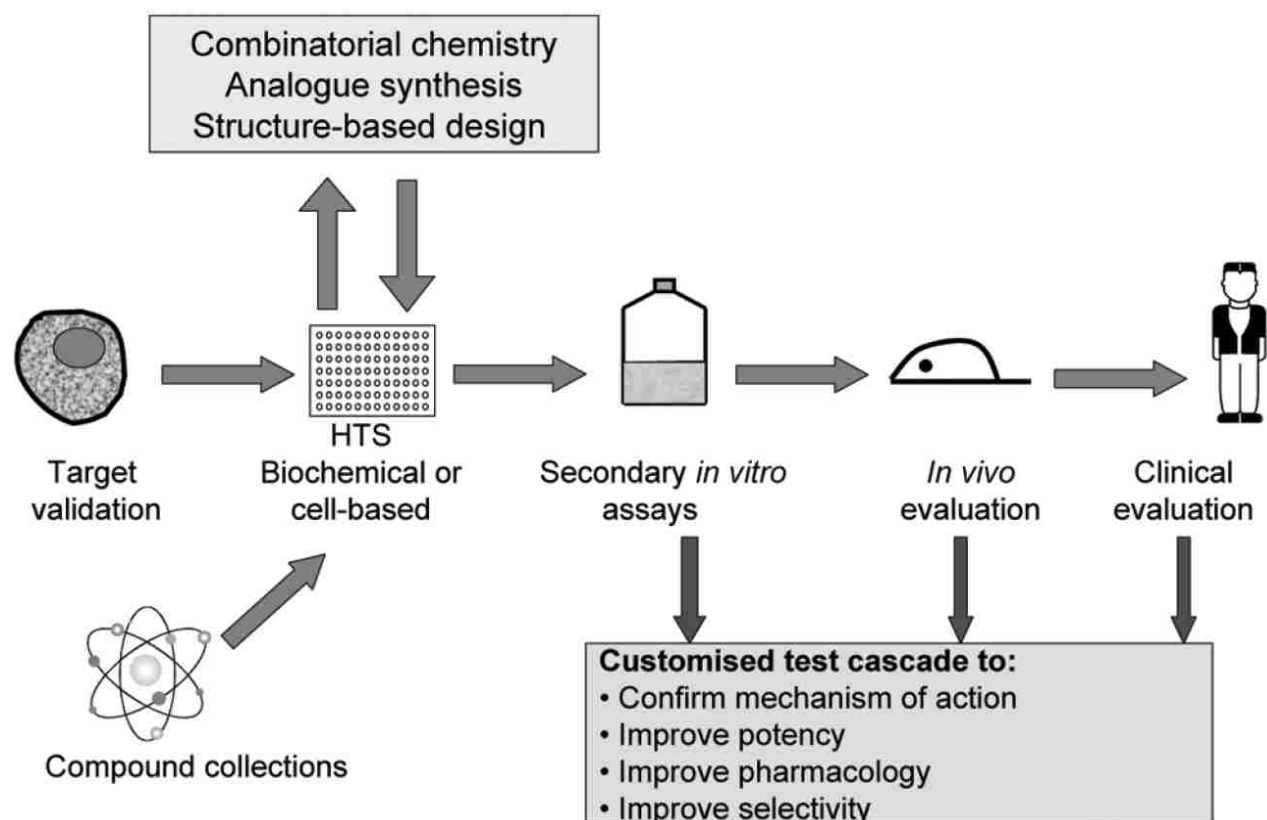
Figure I.1 Overview of the drug discovery pipeline showing the central role of high throughput screening (HTS) in the mechanism-based drug discovery process. Adapted with permission from Aherne *et al.*[8]

I.2 High Throughput Screening and High Throughput Sample Processing

The configuration of the screening platform in the drug discovery pipeline for high throughput processing is vital in maximizing the overall efficiency of the drug discovery process. This would allow for the ability to process multiple samples in a parallel fashion with a resultant reduction in the time requirement for the drug screening process. High throughput sample processing has also become the primary goal in other applications, such as molecular diagnostics and genome sequencing due to the large number of samples that must be interrogated. Obviously

from the illustration shown in Figure I.1, high throughput screening (HTS) plays a pivotal role in the drug discovery process with its utility spreading from the structure-based design or analogue synthesis of compounds (combinatorial chemistry) via the 'hit to lead' process to the generation of preclinical drug candidates.[8] Thus, HTS has remained the essential starting point in the drug discovery process and has rapidly evolved into a highly efficient, robust, integrated and information-rich scientific discipline. Assay throughput has been continuously increased from the traditional 96-well plates to higher density plate systems, for example, the use of microtiter plates with a 9,600-well configuration.[9-12] The increasing demands to screen larger libraries of compounds against a number of therapeutic targets has incited technological advancements towards automated HTS. This trend was accompanied by miniaturization to reduce development and operating costs as well. While miniaturization facilitates assay automation and the realization of higher throughput formats through the use of parallel sample processing, it also reduces the amount of precious biological materials and chemical reagents used per assay.

This advancement and need is being pursued through the use of microfabricated devices designed to perform continuous flow assays appropriate for HTS.[13,14] For example, the potential of microfluidic systems for large-scale and high performance screening was demonstrated through the use of microfabricated microchannel array systems with automatic sample loading from microtiter plates to screen 96 samples in less than 90 s.[15] The ultra-small sample volume associated with miniaturization was accompanied with detection challenges due to the ultra-small sampling volume and thus, required the use of sophisticated and high sensitivity detection techniques to readout the assay results.

I.3 Assay Readout Methods

The development of homogeneous assays and the use of high sensitivity detection techniques have become increasingly important in the pursuit of automation, miniaturization, and high throughput in the drug screening process. It is highly required that miniaturized assays be properly designed with suitable readout methods to ensure robustness and reproducibility as well as statistical significance of the assay results.[16]

Homogeneous screening assays are most frequently carried out using scintillation proximity assays (SPA) or fluorescence detection techniques depending on the particular type of target being investigated.[17] Whilst most binding assays for cell surface receptors are often performed using SPA techniques, fluorescent-based methodologies that employ samples such as fluorogenic enzyme substrates, dye-labeled substrates and fluorescent indicators for calcium and other ions are frequently used in enzyme and cell-based assays.[17,18] Other methodologies based on phage-display techniques or heterogeneous assay formats, for example ELISA and agar plate assays[19] have also been employed for screening. Given below will be a brief description of the SPA and fluorescence-based assays typically used in HTS.

I.3.1 Scintillation Proximity Assay (SPA)

The use of SPA techniques[20,21] to measure high affinity binding interactions for cell surface receptors in HTS applications has largely replaced radio-labeled ligands and filtration assays due to the ability of SPA to eliminate separation steps. The technique is essentially based on measuring light emission from a surface bound scintillant as a function of binding interactions between a radio labeled ligand and surface immobilized receptor. Isotopes that produce low

energy emission particles are typically used to ensure that only surface bound ligands are detected.[22-25]

I.3.2 Fluorescence-Based Techniques

Fluorescence-based methodologies are becoming increasingly more popular for HTS applications due to the inherent sensitivity of fluorescence measurements and the industry-wide drift from the use of radioisotopes. Fluorescence techniques most widely used in homogeneous screening assays includes fluorescence resonance energy transfer (FRET), fluorescence polarization (FP), homogeneous time-resolved fluorescence (HTRF), and fluorescence correlation spectroscopy (FCS).[26,27]

- **Fluorescence Resonance Energy Transfer (FRET):** This is essentially a non-radiative energy transfer between donor and acceptor dye molecules with transfer efficiency being dependent on spatial criteria.[28] It can be used to monitor enzymatic activities by measuring changes in observed fluorescence intensity resulting from substrate cleavage by the enzyme such that donor and acceptor drift apart.[29-31]

- **Fluorescence Polarization (FP):** Changes in the rotational diffusion coefficient of small labeled probes upon binding to target molecules is measured using FP techniques.[32] This technique provides rapid analysis of receptor-ligand binding interactions, enzyme-catalyzed hydrolysis of labeled substrates, protein-protein interactions and other binding assays of interest to HTS.[33,34]

- **Homogeneous Time-Resolve Fluorescence (HTRF):** Fluorescence signals from homogeneous samples are often hampered by background signal arising from sample matrix. One method of minimizing this problem is through the use of the time-resolved technique in which pulsed excitation sources and gated detectors are employed to allow the decay of background fluorescence before sampling the fluorescence signal of interest. HTRF utilize the advantage offered by europium crystates (i.e. long fluorescence life time and large stokes shift) to exploit energy transfer between an europium donor and suitable acceptors for screening applications.[35,36]

- **Fluorescence Correlation Spectroscopy (FCS):** FCS has emerged as a suitable detection technique for HTS applications.[37] In this technique, measurements are carried out using confocal optics to provide focused excitation light with the associated reduction in probe volume such that temporal fluctuations in signal as molecules diffuse in and out of the probe volume is observed. Autocorrelation analysis of time-dependent fluorescent signals generate information about the diffusion characteristics of the particles or molecules. This technique is also used for monitoring binding interactions since the binding of a fluorescence probe to another molecule results in a change in its diffusion coefficient. It is used in registering molecular events and has demonstrated potential for HTS applications.[37,38]

Chemiluminescence[39] and electrochemiluminescence[40] have both shown detection sensitivities that compete with those of fluorescence and are suitable

for HTS applications.[41] Electrochemiluminescence takes preeminence for HTS applications since reagents can be regenerated to sustain high photon flux rates over longer periods of time.

I.4 Need for Single-Molecule Sensitivity

Single molecule detection (SMD) represents the highest sensitivity in any analytical measurement and therefore possesses the ability to eliminate sample processing steps in multi-step assays as well as providing exquisite analytical sensitivity. For example, SMD provides the ability to detect biological components in their native concentrations without sample enrichment steps such as PCR amplification, and can record subtle changes in biochemical reaction profiles. In addition, SMD reveals detailed information on molecular behavior such as complex fluctuations phenomena that are otherwise hidden within ensemble average techniques.[42-45] These, together with the reduced assay time and short readout times associated with SMD, have given the technique immense recognition as a powerful analytical tool for biochemical assays especially in enhancing high throughput sample processing.[26,46,47] The major advantages of SMD toward HTS are high statistical accuracy, even at measurement times of ~1 s, the ability to provide for the sensitivity demand of HTS with the pursuit of miniaturization,[48-52] and most importantly, the low consumption of precious biological materials brought about by the ability to monitor reactions efficiently in ultra-small volumes, which provides a drastic reduction in assay cost.[26,46] Typically, the technique employs ultra-small sample volumes with appropriate sample concentrations that allows sampling of exactly one molecule at any given time. This is illustrated in Figure I.2
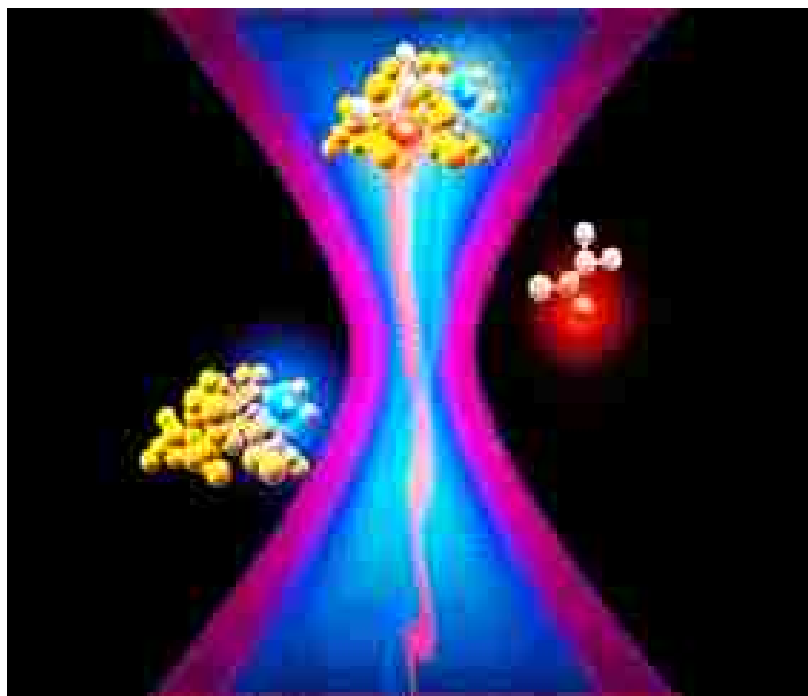
Figure I.2 Illustration of fluorescence SMD with a tightly focused laser that generates femtoliter probe volumes such that the appropriate sample concentration is selected to keep single molecule occupancy at ~0.1. Only one molecule is sampled in the probe volume at any given time.

I.5 Research Focus

The overarching goal of my research area is the design of a microfluidic system for drug discovery (HTS) using near-IR fluorescence detection with single molecule sensitivity. A conceptual rendition of the target fluidic system with high throughput and automation capabilities is represented in Figure I.3.

In this dissertation, I will focus on the development of ultra-sensitive detection systems for the rapid flow-based analysis of biological samples in a high throughput format. In one development, an ultrasensitive fluorescence detection system with a wide field-of-view (FoV) microscope was constructed to transduce fluorescence signals from single chromophores that were electrokinetically transported through a
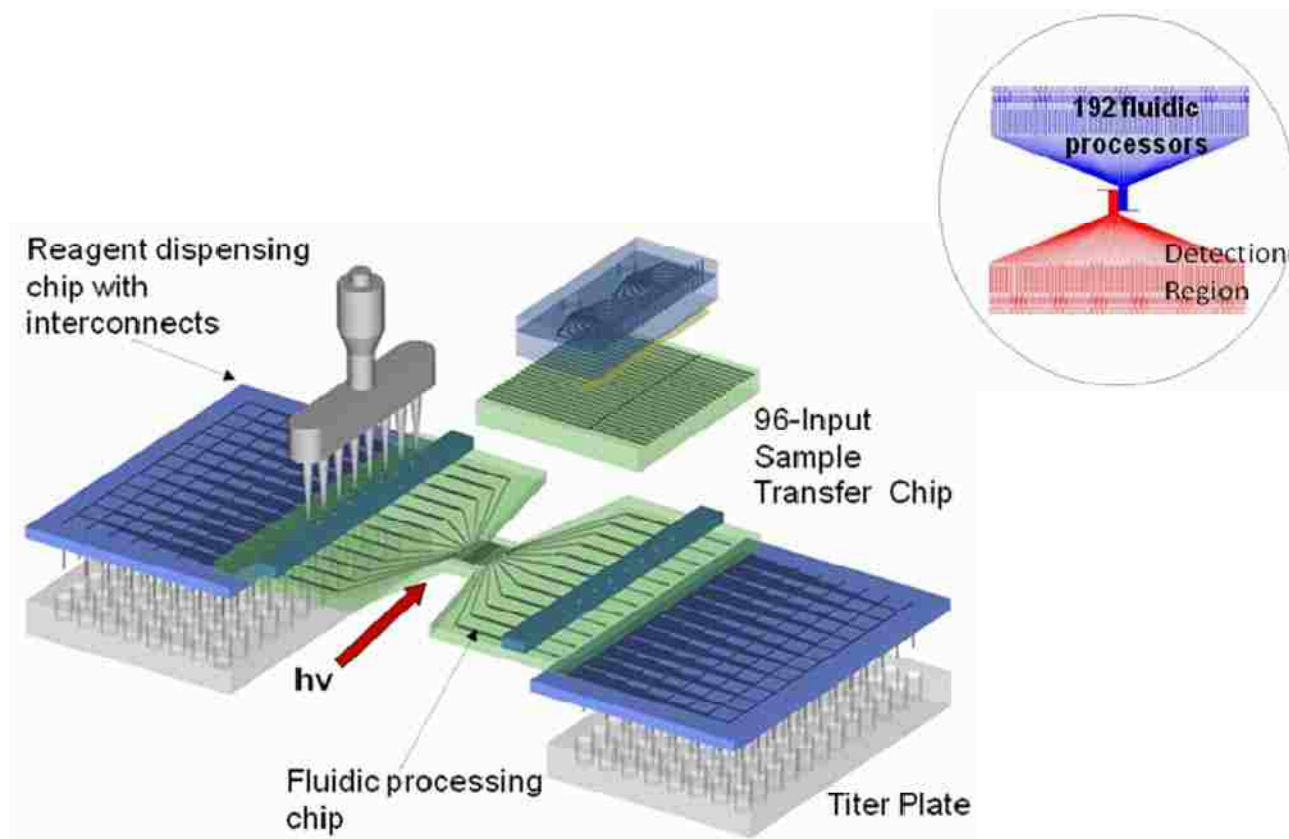
Figure I.3 Integrated fluidic system for performing HTS assays. The system will be configured on a 6" wafer and the wafer shown has 192 processors. The wafer consists of a stack of fluidic chips, with one chip used for containing the substrates and buffer reagents required for the HTS, a 96-element transfer chip to move drug candidates to the processor wafer and the HTS processor chip containing passive mixers, 2-phase flow generator and detector elements. The system will be operated in a 2-phase flow format with an inert separator liquid to significantly increase processing throughput.

series of tightly packed fluidic channels poised on PMMA and contained within the FoV of the detection system. The system was used to monitor biochemical reactions at the single-molecule level in a continuous flow format. The potential of this system was expanded through the fabrication of a high density fluidic device (microchip) with individual reactors (vias) on the polymeric platform with suitability for HTS applications (drug discovery). In another development, the ability to enhance sensitivity in a flow-based biochemical assay was investigated using a novel

integrated embedded waveguide system. The embedded waveguide was used to effectively generate evanescence excitation across a series of fluidic channels to allow parallel excitation with subsequent detection of fluorescence signals from the fluidic channels. Finally, in another unrelated area, I focused on the development of a label-free technique using a conductivity sensor for on-chip enumeration of tumor cells as an approach to early disease diagnosis and monitoring efficacy of therapeutic agents (clinical evaluation of drug potency), which also form part of the drug discovery pipeline.

I.6 References

(1)   Drews, J. *Science* **2000**, *287*, 1960 - 1964.

(2)   Gibbs, J. B. *Science* **2000**, *287*, 1969-1973.

(3)   Leibl, M. *J. Comb. Chem.* **1999**, *1*, 3 - 24.

(4)   Rademann, J.; Jung, G. *Science* **2000**, *287*, 1947-1948.

(5)   Schreiber, S. L. *Science* **2000**, *287*, 1964-1969.

(6)   Fattori, D.; Squarcia, A.; Bartoli, S. *Drugs R. D* **2008**, *9*, 217-227.

(7)   Hughes, I.; Hunter, D. *Curr. Opin. Chem. Biol.* **2001**, *5*, 243-247.

(8)   Aherne, G. W.; McDonald, E.; Workman, P. *Breast Canc. Res.* **2002**, *4*, 148-154.

(9)   Major, J. *J. Biomol. Screen* **1998**, *3*, 13-17.

(10)   Oldenburg, K. R.; Zhang, J. H.; Chen, T. M.; Maffia, A.; Blom, K. F.; Combs, A. P.; Chung, T. D. Y. *J. Biomol. Screen* **1998**, *3*, 55-62.

(11)   Stahl, W. *J. Biomol. Screen* **1999**, *4*, 117-118.

(12)   Divers, M. *J. Biomol. Screen* **1999**, *4*, 177-178.

(13)   Khandurina, J.; Guttman, A. *Curr. Opin. Chem. Biol.* **2002**, *6*, 359-366.

(14)   Sundberg, S. A. *Curr. Opin. Biotechnol.* **2000**, *11*, 47-53.

(15) Shi, Y. N.; Simpson, P. C.; Scherer, J. R.; Wexler, D.; Skibola, C.; Smith, M. T.; Mathies, R. A. *Anal. Chem.* **1999**, *71*, 5354-5361.

(16) Major, J. *J. Biomol. Screen* **1999**, *4*, 119-119.

(17) Zysk, J.; Baumbach, W. *Comb. Chem. High Throughput Screen.* **1998**, *1*, 171 - 183.

(18) Hill, D.; Wrigley, S.; Nisbet, L. *Adv. Biochem. Eng. Biotechnol* **1998**, *59*, 73 - 121.

(19) Walsh, J. C. *J. Biomol. Screen* **1998**, *3*, 175 -181.

(20) Sittampalam, G. S.; Kahl, S. D.; Janzen, W. P. *Curr. Opin. Chem. Biol.* **1997**, *1*, 384-391.

(21) Bosworth, N.; Towers, P. *Nature* **1989**, *341*, 167-168.

(22) Graziani, F.; Aldegheri, L.; Terstappen, G. C. *J. Biomol. Screen* **1999**, *4*, 3-7.

(23) Bosse, R.; Garlick, R.; Brown, B.; Menard, L. *J. Biomol. Screen* **1998**, *3*, 285-292.

(24) Kariv, I.; Stevens, M. E.; Behrens, D. L.; Oldenburg, K. R. *J. Biomol. Screen* **1999**, *4*, 27-32.

(25) Parandoosh, Z.; Knowles, S. K.; Xiao, X. Y.; Zhao, C.; David, G. S.; Nova, M. P. *J. Biomol. Screen* **1998**, *3*, 293-298.

(26) Gribbon, P.; Sewing, A. *Drug Discov. Today* **2003**, *8*, 1035 -1043.

(27) Pope, A. J. *Drug Discov. Today* **1999**, *4*, 350 - 362.

(28) Stryer, L. *Annu. Rev. Biochem.* **1978**, *47*, 819-846.

(29) Grahn, S.; Kurth, T.; Ullmann, D.; Jakubke, H. D. *Biochim. Biophys. Acta-Protein Struct. Molec. Enzym.* **1999**, *1431*, 329-337.

(30) Harrison, J.; Liu, X.; Balasubramanian, S. *Nucleic Acids Res.* **1999**, *27*, e14.

(31) Kakiuchi, N.; Nishikawa, S.; Hattori, M.; Shimotohno, K. *J. Virol. Methods* **1999**, *80*, 77-84.

(32) Nasir, M.; Jolley, M. *Comb. Chem. High Throughput Screen.* **1999**, *2*, 177-190.

(33) Seethala, R.; Menzel, R. *Anal. Biochem.* **1998**, *255*, 257-262.

(34) Bolger, R.; Wiese, T. E.; Ervin, K.; Nestich, S.; Checovich, W. *Environ. Health Perspect.* **1998**, *106*, 551-557.

(35) Moore, K. J.; Turconi, S.; Miles-Williams, A.; Djaballah, H.; Hurskainen, P.; Harrop, J.; Murray, K. J.; Pope, A. J. *J. Biomol. Screen* **1999**, *4*, 205-214.

(36) Kolb, A. J.; Kaplita, P. V.; Hayes, D. J.; Park, Y. W.; Pernell, C.; Major, J. S.; Mathis, G. *Drug Discov. Today* **1998**, *3*, 333-342.

(37) Auer, M.; Moore, K. J.; Meyer-Almes, F. J.; Guenther, R.; Pope, A. J.; Stoeckli, K. A. *Drug Discov. Today* **1998**, *3*, 457-465.

(38) Koltermann, A.; Kettling, U.; Bieschke, J.; Winkler, T.; Eigen, M. *Proc. Natl. Acad. Sci. U. S. A.* **1998**, *95*, 1421-1426.

(39) Creton, R.; Kreiling, J. A.; Jaffe, L. F. *Microsc. Res. Tech.* **1999**, *46*, 390-397.

(40) Knight, A. *Anal. Chem.* **1999**, *18*, 47-62.

(41) Pasini, P.; Musiani, M.; Russo, C.; Valenti, P.; Aicardi, G.; Crabtree, J. E.; Baraldini, M.; Roda, A. *J. Pharm. Biomed. Anal.* **1998**, *18*, 555-564.

(42) Barkai, E.; Jung, Y.; Silbey, R. *Annu. Rev. Phys. Chem.* **2004**, *55*, 457 - 507.

(43) Lee, A. I.; Brody, J. P. *Proc. of SPIE* **2005**, *5699*, 482 - 490.

(44) Xie, X. S.; Lu, H. P. *J. Biol Chem* **1999**, *274*, 15967-15970.

(45) Medina, M. A.; Schwille, P. *Bioessays* **2002**, *24*, 758 - 764.

(46) Eggeling, C.; Brand, L.; Ullmann, D.; Jager, S. *Drug Discov. Today* **2003**, *8*, 632 - 641.

(47) Hintersteiner, M.; Auer, M. *Ann. N.Y. Acad. Sci.* **2008**, *1130*, 1-11.

(48) Moore, K. J.; Turconi, S.; Ashman, S.; Ruediger, M.; Haupts, U.; Emerick, V.; Pope, A. J. *J. Biomol. Screen.* **1999**, *4*, 335-353.

(49) Gribbon, P.; Schaertl, S.; Wickenden, M.; Williams, G.; Grimley, R.; Stuhmeier, F.; Preckel, H.; Eggeling, C.; Kraemer, J.; Everett, J.; Keighley, W. W.; Sewing, A. *Curr. Drug Discov. Technol.* **2004**, *1*, 27-35.

(50) Rudiger, M.; Haupts, U.; Moore, K. J.; Pope, A. J. *J. Biomol. Screen.* **2001**, *6*, 29-37.

(51)   Haupts, U.; Rudiger, M.; Ashman, S.; Turconi, S.; Bingham, R.; Wharton, C.; Hutchinson, J.; Carey, C.; Moore, K. J.; Pope, A. J. *J. Biomol. Screen.* **2003**, *8*, 19-33.

(52)   Jager, S.; Garbow, N.; Kirsch, A.; Preckel, H.; Gandenberger, F. U.; Herrenknecht, K.; Rudiger, M.; Hutchinson, J. P.; Bingham, R. P.; Ramon, F.; Bardera, A.; Martin, J. *J. Biomol. Screen.* **2003**, *8*, 648-659.

CHAPTER 1

SINGLE-MOLECULE DETECTION: THE ULTIMATE SENSITIVITY IN ANALYTICAL

MEASUREMENTS

1.1 Introduction

The scientific community has witnessed tremendous progress in the field of single-molecule research, which is continuously expanding due to technological advances and the promise of unparalleled capabilities to provide incredible molecular information that were hitherto hidden in conventional ensemble techniques. Whilst standard ensemble methods generate results from large numbers of molecules, which correspond to their average properties, single-molecule detection (SMD) allows the interrogation of exactly one molecule in a complex matrix, and represents the ultimate detection limit defined by the inverse of Avogadro's number (1.66×10^{-24} or 1.66 yoctomole). This allows for construction of actual distributions of complex phenomena, such as folding states of biomolecules, molecular configurations and stages of enzymatic cycles.[1] Another benefit of single molecule studies is the ability to monitor molecular dynamics. For example, it can give detailed information about the stochastic motion of DNA enzymes or molecular motors in biological systems. In addition, single-molecule detection could be a local reporter in the nanoenvironment such that small changes in its immediate surrounding can be clearly observed. These changes could be in the form of the presence of reactive functional groups, ions, atoms or electrostatic charges. Also, the ability to observe individual molecular events eliminates the need for synchronization, especially for molecules undergoing time-dependent processes such as triplet state crossing, thus enabling measurement of spectral shift or temporal fluctuations as a function of natural or induced perturbations in biological systems with

high efficiency.[2,3] Finally, single-molecule methods eliminate sample preprocessing steps, for example, it allows measurement of native concentrations of cellular components, which are often present in few copies within biological cells.[4-6] The science of single molecule spectroscopy spans several fields such as physics, chemistry and biology and thus has promoted excellent collaborations for making key advances in scientific research.

Early approaches to single-molecule detection included optical detection of multiply labeled single antibody molecules[7] and detection of current from single ion channels in membranes.[8] Subsequently, several exciting developments were made using various experimental approaches.[9,10] These included, optical detection of single chromophores in solids at low temperature,[11,12] detection of single fluorophores under biologically relevant conditions,[13-15] imaging individual DNA molecules in water,[16,17] and measurement of individual kinesin movements along a microtubule.[18,19] This field of research has evolved through the last two decades to a status of a powerful and compelling technique for exploring molecular behavior at the nanoscale.[20,21]

A recent search using the PubMed data base (www.pubmed.gov) as conducted by Ha and coworkers[22,23] showed a trend that appeared to be exponential with a doubling time of 2.2 years (see Figure 1.1) in terms of single-molecule research. This rapidly increasing research interest in single-molecule studies has motivated frequent breakthroughs in imaging and analyzing techniques, resulting in over 400 United States patents[24] and consequently facilitating advances in biological sciences. For example, videos of the motion and biochemistry of macromolecular machines can now be generated at the single-molecule level, which are helpful in elucidating their mechanism and could potentially lead to the development of new drugs.[24-27]

Figure 1.1 Growth pattern of single molecule fluorescence research (appearing to be exponential with doubling time of 2.2 years). (a) Number of single-molecule publications per year. Data was obtained by searching the PUBMED data base with the keyword "single-molecule fluorescence". Technical advances in FRET experiments are shown in gray; (b) technical advances in single-molecule tracking: translocation (purple), rotation (orange); (c) technical advances in live cells studies (green). Adopted with permission.[23]

The two primary approaches for SMD are fluorescence and manipulation (force). Fluorescence techniques for SMD include FRET, polarization, lifetime, localization and intensity while manipulation includes optical and magnetic tweezers and atomic force microscopy (AFM). In this review and with regards to our research goal, particular attention will be given here to fluorescence techniques, however, a detailed discussion of manipulation methods can be found in selected papers.[9,28-33]

1.2 Fluorescence Single-Molecule Detection

With emerging technology, the utility of fluorescence spectroscopy in single molecule studies is becoming even more powerful due to the inherent sensitivity of

fluorescence detection.[23] To be able to probe the molecule of interest, a laser beam is used to induce electronic transitions with the resulting optical absorption detected indirectly by monitoring the fluorescence emission.[12] Appropriate dilution conditions are required to ensure that one molecule is resident in the probe volume (analysis volume) at any given time. This would mean for example, acquiring fluorescent signal from a 10^{-15} liter volume of a 1.66 x 10^{-9} M (maximum concentration) solution. Obviously, fluorescence measurements from the molecule of interest is done in the presence of trillions of solvent molecules as well as noise from the detection system, thus techniques are employed to spectrally isolate the single-molecule fluorescence from unwanted signal emanating from its immediate vicinity. This is often achieved through the use of specially designed interference and/or Raman notch filters.[11]

1.2.1 Basic Principle of Single-Molecule Fluorescence

There are two basic requirements for realizing single-molecule sensitivity using fluorescence: *(1)* the use of ultra small probe volumes and *(2)* ensuring a signal-to-noise ratio (SNR) that is greater than unity (SNR >3 gives a statistical result with 99.7% certainty) for the single-molecule signal. In most fluorescence-based single-molecule experiments, the small probe volume requirement is obtained by focusing the laser beam to a diffraction limited spot, however, appropriate concentrations of the analyte molecule of interest contained in an ultrapure host matrix must also be selected based on Avogadro's criterion to keep molecular occupancy lower than unity in the probe volume. This is important to avoid double occupancy at a reasonable sampling time such that any signal registered is indeed from a single molecule. The required SNR is obtained through adequate suppression of background signals, which mainly originate from undesirable fluorescent impurity in the sample, Raman scattering from the solvent,

Rayleigh scattered radiation at the pumping wavelength and residual fluorescence from the optical system.[34] The challenge therefore is to increase the signal size from the single molecule hidden in its host matrix as much as possible. This is achieved, in addition to using a small focal volume by using fluorophores with large absorption cross sections, high photostabilities and a weak tendency for triplet state transitions. Also, the pumping laser must be operated below optical saturation of the molecular absorption. Although the number of photons emitted by a single molecule per second is much smaller compared to the number of photons per second from the incident laser beam, the Stokes' shift associated with the molecular absorption phenomena makes it possible to carefully isolate the weak fluorescence from a single molecule. Illustration of the prominent features in the energy level diagram of single-molecule fluorescence is shown in Figure 1.2. Typically, the ground state (S_0) molecule absorbs energy from the pumping laser to undergo an electronic transition to a higher electronic energy level (S_1), which quickly relaxes to the lowest energy level of the excited state (S_1) from which fluorescence photons are emitted. Energy losses due to vibrational relaxation causes red-shifts in the emission wavelength (Stokes shift). The molecule can undergo several absorption-emission cycles prior to photobleaching. It is also important to note that there is a finite probability for intersystem crossing (ISC) into the triplet states, which often results in fluorescence intermittency or photoblinking in single-molecule experiments depending on the properties of the fluorophore and experimental conditions.[35,36]

1.2.2 Fluorophore Consideration for SMD

Fluorophores can be referred to as molecular spies in single molecule experiments with information feedback channels occurring as fluorescence. Thus, when

attached to biological molecules, they reveal information that depicts the molecular
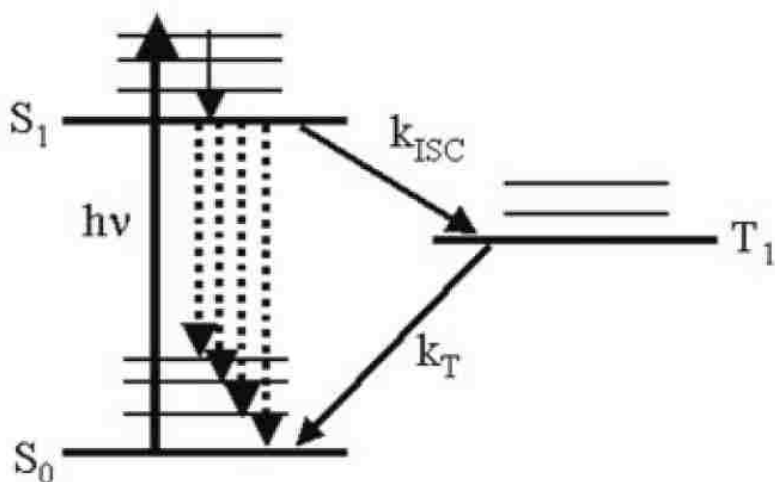
Figure 1.2 Energy level diagram for single molecule spectroscopy showing the ground singlet state (S0), first excited state (S1), lowest triplet state (T1), and other intermediate states. Single molecules can be recycled many times through this scheme to generate millions of photons. Adopted with permission.[20]

processes in the vicinity of the host molecule. However, single dye molecules emit

limited amounts of fluorescence, which must be maximized to facilitate a clear

observation of processes when placed in its nanoenvironment. Consequently, an ideal

fluorophore is required for a successful single molecule experiment. Fluorophores

should stay photoactive under intense illumination, possess high absorption cross-

sections and fluorescence quantum yields, does not modify the properties of the host

molecule and should show steady emission intensity. Typical fluorescent molecules

used for single molecule studies originate from the general classes of laser dyes used in

biological fluorescent labeling. These include rhodamines, cyanines, oxazines, terrylene

or perylene diimide.[37-39] In addition, classes of genetically expressed proteins like green

fluorescent protein (GFP) have been employed for single-molecule fluorescence

studies.[40,41] In the cyanine family, Cy3 and Cy5 are extensively used either individually

or as a FRET pair.[42-44] These dyes have high photostability and good fluorescence quantum yields.[45] Other popular fluorophore includes Cy5.5 and Cy7. In the rhodamine family, tetramethylrhodamine,[46,47] rhodamine 6G, Texas Red, and bis-sulfonerhodamine have been used. Other fluorophores of interest includes Alexa dyes[23] and some new classes of single molecule fluorophores found among molecules originally optimized for non-linear optics.[48] In addition, some proteins are naturally fluorescent with the presence of one or many fluorophores serving as a co-factor, and have been used to obtain useful information for single-molecule interrogation, for example in the cases of flavoenzymes[49,50] and complexes containing bacteriochlorophyll molecules.[51] Novel fluorescent dyes, such as the phthalocyanine derivatives,[52] have been synthesized and used for molecular single molecule studies as well. These dyes have been characterized with self quenching, resulting from aggregation and thus eliminate the need for a separate quencher in RET-based experiments.[53]

1.2.3 Physical Effects that Limit Fluorescence Emission from Single Molecules

The major physical effect related to single-molecule fluorescence is photobleaching, which is an irreversible process that causes molecules to eventually change to another, non-fluorescent form. This is true for almost all molecules in aqueous solution and typically occurs after emission of specific number of photons. Under favorable conditions, individual molecules can emit on the average $10^5 - 10^6$ fluorescence photons before photobleaching. Although, there are many factors responsible for photobleaching, in most cases, it is mainly due to photo-oxidation. Thus, methods such as flooding the system with inert gases,[54] operating the detection system in vacuum,[55] and incorporation of enzymatic oxygen scavengers[56,57] to reduce the presence of molecular oxygen can help to reduce this effect.

Another physical effect is optical saturation. The amount of photons emitted per second scales linearly with the laser power as long as the saturation point is not exceeded.[58] However at optical saturation, the absorption cross section from the molecule decreases such that further increases in laser power only generate more background with no increase in the amount of emitted photons. The net effect of this is a decrease in the SNR for the fluorescence measurement. It is also important to note that the scattering signal is always linear with laser power; therefore, appropriate conditions are required to balance the relationship between these factors in order to maximize the fluorescence signal from single molecules.

1.2.4 The War Against Background Signal

A major challenge in designing single-molecule experiments is the ability to conquer or reduce background signal. This is because almost all single-molecule experiments are background limited. As noted previously, background signal may arise as a result of residual fluorescence from the solvent system used, scattered radiations, and/or residual emission from excitation sources that extend into the spectral range for fluorescence detection especially when a diode laser is employed as the excitation source.[20] These sources of background, although critical, can be minimized by using multiple filters and high quality optical components. Other sources, such as elastic Rayleigh scattering from the sample itself as well as from its immediate environment (e.g. backscattering from sample container) can be reduced through the use of ultraclean, scratch-free substrates of the highest quality and interference filters. Unfortunately, red-shifted Raman scattering from the host matrix and residual fluorescence from impurities in the sample or host matrix provide a greater problem. Both are proportional to the size of the probe volume, and though a logical step is to

reduce the probe volume size as much as possible, impurities or molecular components of the host matrix can generate very strong residual fluorescence. This problem is more pronounced when working in the blue or ultra-violet spectral regions. It is therefore paramount to use ultrapure solvents for samples to be interrogated. A prediction of the possible emission wavelength of an unavoidable biological matrix may be helpful in selecting the right fluorophore and optical filtering systems that will minimized the effect especially when working in the UV region. Another method of overcoming this problem is to work in the near infra-red spectral region where interference from unwanted emissions is highly minimal.

1.3 Techniques: Instrumentation for SMD

Typical optical instruments used for single-molecule measurements are based on three major experimental formats. These are confocal, scanning and wide-field methods.[59] Essentially, the optical configuration for each of these methods is aimed at limiting the observed volume and carefully isolating the small number of photons emitted by a single molecule. All emerging single molecule fluorescence techniques are based on these methods which are considered in detail below.

1.3.1 Confocal Method for SMD

The observation volume in fluorescence measurements is drastically reduced through the use of confocal optics, which allow for rejection of signal from above and below the focal plane of a tightly focused excitation source. Figure 1.3a shows a simplified schematic of a typical instrument used for confocal fluorescence detection. Although this can also be configured in a trans-illumination format, the epi-fluorescence (epi-illumination) format is the most common optical design for confocal microscopy and this format has been described in detail in many reports.[20,60-63] Essentially, a collimated

laser beam is directed through a high numerical aperture (NA) microscope objective using a dichroic beam splitter. This results in the generation of a focused diffraction limited laser spot at the sample plane (see Figure 1.3b). All fluorophores within the laser spot are excited and fluorescence emission as well as backscattered light from the substrate and Raman scattering from the sample matrix are collected by the same microscope objective, passed through the dichroic beam splitter and subsequently through other appropriate emission filters to isolate the fluorescence emission of interest, which is then focused on the detector (usually a single element detector such as SPAD) through a pinhole aperture located on the optical plane of the emitted fluorescence. The pinhole serves as a spatial filter that rejects out-of-focus light. This is called the confocal advantage. It is important to note that the excitation volume is defined by the size of the laser spot, therefore the use of high NA microscope objectives, which generate small laser spot-sizes, helps in minimizing the observed volume to improve the SNR in SMD by both increasing the signal (high collection efficiency) and reducing background. A careful selection of the proper size pinhole is very important in optimizing and isolating the single molecule fluorescence signal. Although smaller pinholes are difficult to align, they give superior axial resolution. Excellent treatment of pinhole selection has been given by Corle *et al.*[64] The spatial size of the fluorescence at the pinhole is simply determined by the diameter of the diffraction limited laser spot multiplied by the magnification of the microscope objective. For example, the spatial spread of the fluorescence collected from a laser spot size of 3 μm using a 40x microscope objective would be ~120 μm. In this case, a pinhole with a diameter of 80 μm will reduce the amount of fluorescence transmitted to the detector but will give a better axial resolution. On the contrary, a pinhole with a diameter of 150 μm

will transmit more fluorescence to the detector, but will generate poorly resolved signal and high background. Therefore, a perfect correlation of this factor with the size of the pinhole allows for better fluorescence transmission through the confocal aperture.

(a)
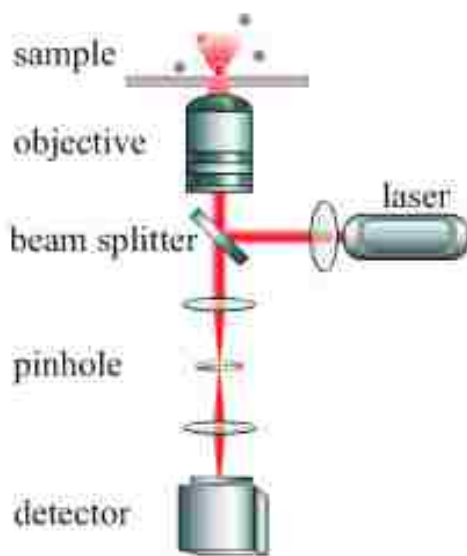
(b)
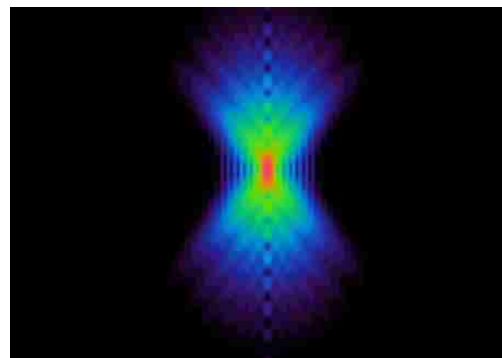
Figure 1.3. (a) A simplified schematic of confocal optics for single-molecule detection. Adapted with permission from Tinnefeld *et al.*[65] (b) A pictorial representation of the focused laser spot produced by a confocal set up. The red spot represents the focal volume.

1.3.2 Scanning Methods

The availability of highly accurate motorized stages that provide resolution down to molecular sizes has created opportunities for fluorescence image acquisition using a single element detector. The fluorescence image in this case is a reconstructed image obtained by raster scanning the sample. There are basically two scanning methods used for SMD. These are; confocal microscopy that utilize the confocal advantage (see above) and near-field scanning optical microscopy (NSOM), which creates a laser spot smaller than the diffraction limit.

In confocal microscopy (confocal imaging), the instrumentation is similar to that shown in Figure 1.3a except that in this case, a computer controlled motorized sample stage is employed to facilitate the scanning. A typical single molecule image of a green fluorescence protein (GFP) mutant 10c collected using confocal optics and stage scanning is shown in Figure 1.4. The size of the fluorescence spots are about 500 nm in diameter, which is determined by the optical resolution and not the size of the molecule.
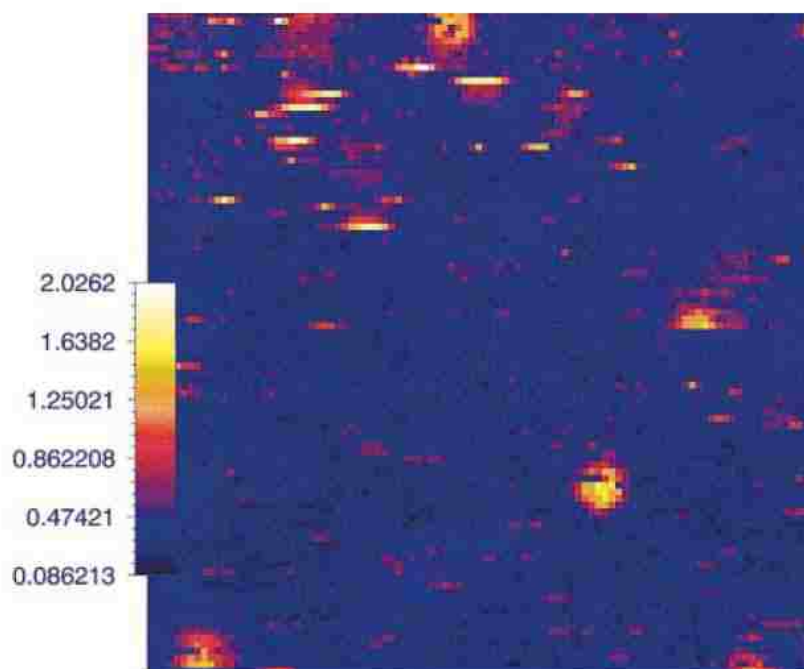
Figure 1.4 Fluorescence image of a single GFP mutant 10c collected using confocal scanning microscopy. Fluorescent spots are about 500 nm for each GFP molecule. Adopted with permission. [66]

NSOM is based on a simple principle.[67,68] In this case, a highly localize excitation is obtained using an optical fiber to create a relatively smaller laser spot. The laser spot is generated from a narrow aperture produced by a modified optical fiber (see Figure 1.5a). In early studies using NSOM, a single-mode optical fiber was heated and pulled until it broke, forming a narrow tip that was much smaller than the original fiber

core.[69] The sides of the fiber are then coated with aluminum to form a waveguide for the light travelling through the optical fiber with a tiny aperture, which is typically 70 - 80 nm in diameter.[70] Laser light is focused to enter the larger distal end of the fiber while the tip of the fiber is positioned near the sample (~5 nm from the surface) using components similar to those developed for probe techniques, such as atomic force microscopy (AFM). While the fiber is located at a known distance from the sample, the stage is scanned to create fluorescence images at the far-field end using traditional optics and a single element detector. In this format, only a small region of the sample is excited, thereby eliminating the need for a confocal aperture. Figure 1.5b shows a typical NSOM image of single molecules of the dye, oxazine 720, in PMMA with fluorescent spots that are below 100 nm in diameter. The spatial resolution in this image is not limited by the optical resolution set by diffraction, but is determined by the diameter of the probing fiber when in the near field with respect to the sample. NSOM has been used to reveal heterogeneity among spectral properties of a single emitter as a function of time[71] and also to measure single-molecule fluorescence lifetimes.[72] The major advantage of NSOM includes the reduced sample volume offered by the extremely reduced laser spot size, which generates low background counts and immediate orientation information. Also, by monitoring the position of the scanned fiber tip, topographical information can be obtained with the fluorescence image.[20] However, this technique is limited to flat samples because of the brittle nature of the fiber tip, which is susceptible to breakage. Also, imaging single molecules far from the surface is impossible due to the fact that the near field regime quickly disappears or disperses in the z-direction, thus limiting the application of NSOM in many biological systems, such as the interior of a cell. In addition, it is difficult to consistently make fibers with the same aperture size.

Nonetheless, a potential solution to some of these limitations is the use of apertureless NSOM techniques, which utilize ultrasharp tips as an antenna to localize the excitation region.[73]
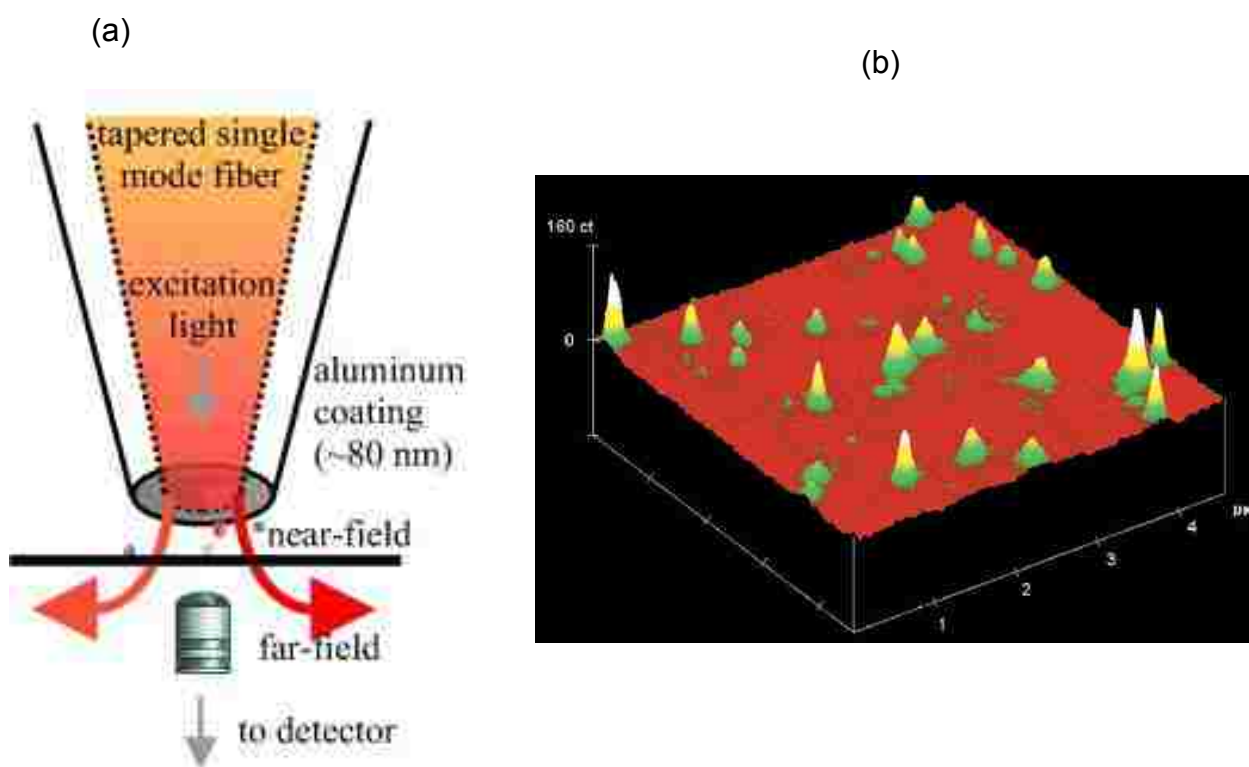
Figure 1.5 (a) Schematic representation of instrumentation used for NSOM. Adapted with permission.[65] (b) Single molecule image of Oxazine 720 molecules acquired with NSOM, adapted with permission.[74]

1.3.3 Wide-Field Methods

Similar to traditional microscopy, wide-field methods for SMD utilize an excitation source (usually a laser) to illuminate an area several microns in diameter. Fluorescence emission from single molecules within the illuminated area are properly isolated and passed to a two-dimensional array detector such as a CCD. Single-molecule studies

performed in this fashion provide two major advantages: (a) simultaneous observation of several individual chromophores and (b) the ability to monitor individual chromophores at near video frame rates to allow for the observation of real time translation of single molecules. However, wide field microscopy methods have a primary limitation that stems from the fact that the maximum frame acquisition rates for CCD cameras is much slower than the response time of single element detectors. This limitation has been greatly curtailed with technology advancements in CCD designs, which have made available ultrasensitive frame transfer electron multiplying CCDs (EMCCDs) capable of generating amplified fluorescence signal through their intrinsic signal cascade characteristics. Although, a large region of the sample is imaged onto the detector's active area, the ability to determine single molecule position is controlled by the size of the CCD pixels and the total magnification of the optical system. Spatial resolution is enhanced by dispersing the image over a greater number of CCD pixels by using a CCD with smaller pixel sizes and a large pixel array. Because single molecule photobleaching limits the total number of detected photons and one needs to collect sufficient numbers of photons per pixel for a given integration time to be able to maintain a reasonable SNR, appropriate magnification must be carefully selected in designing the optics for wide-field imaging of single molecules. Although, CCD image signal processing operations, such as binning, can assist in improving SNR when high magnification and high NA microscope objectives are used, it does so at the expense of spatial resolution.

There are basically two techniques for wide-field single molecule studies; these are epi-fluorescence and total-internal reflection (TIR) microscopy. Implementations of both techniques are discussed below.

1.3.3.1   Epi-Fluorescence Microscopy

Epi-fluorescence microscopy has been used for many years for biological applications and was first applied to room temperature single-molecule experiments in studying a biomolecular motor.[42] A simplified schematic of the instrumentation used for epi-fluorescence microscopy is shown in Figure 1.6. An approach for achieving wide area illumination (excitation) is to use a non-collimated excitation beam, which is focused on the back aperture of the microscope objective. The result is a collimated output from the front aperture of the microscope objective with the field of illumination determined by the size of the microscope's aperture. An easy method of accomplishing this is to use a lens with the appropriate focal length situated within the optical path of the excitation light. A high NA microscope objective is usually employed to maximize the detected fluorescence. Also, the flatness of field for the objective is an important consideration in wide-field imaging, especially in situations that require careful quantification of distance molecules across the image plane. Consequently, microscope objectives with the highest flatness of field, such as those designated as "Plan Apo" or "Plan Fluor" are typically used for wide-field imaging. Furthermore, it is very important for the microscope objective to have very low residual fluorescence artifacts, especially in the region of interest. The resulting single-molecule fluorescence is collected with the same objective (epi-fluorescence) and carefully isolated using the appropriate optical filters prior to being focused onto the CCD camera. Wide-field SMD has been applied in the study of the motion of critical structures in single cell membranes[75] and has also been used to explore diffusion of single molecules of transmembrane proteins embedded in live cells.[76] Recently, the ability of wide-field SMD to monitor biochemical

reactions was demonstrated in studying thermal denaturation and the melting profile of labeled DNA molecules in a FRET assay.[77]
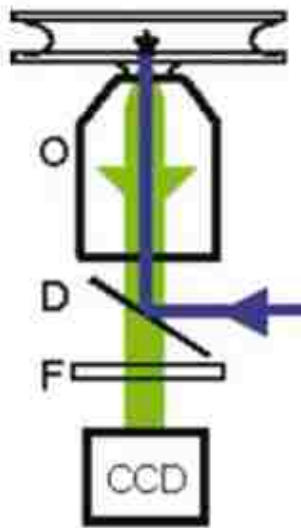
Figure 1.6 Schematic of epi-fluorescence optics; objective (O), dichroic filter (D), emission filter (F). Adopted with permission.[20]

1.3.3.2   Total-Internal Reflection (TIR) Fluorescence Microscopy

TIR fluorescence measurements utilize the exponential decay of an evanescent field generated at a high-index to low-index boundary when light is incident on a low-index medium from a high index material at an angle greater than the critical angle (the angle at which total-internal reflection occurs). The decaying evanescent field penetrates into the low-index medium to a small distance often referred to as the penetration depth. This distance is typically ~150 nm for green laser excitation, which implies that only fluorophores that are sufficiently close to the boundary will be excited while those further away in the bulk sample will not be excited. As a result, only a very

small volume of the sample is observed. Implementation of TIR fluorescence for SMD can be achieved using a prism that is coupled to a microscope cover glass or a thin glass substrate (or any other suitable substrate of high refractive index) using index matching oil. TIR is achieved when the laser beam is launched into the prism above the critical angle, which generates an evanescent field at the interface.[78] A schematic drawing of a prism-type TIR set-up used for imaging single dyes[79] and single GFPs[80] is shown in Figure 1.7a.

Another method by which TIR is implemented for SMD is to couple the input laser beam through the edge of a high NA microscope objective such that illumination occurs around the sides of the glass-water interface, where the launch angle is above the critical angle. This creates an evanescent field that excites a thin plane of the sample near the interface. This method was first implemented by Funatsu *et al*.[42] and is called through the objective TIR.[81] This is represented in Figure 1.7b.

An optical fiber has also been used to generate evanescent field excitation through TIR. In this case, a section of the core of the optical fiber is exposed to the fluorophore such that when light is coupled into the optical fiber, the evanescence wave field generated on the core surface is used to excite the fluorophore in close proximity to the fiber surface. A simplified set up for this technique is represented using the schematic diagram shown in Figure 1.7c.[82]

A typical image acquired using TIR optics is shown in Figure 1.8. This image was obtained using the prism-type TIR configuration. Note also that this is one method by which single molecule fluorescence data is displayed for easy comparison of the relative intensities of individual molecules. Due to the low background of this image, information, such as molecular diffusion, can easily be extracted.

(a)   (b)

(c)
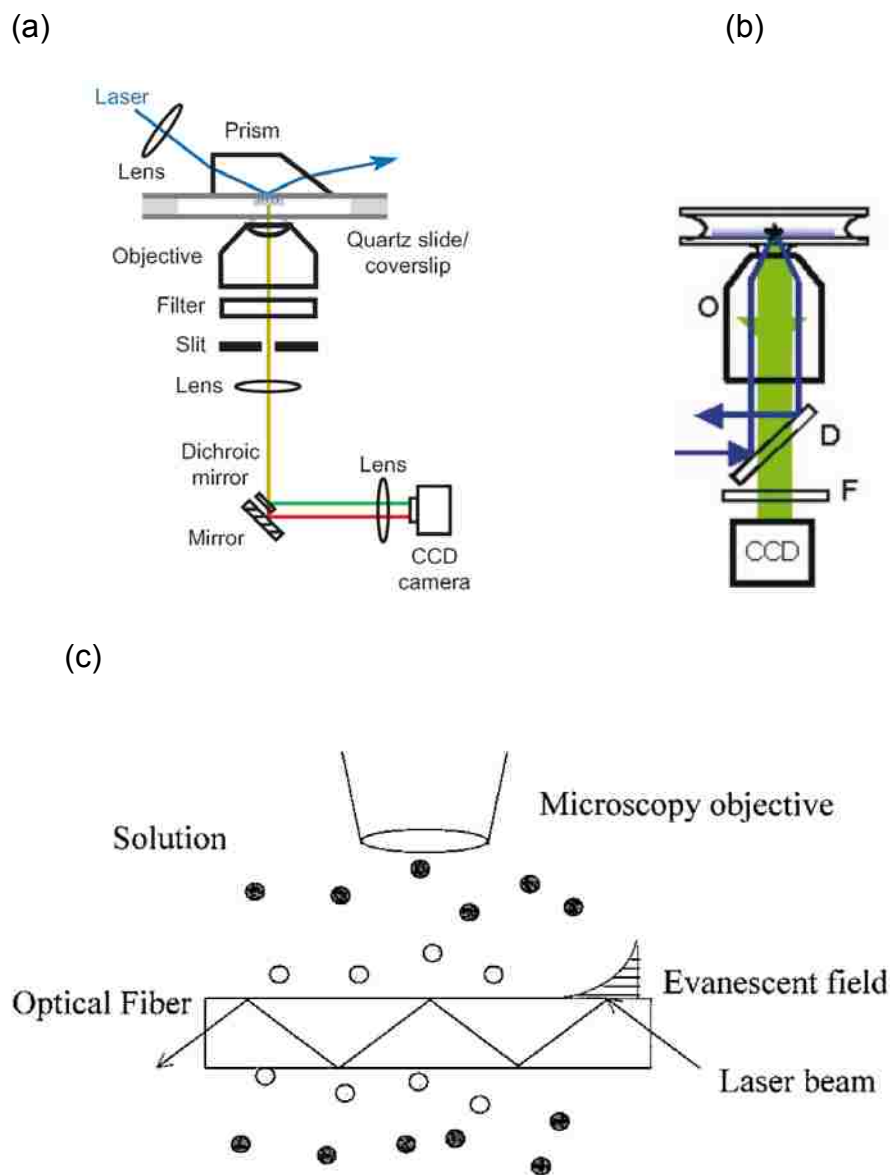
Figure 1.7 (a) Schematic diagram of a prism-type TIR experiment. Adapted with permission.[22] (b) Schematic diagram of an objective-type TIR; adapted with permission.[20] (c) Excitation through an optical fiber; adapted with permission.[82]

1.3.4 Detectors for SMD

The ability to detect single-molecule fluorescence depends not only on the optical design of the detection system but also on the efficiency of the readout device. Such devices should generate minimal dark noise and posses high quantum efficiency to be
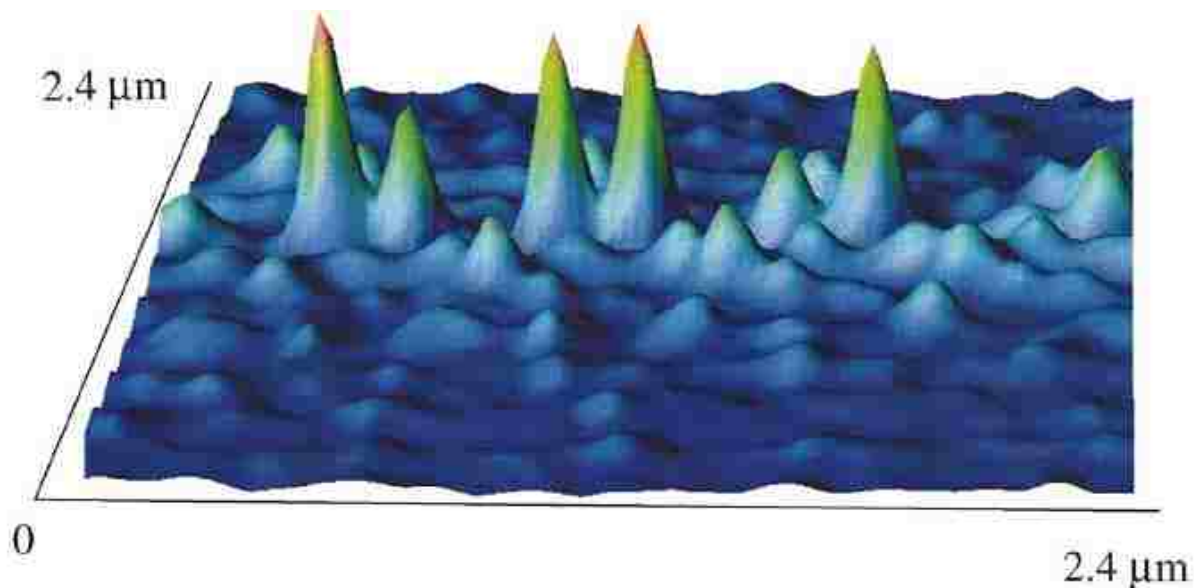
Figure 1.8 A typical single molecule image of GFP mutant T203Y acquired with a CCD using TIR fluorescence; adapted with permission.[66]

able to register fluorescence signals from single molecules. Thus, an important consideration in designing the instrumentation for single molecule experiments is the selection of an appropriate readout device with a matching capability for the particular single-molecule experiment format. Detectors for SMD are classified into two groups: single element detectors and two-dimensional array detectors. Each of these classes of detectors has unique capabilities and characteristics for different experimental approaches. While single element detectors are mainly used for point-by-point fluorescence detection (e.g. in confocal methods and scanning methods), two-dimensional array detectors are used for wide-field microscopy.

1.3.4.1   Single Element Detectors

Early single-molecule experiments utilized photomultiplier tubes (PMTs) to register fluorescence from single molecules diffusing through a tightly focused laser spot.[13] PMTs have large active areas (photocathode), which can be greater than a

square centimeter, and are generally able to multiply single photon events by a million-fold while at the same time offering suitable temporal response with low dark noise levels when cooled. However, they typically have low quantum efficiencies (about 20%), which further decreases at longer wavelengths thus limiting their use in SMD for extended-red fluorophores. Also PMTs require high voltages to operate and have several pieces of electronic components for single photon counting, which makes the design a little complex.

A more simple and generally preferred detector for single-molecule fluorescence is single photon avalanche photodiodes (SPADs), which offer several advantages compared to PMTs. SPADs are available in small integrated packages with on-board amplification and requires only ~5 V to operate. SPADs have quantum efficiencies greater than 60% in the visible region of the electromagnetic spectrum with up to 90% in the near-infrared (NIR). Generally with SPADs, a detected photon is converted to a digital output pulse, which is counted using a computer-based digital acquisition board.[83] SPADs also have low dark count rates (25 – 100 cps) comparable to the best cooled PMT. The only disadvantage of SPADs compared to PMTs is the small active area of the SPAD (~200 µm in diameter), which creates a challenge in the design of a typical fluorometer since most of the collected photons could fall on the non-active regions of the SPAD and thus will not be detected. However, this limitation becomes an advantage in confocal imaging where the small active area can be used as a confocal aperture to improve the signal quality.

1.3.4.2 Two-Dimensional Array Detectors

Wide-field methods for SMD employ array detectors, such as microchannel plates or CCDs. The microchannel plate detector is a large area PMT that is configured

to register fluorescence signal in two dimensional x-y formats. Although this detector can provide fast timing information, it has a low quantum efficiency, comparable to that of a conventional PMT. The detector of choice for wide-field microscopy is the CCD, due to its intrinsically high single photon detection efficiency with low read noise. A CCD contains an array of pixels, each of which acts like an individual detector[84] and makes it possible to register multiple isolated fluorescent signals on a single CCD chip.

Back-illuminated CCD cameras have been used in astronomy and spectroscopy. This type of CCD camera has high quantum efficiency ranging from 70 – 80% in the red and infrared regions and they are built with liquid nitrogen cooling to operate at ~120°C to reduce dark counts down to the level of 1 electron/pixel/h. However, these detectors are limited by their characteristic read noise (~20 electrons for each analog-to-digital conversion) and operate with low speed. Consequently, they are best used in situations that allow long signal averaging times.

Another generation of CCD is the intensified frame transfer CCD cameras, which are designed with optical integration using a photocathode, fiber bundle, microchannel plate, phosphor screen, and Si CCD chip. Photons are first detected by the photocathode, and the emitted electrons are amplified in the microchannel plate that is coupled to the photocathode using a fiber bundle. Subsequently, the phosphor screen generates photons from the amplified electrons, which are converted back to electrons by a front-illuminated Si CCD detector. A fast analog-to-digital converter (ADC) is used to generate digital numbers from the electrons in each CCD well. The advantage of this design is the ability to multiply the detected photoelectrons prior to readout and continuous readout provided by the frame-transfer mode. In the frame transfer mode, the entire frame of the CCD is transferred to a non-photosensitive area following each

exposure. Also the use of a fast ADC allows these detectors to operate at high frame rates (near video frame rates) without sacrificing single photon detection efficiencies. While these detectors provide for high speed imaging, they are characterized by a low quantum efficiency, excess noise from the multiplication process and non-uniform gain over the microchannel plate.

The back-illuminated frame-transfer CCD camera is another class of detectors designed with fast ADC capabilities that operate without large increases in read noise. This design provides for uniform sensitivity from pixel-to-pixel and retains the high quantum efficiency of back-illuminated CCDs.[84]

Further developments in CCD technology have recently made available ultra-sensitive frame-transfer CCDs designed with on-chip multiplication gain. In this design, the last row of the CCD wells is connected to a series of additional wells such that secondary emission is generated as the electrons are passed from well-to-well. This can result in a multiplication gain of ~1000 depending on the number of pixels in the serial register. This detector is finding wide spread applications in SMD with a major advantage of signal amplification, reduced read noise and continuous imaging at video frame rates.

1.3.5 SMD Data Analysis

Single-molecule fluorescence is governed by photon statistical models,[85-88] which allows for the derivation of experimentally measurable characteristics of interest such as the autocorrelation function or photon burst distribution.[89]

SMD experiments are usually characterized by low SNR, thus creating a challenge in the ability to clearly distinguish background noise from single-molecule signal as well as distinguishing different molecules by their emitted photons. The autocorrelation

36

function has been shown to be a useful tool for dissecting the average motion of small molecules.[13,89] It has also been demonstrated as a sensitive indicator of fluorescence signal produced by individual molecules as they traverse through a focused laser beam.[13,14] For a data set d(t) consisting of N consecutive values of the number of photons detected in a specific time interval (τ), the digital autocorrelation function $A(\tau)$ is given by:[13,14]

$$A(\tau) = \sum_{t=0}^{N-1} d(t)d(t + \tau)$$

(1.1)

Where $d(t + \tau)$ represents the data point (value) at time $t + \tau$. A plot of the function A (τ) for a given experimental data set would generate a peak, which is easily distinguishable from background signals. The autocorrelation peak is an indicator of the presence of molecular species in the probe volume. In the absence of emitting species in probe volume, the peak disappears. This is because the random noise of the background is not recognized by the autocorrelation function. The width of the autocorrelation peak is a measure of the time a dye molecule stays in the probe volume (molecular transit time). It can be used to discriminate different molecular species based on their transit time. The autocorrelation function will indicate that a high sensitivity (molecular level) is achieved in the experimental measurement. However, this type of analysis is not able to identify single molecules as they migrate through the excitation volume.

A more quantitative approach for identifying the passage of individual molecules through an illuminated volume element is the use of the weighted quadratic sum (WQS);[13,14,90]

$$S(t) = \sum_{\tau=0}^{k-1} w(\tau)d(t + \tau)^2$$

(1.2)

where k is the approximate time interval representing the lower limit of the molecular transit time or the average photobleaching lifetime of the dye molecule, and ω(τ) is a weighting function chosen to best distinguish the single molecule signal from background fluctuations. Usually ω(τ) is chosen to compensate for the time interval between when the molecules approach the excitation volume and the photobleaching lifetime of the molecule (sometimes, ω(τ) represents a Gaussian). For the WQS, S(*t*) will have a sharp maximum whenever emitting dye molecules flow through the laser such that when a threshold value S_{th} is set, the data set is sufficiently filtered from background interference. In other words, a signal S can be clearly identified as a single molecule signal when S(t) > S_{th} . This quantitative information can be used to calculate the detection efficiency (DE) of the detection system by using;

$$DE = M_d/M_{en} \qquad\qquad (1.3)$$

where M_d is the number of molecules detected and M_{en} is the number of molecules that enter the detection volume.

The maximum-likelihood criterion (MLC) is another tool, which can be used to process single-molecule data.[90] This is based on a probability distribution of background noise and single-molecule signal.[91] For a given data set N, the probability that N represents single-molecule events (P_{mol}) and the probability that N represents background fluctuations (P_{noise}) both are calculated and fitted into the MLC function (*M*):[90]

$$M = \ln\left[\frac{P_{\mathrm{mol}}(\{N_i\})}{P_{\mathrm{noise}}(\{N_i\})}\right]$$

(1.4)

M > 0 = molecule present

M < 0 = no molecule present

The MLC simply states that the process with the highest probability is the most likely.

1.3.6 High Throughput SMD

The advent of wide-field imaging and improved technology in CCD design (see section 1.3.3) has created an opportunity for throughput enhancement in single molecule experiments. This allows for the simultaneous study of several surface bound single molecules[92] and monitoring of molecular motion in solution.[93,94] Also, advancements in micro-total analysis systems (μ-TAS)[95] has enabled parallelization of SMD experiments, which has allowed maximizing throughput via parallel multi-sample processing in short analysis times.

1.4 Merging Microfluidics with SMD

Microfluidics can be defined as the technology of systems capable of processing and manipulating minute amounts of fluid (liquid samples) using micrometer-scale channels. These systems or devices consist of microfabricated structures, which can be designed to produce diagnostically useful systems (e.g micro-total analysis system, *μ-TAS*) for such applications as point-of-care (POC) measurements.[95-98] There has been a rapid growth and wide spread applications of microfluidic technology since the conceptualization of miniaturized chemical analysis systems in the early 1990s.[99,100] Presently, it is adopted in various fields of applied research, such as DNA sequencing,[101,102] immunoassays,[103] protein analyses,[104] and clinical diagnostics.[105] Microfluidic-based systems possess unique advantages, such as sample miniaturization, reductions in reagent consumption, short analysis times and the ability to integrate several processing steps into a single system, which simplifies routine

operations and also eliminates sample cross contamination. In addition, these devices are viable platforms for parallel processing of multiple assays (High Throughput Screening, HTS) due to the inherent ability to generate multiple fluidic processors over small footprints suitable for optical imaging.[106-108] Other benefits include the ability to automate fluid handling and drastically reduce assay cost.

While microfluidic channels provide the interface required to handle small sample volumes, SMD allows for the localization, counting, and identification of individual molecules present in the small volume. Thus, by merging microfluidic technology with SMD, the optimal requirement for the analysis and manipulation of samples on a single-molecule scale can be achieved; such merger would facilitate system integration and automation suitable for increasing throughput in biochemical screening such as HTS in drug discovery.[108] In more specific terms, SMD in combination with microfluidics offers new tools for research; *First,* single-molecule analysis permits a reduction in the number of molecules needed per assay, thus the total sample volume and the sample concentration can be drastically decreased. This is particularly important when dealing with such systems as biological cells that have few copies of target analytes. *Second,* the identification of single molecules greatly reduces the time required for data acquisition; consequently miniaturized samples are analyzed with increased speed and high statistical accuracy. *Third,* mixtures of analytes can be analyzed in a flow-based format with higher molecular detection efficiency by employing distinct identification tags (multiplex single-molecule detection). *Fourth*, the ability to carry out multiple assays in parallel with single-molecule sensitivity (high throughput SMD).

Silicon and glass have been traditionally employed for creating microfluidic devices[109, 110] based on fabrication techniques developed in the microelectronics sector.

Successful fabrication on these substrates has been accomplished using several methods such as lithography, plasma etching or reactive-ion etching techniques.[111,112] The attractiveness of glass and quartz as classic materials for microfluidic applications includes their well-defined surface chemistry, good electro-osmotic properties and excellent optical properties, which are suitable for fluorescence measurements. However, the fabrication modalities are quite challenging and relatively expensive. This result into a search for alternative materials, that are more conducive to large-scale production.

1.4.1 Polymers as Fluidic Chip Substrate for SMD

Polymer materials offer important advantages in microfluidic device production. This is essentially due to their wide range of material properties, which can be selected for diverse applications. In addition, they are generally low-cost materials with good processibility requiring simple fabrication procedures to make devices allowing for the inexpensive replication of microstructures and the mass production of disposable microchips.[113] However, many polymers display poor optical properties that may not be conducive to ultra-sensitive fluorescence measurements required for SMD and thus, a careful selection of a suitable polymer for microfluidic construction must be made based on their properties to ensure high performance for the intended application.[113-116] For SMD, properties that are of fundamental importance include the optical transparency, autofluorescence levels, biocompatibility and chemical resistance. Other properties such as the glass transition temperature, machinability, tensile strength and thermal conductivity are important in selecting the appropriate material. A compilation of physical and chemical properties of the most widely used polymers for microfluidics applications is shown in Table 1.1 (adopted from Becker *et al.* [115]).

1.4.2 Microfabrication Techniques

Fabrication of the desired fluidic structures on polymers for SMD can be achieved by several methods including lithography, UV-laser ablation, hot embossing, injection molding, direct micromilling, or soft lithography. Detailed descriptions of these methods can be found in selected reviews.[117-120] However, a brief description of LiGA is given below;[121,122]

1.4.2.1 LiGA

A common approach for large –scale production of microfluidic devices using a polymer substrate is LiGA; a German acronym for lithography, electroplating and molding. This process is normally employed to fabricate high quality mold inserts for mass production of polymer parts (microfluidic devices). It employs either a synchrotron source (X-ray LiGA) or UV light (UV-LiGA) as appropriate for a particular microfluidic design.[123] In X-ray LiGA,[124] an X-ray sensitive resist, such as PMMA, is coated on a plating base (e.g. stainless steel), which is then exposed to X-rays to form microstructures using an appropriate X-ray mask that has the defined pattern. The exposed photoresist is then removed in a developing step using a GG developer (a mixture of water, 2-(2-butoxyethoxy)ethanol, tetrahydro-1,4-oxazine and 2-aminoethanol),[125] which is a solvent that dissolves the exposed portion of the resist. Following this step is an electroplating process that fills up the voids between the polymeric features with metal (usually Ni), which is deposited over the top of the patterned resist to a thickness of ~5 mm to obtain a metal mold. A schematic of the LiGA processing steps using X-ray photopatterning is shown in Figure 1.9. After the electroplating process, the polymeric resist is removed to generate the metal mold

Table 1.1 Physical and chemical properties of most widely used polymers for microfluidic applications. Adopted from Becker *et al.*

Name	Trade name (examples)	Density (g cm⁻³)	T_g (°C)	Heat distortion temperature (°C)	Resistivity (Ω cm⁻¹)	Water absorption (%)	Refractive index	Young's (tensile) modulus (MPa)	Thermal expansion coeff. (10⁻⁶/K)	Resistant against	Not resistant against	Organic solvent stability
PMMA	Perspex, Plexiglas	1.19	110	90	1×10^{15}	2	1.492	3,200	80	Acids, bases (medium conc.), oil, petrol	Alcohols, acetone, benzole, UV radiation	Attacked by most solvents (e.g. acetone, benzene, dichloromethane)
PC	Makrolon, Calibre, Lexan, Trirex	1.19–1.24	148	125	1×10^{14}	0.30	1.58–1.6	2,200–2,400	70	Alcohols, acids	Hydrocarbons, ketones, KOH	Attacked by most solvents (e.g. acetone, methylene chloride)
PP	Ektar, Fortilene, Hostalene	0.9	0–10	100–110	$>1 \times 10^{14}$	0.01–0.1	1.49	1450	100–200	Acids, bases, Alcohol, organic solvents, fats	Petrol, benzole, hydrocarbons	Xylol, tetraline, decaline
PS	Styron, Noryl	0.9–1.24	100	70	$>1 \times 10^{16}$	<0.4	1.59	2,300–4,100	30–210	Bases, alcohols	Hydrocarbons	Attacked by most solvents (e.g. acetone, benzene, dichloromethane)
PE (LD/HD)	Rexlon, Bapolene, Dowlex	0.91 (LD) 0.967 (HD)	110/140	80/100	10^{15}–10^{16}	<0.015	1.51 (LD)	200/1,000	170/200	Acids, bases, alcohols, oil	Hydrocarbons	Trichlorobenzole, xylole, hexane
COC	Topas, Zeonor	1.02	78	170	$>1 \times 10^{14}$	0.01	1.53	2,600	70	Acids, bases		
COP	Zeonex	1.01	138	140	$>1 \times 10^{17}$	0.01	1.525	2,400	70			
PEEK	PEEK	1.3	143	250	$>1 \times 1,016$	0.5		3,700	17	Most organic and inorganic substances	Conc. nitric acid, sulfuric acid, UV light	
PDMS	Sylgard	1.03	–120	200	1.2×10^{14}	0.1	1.43		960	Weak acids and bases	Strong acids, hydrocarbons	
SU-8		1.19	210		2.8×10^{16}		1.58	2,000	52	Acids, bases, most solvents		
PI	Kapton	1.42	360–410	400	$>1 \times 10^{12}$	2.9–4	1.7	2,500	20	Acids, bases, solvents		No known solvents

master, which can be used to replicate polymer microstructures repeatedly through injection molding or hot embossing.

UV-LiGA operates with the same principle except that a UV light source is used instead of X-rays.[126,127] This approach has been used to produce high aspect ratio patterns using SU-8 as the resist.[128]

1.4.2.2   Hot Embossing

This is a replication technology used to transfer fluidic patterns from a mold master into the required polymer substrate.[129,130] The pattern on the mold master can be made either by micromachining[131,132] or by a lithography-based approach such as LiGA. Hot embossing is done in three steps; *first,* the suitable polymer material is placed between two metal plates (one contains the mold master) and heated to above its glass transition temperature (T_g). *Second,* a controlled force is then applied onto the soften polymer by pressing the heated mold master under vacuum for few minutes. *Third,* the metal plate and polymer substrate are cooled below the T_g of the polymer prior to the withdrawal of the metal plates to form the desired pattern in the polymer. This technique is very simple and cost effective. It has a fast processing time of ~5 mins and can be used to produce thousands of parts from a single mold master. Examples of parts fabricated using this technology are shown in Figure 1.9

1.4.2.3   Thermal Annealing

Following the transfer of the fluidic pattern into the polymer substrate as described above, the next step is the creation of the fluidic channels. This is mostly done by thermal annealing. In this process, a thin polymer sheet, often referred to as cover sheet, which should be of the same (or similar) material properties (especially the glass transition temperature, T_g) as the substrate bearing the fluidic pattern, is used to

enclose the fluidic pattern by thermally bonding it to the substrate to create the fluidic

channels. Thermal annealing proceeds in four steps: (1) the thin polymer sheet is cut to
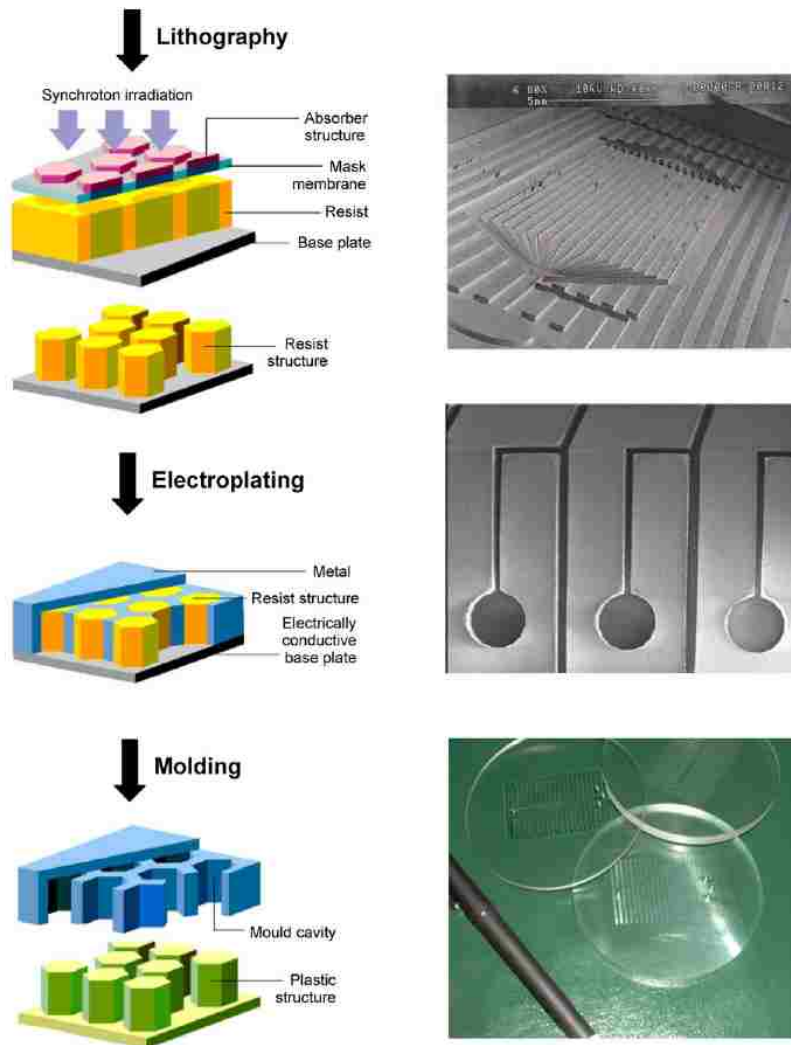
Figure 1.9 X-ray LiGA processing steps for making a metal mold master and molding on polymer substrates. The process begins with a lithography step using X-ray mask and a photoresist to create the desired pattern. After development, the voids left by the resist are filled with metal in the electroplating step to create the desired structures on a metal mold which is then used for molding by transferring the structures on the mold to the polymer substrate. Scanning electron micrograph of metal mold and polymer parts produced with this process are also shown. Adopted with permission.[121,133]

the appropriate size and placed on the polymer substrate containing the fluidic patterns

to enclose the patterns; (2) the assembly is sandwiched between glass plates and

clamped together; (3) heat is applied, usually in a temperature controlled oven to raise the temperature to slightly above the T_g of the polymer substrate for a reasonable length of time; (4) the assembly is allowed to cool to room temperature to generate the fluidic chip.

1.4.3 Single Channel SMD

Most flow-based single-molecule experiments are performed in a single fluidic channel using confocal optics (see section 1.3.1) and single element detectors such as a SPAD (see section 1.3.4.1). In this format, the fluidic channels provide for a conducive environment for effective sample manipulation and delivery while the single element detector and confocal configuration provide for a high sampling rate (defined by the response time of the detector) and high sensitivity. The sampling rate simply represents the frequency of data collection by the detector. For example, if a target analyte (or molecule) traversed the probe volume with a transit time of 1 s, a detector element with a respose time of 0.1 s will generate 10 data points (i.e. 10 data points per second) for the analyte signal to represent a Gaussian peak.[134-139] While this format generates high detection efficiency, which is simply the percentage of molecules detected above a threshold value, and favorable SNR, it is characterized with a low sample processing throughput.[140] The throughput limitation associated with single channel SMD is addressed using a multichannel configuration and a suitable detection system for parallel readout of results.

1.4.4 Multi-Channel SMD

In multi-channel single-molecule experiments, the samples are dynamically transported through a series of fluidic channels and single molecules are interrogated using wide-field illumination (see section 1.3.3). The resulting fluorescence signals from

flowing molecules in the fluidic channels are imaged onto an array detector, such as a CCD for parallel readout. In this configuration, the increase in throughput is directly related to the number of channels patterned onto the fluidic substrate that are interrogated. The potential of this experimental format for drastic reductions in sample processing times suitable for high throughput biochemical analysis has been demonstrated in recent reports.[77,141]

There are basically two methods for excitation to perform high throughput single-molecule experiments in a multi-channel fashion: epi-illumination and waveguide excitation (see section 1.3.3.1). In epi-illumination for multi-channel SMD,[77] the fluidic channels must be configured in a high packing density format and confined within the excitation volume, which is defined by the optical design, such that molecules traversing each fluidic channel can be identified via optical imaging. The fluidic channels should also be constructed with the appropriate dimensions to minimize background fluorescence from the sample matrix.

Waveguide excitation possesses the potential for improved sensitivity since it utilizes a confined evanescent field with a small penetration depth (~350 nm) and thus generates ultra-small probe volumes suitable for maximizing the single-molecule fluorescent signal. However, the challenge in this technology lies on the ability to fabricate an integrated system with a fluidic network and waveguide suitable for multi-channel flow-based SMD. This configuration was recently reported by Soper's group,[142] which employed two different substrates to create a fluidic system with integrated orthogonal waveguide for high throughput fluorescence measurements. Exploitation of this technology could expand the use of single-molecule fluorescence especially in high throughput biochemical screening applications.

1.4.5 CCD Operational Formats for Multi-Channel SMD

CCD detection technology allows for different software-controlled operational modes suitable for single molecule studies in biochemical assays. The traditional operational mode of CCDs is the snap-shot mode, where a CCD image is taken and processed before the next image is captured. This is generally characterized by a low duty cycle, which in this case depends on the total integration time for an image. The ability to track single molecules with 100% duty cycle in multi-channel SMD applications has been demonstrated by operating the CCD in a time-delayed integration (TDI) mode[141] or in frame transfer mode (FTM). [77]

1.4.6 Time-Delayed Integration (TDI) Mode

In this mode of operation, the CCD pixels of the array are exposed for the entire duration of an experiment to continuously collect fluorescence signals from flowing single molecules. The CCD chip is configured using the interface software to read out one row at a time instead of the entire chip. The parallel shift of the CCD is then synchronized with the linear velocity of the flowing single molecule so that photogenerated signal is collected into the same potential well of the CCD array thereby enhancing the SNR while at the same time increasing the duty cycle of the detection system. In this case, the SNR scales with $N^{1/2}$, where N is the number of rows in the CCD camera. A more detailed description of the TDI mode can be found in Emory *et al.*[141]

1.4.7 Frame Transfer Mode (FTM)

The FTM allows for continuous imaging with 100% duty cycle to track fluorescently labeled molecules at near video frame rates as the molecules traverse an interrogation zone. Frame transfer CCDs are constructed with the CCD chip divided into

two halves: a photosensitive area and a non-photosensitive (image storage) area. Once an image is taken, it is immediately transferred from the sensor area to the frame transfer area and immediately followed by another image being collected while at the same time, the stored image is being read out through the serial register. This allows for high speed imaging and it is suitable for monitoring molecular motion in fluidic systems. A schematic representation of a frame transfer CCD chip is shown in Figure 1.10. Another added feature to most frame transfer CCDs, especially the EMCCDs, is on-chip multiplication gain, which provide for single-molecule sensitivity. The on-chip gain is a signal boosting process that multiplies photo-generated charges above the read noise and occurs before the charges reach the readout amplifier. This process can generate gain factors greater than 1000x. The technology employs an extended serial register called a multiplication register (see Figure 1.10), where electrons are multiplied via impact ionization that is initiated and sustained by applying higher than typical CCD clock voltages (up to 50 V). For most cascade CCDs, the clock voltage is controlled by a 12-bit analog-to-digital (ADC) converter. This technology provides for single-molecule sensitivity even at supravideo frame rates.

1.5 Biochemical Applications of SMD

A new environment for biochemical research has been realized by emerging SMD techniques. In its present status, SMD has provided unprecedented insight toward the understanding of functional details in many biological areas such as molecular motors,[21,143-145] nucleic acid enzymes,[146-148] RNA activities,[149-152] protein folding,[153-156] enzymology,[157-162] gene expression,[26,163] and mutational analysis.[164] Detailed discussions on these and other applications can be found in selected reviews.[22,65,165-175]
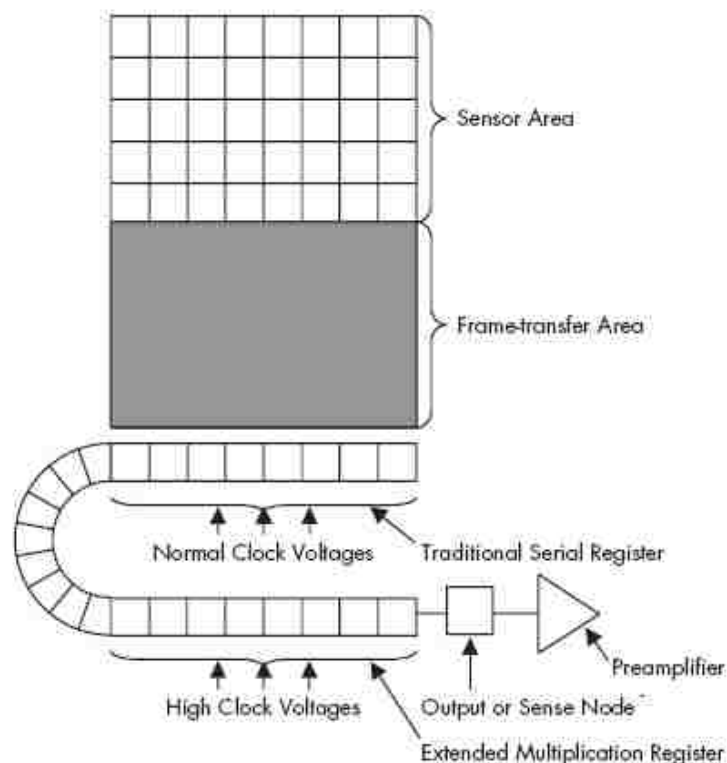
Figure 1.10 A schematic representation of a frame transfer CCD chip with on-chip multiplication gain. Images are taken with the sensor area and immediately transferred to the frame transfer area. Prior to being read out, the collected charges that form the image are multiplied many times in the multiplication register to enhance sensitivity.

However, specific examples are given below, which are related to two commonly applied assay format for HTS: receptor binding assays and competition- / inhibition-based assays.

1.5.1 Protein Kinase Assay

SMD technology can be readily applied to kinase-type assays to generate high quality data such as molecular distribution of phosphorylated products. A typical example representing an indirect competition-based assay format is given in Figure 1.11, which shows components in a kinase inhibition assay. In this illustration, the production of phosphorylated product is measured using the change in polarization as a

result of the displacement of a fluoro-labeled pre-phosphorylated peptide from the specific antibody.[176] This has been demonstrated at Pfizer Sandwich using the first generation EVOscreen Mark-II technology[173] to measure molecular brightness in each polarization direction in a kinase screening assay. In this screening platform, high quality measurements of fluorescence polarization were demonstrated using single molecule detection in a 1 µL volume of the assay.[176]
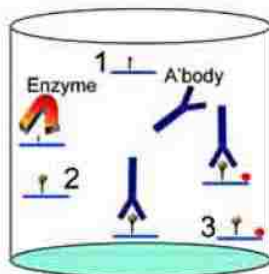
Figure 1.11 Components in a kinase inhibition assay using antibody recognition. The phosphorylated product displaces a pre-phosphorylated fluoro-labeled reporter peptide from the antibody. 1: non-phosphorylated petide substrate, 2: phosphorylated peptide product, 3: pre-phosphorylated fluoro-labeled reporter peptide. Molecular brightness in each polarization direction arising from the free and antibody-bound state can be measured. Adapted with permission.[176]

1.5.2 Membrane Receptor-Ligand Assay

The binding of a fluoro-ligand to a sub-cellular component such as a receptor in a membrane preparation will generate two distinct fluorescent species due to the high local concentration of the membrane receptor. The two fluorescent species represent the free ligand and the ligand bound to the receptor (see Figure 1.12). Introduction of test compounds into the assay will lead to competitive binding of the test compound and the labeled ligand with the receptor. SMD detection technology can then be used to construct fluorescence intensity distributions of the different species in the assay to determine both the degree of binding and the populations of free and membrane-bound

ligand. This has been implemented using the second generation Evotec screening system (EVOscreen Mark-III) in a vesicle-based assay.[177] The assay was configured by preparing vesicles from cells containing the β_2 adrenergic receptor and employing a Rhodamine Green-labeled ligand (CGP12177A).[178] Binding interactions of ligands to vesicles were monitored, which allowed quantification of bound and unbound ligands using fluorescent intensity distribution analysis (FIDA).[179,180]
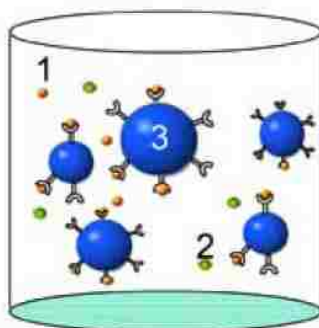
Figure 1.12 Schematic representation of a receptor binding assay showing the principle assay components. 1: free ligand, 2: autofluorescent compound, 3: membrane associated receptor/ligand complex. Adapted with permission.[176]

1.5.3 Future Perspective

SMD technologies have evolved to provide previously unattainable wealth of molecular information in biochemical assays. Besides the ability to distinguish different fluorescing species, such as bound and unbound labeled molecule in one sample, the techniques also provide for the ability to measure multiple, species-resolved parameters. For example, molecular counts, size and brightness can be measured simultaneously, which are useful parameters that can be used to clearly distinguish real hits from false positives in drug screening. In addition, artifacts induced by auto-fluorescent compounds, biological reagents as well as technical errors can be clearly discriminated when analyzing SMD data, which will facilitate the drug validation process

by ensuring that drug candidates for clinical trial have reasonable potency for the target. The technology is currently driving drug discovery research to higher throughputs especially the high sensitivity advantage, which is a major challenge in miniaturized HTS. A combination of SMD with microfluidics will govern and lead the future of drug discovery.

1.6 References

(1)   Nahas, M. K.; Wilson, T. J.; Hohng, S. C.; Jarvie, K.; Lilley, D. M. J.; Ha, T. *Nat. Struct. Mol. Biol.* **2004**, *11*, 1107-1113.

(2)   Moerner, W. E. *Science* **1997**, *277*, 1059.

(3)   Basche, T.; Kummer, S.; Brauche, C. *Nature (London)* **1995**, *373*, 132.

(4)   Guptasarma, P. *Bioessays* **1995**, *17*, 987-997.

(5)   Ghaemmaghami, S.; Huh, W.; Bower, K.; Howson, R. W.; Belle, A.; Dephoure, N.; O'Shea, E. K.; Weissman, J. S. *Nature* **2003**, *425*, 737-741.

(6)   Bon, M.; McGowan, S. J.; Cook, P. R. *FASEB J.* **2006**, *20*, 1721-1723.

(7)   Hirschfeld, T. *Appl. Optics* **1976**, *15*, 2965-2966.

(8)   Neher, E.; Sakmann, B. *Nature* **1976**, *260*, 799-802.

(9)   Deniz, A. A.; Mukhopadhyay, S.; Lemke, E. A. *J. R. Soc. Interface* **2008**, *5*, 15 - 45.

(10)   Moerner, W. E. *Proc. Natl. Acad. Sci.* **2008**, *104*, 12596-12602.

(11)   Moerner, W. E.; Kador, L. *Anal. Chem.* **1989**, *61*, A1217-A1223.

(12)   Orrit, M.; Bernard, J. *Phys. Rev. Lett.* **1990**, *65*, 2716 - 2719.

(13)   Shera, E. B.; Seitzinger, N. K.; Davis, L. M.; Keller, R. A.; Soper, S. A. *Chem. Phys. Lett.* **1990**, *174*, 553-557.

(14)   Soper, S. A.; Davis, L. M.; Shera, E. B. *J. Opt. Soc. Am. B* **1992**, *9*, 1761-1769.

(15)   Soper, S. A.; Mattingly, Q. L.; Veguntat, P. *Anal. Chem.* **1993**, *65*, 740-747.

(16) Lindsay, S. M.; Thundat, T.; Nagahara, L.; Knipping, U.; Rill, R. L. *Science* **1989**, *244*, 1063-1064.

(17) Engel, A. *Annu. Rev. Biophys. Biophys. Chem.* **1991**, *20*, 79-108.

(18) Howard, J.; Hudspeth, A. J.; Vale, R. D. *Nature* **1989**, *342*, 154-158.

(19) Block, S. M.; Goldstein, L. S. B.; Schnapp, B. J. *Nature* **1990**, *348*, 348-352.

(20) Moerner, W. E.; Fromm, D. P. *Rev. Sci. Intrum.* **2003**, *74*, 3597-3619.

(21) Greenleaf, W. J.; Woodside, M. T.; Block, S. M. *Annu. Rev. Biophys. Biomol. Struct.* **2007**, *36*, 171-190.

(22) Cornish, P. V.; Ha, T. *ACS Chem. Biol.* **2007**, *2*, 53-61.

(23) Joo, C.; Balci, H.; Ishitsuka, Y.; Buranachai, C.; Ha, T. *Annu. Rev. Biochem.* **2008**, *77*, 51-76.

(24) Cong, L.; Wissner-Gross, A. D. *Rec. Pat. Nanotechnol.* **2008**, *2*, 1-6.

(25) Brandenburg, B.; Zhuang, X. *Nat. Rev. Microbiol.* **2007**, *5*, 197-208.

(26) Yu, J.; Xiao, J.; Ren, X.; Lao, K.; Xie, S. *Science* **2006**, *311*, 1600 - 1603.

(27) Blainey, P. C.; Van Oijen, A. M.; Banerjee, A.; Verdine, G. L.; Xie, X. S. *Proc. Natl. Acad. Sci.* **2006**, *103*, 5752-5757.

(28) Bustamante, C.; Macosko, J. C.; Wuite, G. J. L. *Nat. Rev. Mol. Cell Biol.* **2000**, *1*, 130-136.

(29) Kienberger, F.; Ebner, A.; Gruber, H. J.; Hinterdorfer, P. *Acc. Chem. Res.* **2006**, *39*, 29-36.

(30) Grier, D. G. *Nature* **2003**, *424*, 810-816.

(31) Gosse, C.; Croquette, V. *Biophys. J.* **2002**, *82*, 3314-3329.

(32) Smith, S. B.; Cui, Y. J.; Bustamante, C. *Science* **1996**, *271*, 795-799.

(33) Strick, T. R.; Allemand, J. F.; Bensimon, D.; Bensimon, A.; Croquette, V. *Science* **1996**, *271*, 1835-1837.

(34) Zander, C. *Fresenius J. Anal. Chem.* **2000**, *366*, 745-751.

(35) Nirmal, M.; Dabbousi, B. O.; Bawendi, M. G.; J., M. J.; Trautman, J. K.; Harris, T. D.; Brus, L. E. *Nature* **1996**, *383*, 802.

(36)   Kuno, M.; Fromm, D. P.; Hamann, H. F.; Gallagher, A.; Nesbitt, D. J. *J. Chem. Phys.* **2000**, *112*, 3117.

(37)   Kulzer, F.; Koberling, F.; Christ, T.; Mews, A.; Basche, T. *Chem. Phys.* **1999**, *247*, 23.

(38)   Blum, C.; Stracke, F.; Becker, S.; Mullen, K.; Meixner, A. J. *J. Phys. Chem. A* **2001**, *105*, 6983.

(39)   Bowden, N. B.; Willets, K. A.; Moerner, W. E.; Waymounth, R. M. *Macromolecules* **2002**, *35*, 8122.

(40)   Moerner, W. E. *J. Chem. Phys.* **2002**, *117*, 10925.

(41)   Harms, G. S.; Cognet, L.; Lommerse, P. H. M.; Blad, G. A.; Schmidt, T. *Biophys. J.* **2001**, *80*, 2396.

(42)   Funatsu, T.; Harada, Y.; Tokunaga, M.; Saito, K.; Yanagida, T. *Nature* **1995**, *374*, 555-559.

(43)   Mujumdar, R. B.; Ernst, L. A.; Mujumdar, S. R.; Lewis, C. J.; Waggoner, A. S. *Bioconjug. Chem.* **1993**, *4*, 105-111.

(44)   Zhuang, X.; Bartley, L. E.; Badcock, H. P.; Russell, R.; Ha, T. *Science* **2000**, *288*, 2048-2051.

(45)   Ha, T. *Methods* **2001**, *25*, 78-86.

(46)   Betzig, E.; Chichester, R. J. *Science* **1993**, *262*, 1422-1425.

(47)   Ha, T.; Enderle, T.; Ogletree, D. F.; Chemla, D. S.; Selvin, P. R.; Weiss, S. *Proc. Natl. Acad. Sci.* **1996**, *93*, 6264-6268.

(48)   Willets, K. A.; Ostroverkhova, O.; He, M.; Twieg, R. J.; Moerner, W. E. *J. Am. Chem. Soc.* **2003**, *125*, 1174.

(49)   Xie, X. S.; Lu, H. P. *J. Biol. Chem.* **1999**, *274*, 15967.

(50)   Lu, H. P.; Xun, L.; Xie, X. S. *Science* **1998**, *282*, 1877.

(51)   Bopp, M. A.; Jia, Y.; Li, L.; Cogdell, R. J.; Hochstrasser, R. M. *Proc. Natl. Acad. Sci.* **1997**, *94*, 10630.

(52)   Nesterova, I. V.; Verdree, V. T.; Pakhomov, S.; Strickler, K. L.; Allen, M. W.; Hammer, R. P.; Soper, S. A. *Bioconjug. Chem.* **2007**, *18*, 2159-2168.

(53)   Nesterova, I. V.; Erdem, S. S.; Pakhomov, S.; Hammer, R. P.; Soper, S. A. *J. Am. Chem. Soc.* **2009**, *131*, 2432-2433.

(54)   Deschenes, L. A.; Vanden Bout, D. A. *Science* **2001**, *292*, 255.

(55)   Weston, K. D.; Carson, P. J.; DeAro, J. A.; Buratto, S. K. *Chem. Phys. Lett.* **1999**, *308*, 58.

(56)   Yasuda, R.; Noji, H.; Kinosita, K.; Yoshida, M. *Cell* **1998**, *93*, 1117.

(57)   Iwane, A. H.; Funatsu, T.; Harada, Y.; Tokunaga, M.; Ohara, O.; Morimoto, S.; Yanagida, T. *FEBS Lett.* **1997**, *407*, 235.

(58)   Mathies, R. A.; Peck, K. *Anal. Chem.* **1990**, *62*, 1786-1791.

(59)   Nie, S. *Annu. Rev. Biophys. Biomol. Struct.* **1997**, *26*, 567-596.

(60)   Robinson, P. J. *Methods Cell Biol.* **2001**, *63*, 89-106.

(61)   Enderlein, J. *The 14th European Conference on Solid-State Transducers (Opto-Chemical Sensors)* **2000**, 607 - 609.

(62)   Inoue, S. *Handbook of biological confocal microscopy* **1995**, 1-17.

(63)   Weber, M. A.; Stracke, F.; Meixner, A. J. *Cytometry* **1999**, *36*, 217-223.

(64)   Corle, T. R.; Kino, G. S. *Confocal Scanning Optical Microscopy and Related Imaging Systems (Academic, San Diego)* **1996**.

(65)   Tinnefeld, P.; Sauer, M. *Angew. Chem. Int. Ed.* **2005**, *44*, 2642-2671.

(66)   Moerner, W. E.; Peterman, E. J. G.; Brasselet, S.; Kummer, S.; Dickson, R. M. *Cytometry* **1999**, *36*, 232- 238.

(67)   Muramatsu, H.; Kim, J. M.; Sugiyama, S.; Ohtani, T. *Rev. Sci. Intrum.* **2003**, *74*, 100-103.

(68)   Vickery, S. A.; Dunn, R. C. *Biophys. J.* **1999**, *76*, 1812-1818.

(69)   Betzig, E.; Trautman, J. K.; Harris, T. D.; Weiner, J. S.; Kostelak, R. K. *Science* **1991**, *251*, 146.

(70)   Hecht, B.; Sick, B.; Wild, U. P.; Decker, V.; Zenobi, R.; Martin, O. J. F.; Pohl, D. W *J. Chem. Phys.* **2000**, *112*, 7761.

(71)   Trautman, J. K.; Macklin, J. J.; Brus, L. E.; Betzig, E. *Nature (London)* **1994**, *369*, 40.

(72) Xie, X. S.; Dunn, R. C. *Science* **1994**, *265*, 361.

(73) Hamann, H. F.; kuno, M.; Gallagher, A.; Nesbitt, D. J. *J. Chem. Phys.* **2006**, *114*, 8596-8609.

(74) Moerner, W. E.; Orrit, M. *Science* **1999**, *283*, 1670-1676.

(75) Schutz, G. J.; Kada, G.; Pastushenko, V. P.; Schindler, H. *EMBO J.* **2000**, *19*, 892.

(76) Vrjlie, M.; Nishimura, S. Y.; Brasselet, S.; Moerner, W. E.; WcConnell, H. M. *Biophys. J.* **2002**, *83*, 2681.

(77) Okagbare, P. I.; Soper, S. A. *Analyst* **2009**, *134*, 97-106.

(78) Davis, L. M.; Parker, W. C.; Ball, D. A. *Proc. SPIE* **2001**, *4262*, 301-311.

(79) Dickson, R. M.; Norris, D. J.; Tzeng, Y-L; Moerner, W. E. *Science* **1996**, *274*, 966.

(80) Dickson, R. M.; Cubitt, A. B.; Tsien, R. Y.; Moerner, W. E. *Nature (London)* **1997**, *388*, 355.

(81) Paige, M. F.; Bjerneld, E. J.; Moerner, W. E. *Single. Mol.* **2001**, *2*, 191-201.

(82) Fang, X.; Tan, W. *Anal. Chem.* **1999**, *71*, 3101-3105.

(83) Li, L.-A.; Davis, L. *Rev. Sci. Intrum.* **1993**, *64*, 1524.

(84) Christenson, M. *Single Molecule* **2000**, *1*, 177-179.

(85) Yang, H.; Xie, X. S. *Chem. Phys.* **2002**, *284*, 423-437.

(86) Enderlein, J.; Robbins, D. L.; Ambrose, W., P; Goodwin, P. M.; Keller, R. A. *J. Phys. Chem. B* **1997**, *101*, 3626-3632.

(87) Ferris, M. M.; Habbersett, R. C.; Wolinsky, M.; Jett, J. H.; Yoshida, T. M.; Keller, R. A. *Cytometry Part A* **2004**, *60A*, 41-52.

(88) Enderlein, J.; Robbins, D. L.; Ambrose, W. P.; Goodwin, P. M.; Keller, R. A. *Bioimaging* **1997**, *5*, 88-98.

(89) Peck, K.; Stryer, L.; Glazer, A. N.; Mathies, R. A. *Proc. Natl. Acad. Sci.* **2008**, *86*, 4087-4091.

(90) Enderlein, J. *Appl. Optics* **1995**, *34*, 514-526.

(91)   Kollner, M. *Appl. Optics* **1993**, *32*, 806-820.

(92)   Uemura, S.; Lizuka, R.; Ueno, T.; Shimizu, Y.; Taguchi, H.; Ueda, T.; Pug;isi, J. D.; Funatsu, T. *Nucl. Acids Res.* **2008**, *36*, e70.

(93)   Xu, X.-H.; Yeung, E. S. *Science* **1997**, *275*, 1106-1109.

(94)   Xu, X.-H. N.; Yeung, E. S. *Science* **1998**, *281*, 1650-1653.

(95)   Vilkner, T.; Janasek, D.; Manz, A. *Anal. Chem.* **2004**, *76*, 3373 -3386.

(96)   West, J.; Becker, M.; Tombrink, S.; Manz, A. *Anal. Chem.* **2008**, *80*, 4403-4419.

(97)   Dittrich, P. S.; Tachikawa, K.; Manz, A. *Anal. Chem.* **2006** *78*, 3887 - 3907.

(98)   Whitesides, G. M. *Nature (London)* **2006**, *442*, 368-373.

(99)   Manz, A.; Graber, N.; Widmer, H. M. *Sens. Actuator.* **1990**, *B1*, 244-248.

(100)   Harrison, D. J.; Manz, A.; Fan, Z.; Ludi, H.; Widmer, H. M. *Anal. Chem.* **1992**, *64*, 1926-1932.

(101)   Schmalzing, D.; Tsao, N.; Koutiny, L.; Chriholm, D.; Srinivasan, A.; Adourian, A.; Linton, L.; McEwan, P.; Matsudaira, P.; Enrlich, D. *Genome Res.* **1999**, *9*, 853-858.

(102)   Paegel, B. M.; Emrich, C. A.; Wedemayer, G. J.; Scherer, J. R.; Mathies, R. A. *Proc. Natl. Acad. Sci.* **2002**, *99*, 574-579.

(103)   Locascio, L. E.; Hong, J. S.; Gaitan, M. *Electrophoresis* **2002**, *23*, 799-804.

(104)   Badal, M. Y.; Wong, M.; Chiem, N.; Salimi-moosavi, H.; Harrison, D. J. *J. Chromatogr. A* **2002**, *947*, 277-286.

(105)   Tian, H. J.; Jaquins-Gerstl, A.; Munro, N.; Trucco, M.; Brody, L. C.; Landers, J. P. *Genomics* **2000**, *63*, 25-34.

(106)   Sundberg, S. A. *Curr. Opin. Chem. Biol.* **2000**, *11*, 47-53.

(107)   Khandurina, J.; Guttman, A. *Curr. Opin. Chem. Biol.* **2002**, *6*, 359-366.

(108)   Khandurina, J.; Guttman, A. *J. Chromatogr. A* **2002**, *943*, 159-183.

(109)   Li, J.; Thibault, P.; Bings, N. H.; Skinner, C. D.; Wang, C.; Colyer, C.; Harrison, J. *Anal. Chem.* **1999**, *71*, 3036-3045.

(110) McClain, M. A.; Culbertson, C. T.; Jacobson, S. C.; Allbritton, N. L.; Sims, C. E.; Ramsey, J. M. *Anal. Chem.* **2003**, *75*, 5646-5655.

(111) Boerner, M. W.; Kohl, M.; Pantenburg, F. J.; Bacher, W.; Hein, H.; Schomburg, W. K. *Microelectron. Eng.* **1996**, *30*, 505-508.

(112) He, B.; Tan, L.; Regnier, F. *Anal. Chem.* **1999**, *71*, 1464-1468.

(113) Becker, H.; Locascio, L. E. *Talanta* **2002**, *56*, 267-287.

(114) Shadpour, H.; Musyimi, H.; Chen, J.; Soper, S. A. *J. Chromatogr. A* **2006**, *1111*, 238-251.

(115) Becker, H.; Gartner, C. *Ana. Bioanal. Chem.* **2008**, *390*, 89-111.

(116) Schuenemann, M.; Harvey, E. C. *Handbook of biosensors and biochips* **2007**, 731-746.

(117) Fionrini, G. S.; Chiu, D. T. *BioTechniques* **2005**, *38*, 429-446.

(118) Maurya, D. K.; Ng, W. Y.; Mahabadi, K. A.; Liang, Y. N.; Rodríguez, I. *Biotechnol.* **2007**, *2*, 1381-1388.

(119) Liu, B. C. *Adv. Mater.* **2007**, *19*, 3783-3790.

(120) Rotting, O.; Ropke, W.; Becker, H.; Gartner, C. *Microsyst. Technol.* **2001**, *8*, 32-36.

(121) Ford, S. M.; Davies, J.; Kar, B.; Qi, S. D.; McWhorter, S.; Soper, S. A.; Malek, C. K. *J. Biomech. Eng.* **1999**, *121*, 13-21.

(122) Soper, S. A.; Ford, S. M.; Qi, S.; McCarley, R. L.; Kelly, K.; Murphy, M. C. *Anal. Chem.* **2000**, *72*, 634A-651A.

(123) Fu, C.; Huang, H. *Microsyst. Technol.* **2007**, *13*, 293-298.

(124) Kupka, R. K.; Bouamrane, F.; Cremers, C.; Megtert, S. *Appl. Surf. Sci* **2000**, *164*, 97-110.

(125) Schmalz, O.; Hess, M.; Kosfeld, R. *Die Angew. Makromol. Chem.* **1996**, *239*, 93-106

(126) Jing, X.; Chen, D.; Fang, D.; Huang, C.; Liu, J.; Chen, X. *Microelectronics. J.* **2007**, *38*, 120-124.

(127) Qu, W.; Wenzel, C.; Jahn, A.; Zeidler, D. *IEEE: Optoelectronic and Microelectronic Materials and Devices* **1999**, *Dec. 14-16*, 380-383.

(128) Lorenz, H.; Despont, M.; Vettiger, P.; Renaud, P. *Microsyst. Technol.* **1998**, *4*, 143-146.

(129) Islam, R.; Glinsner, T. *Proc. SPIE* **2001**, *4560*, 250-255.

(130) Becker, H. *Integrated microfabricated biodevices; advanced technologies for genomics, drug discovery, bioanalysis, and clinical diagnostics* **2002**, 319-350.

(131) Hupert, M. L.; Guy, J. W.; Llopis, S. D.; Situma, C.; Rani, S.; Nikitopoulos, D. E.; Soper, S. A. *Proc. SPIE* **2006**, *6112*, 61120B-61121 - 61120B-61112.

(132) Hupert, M. L.; Guy, J. W.; Llopis, S. D.; Shadpour, H.; Rani, S.; Nikitopoulos, D. E.; Soper, S. A. *Microfluid. Nanofluid* **2007**, *3*, 1-11.

(133) Situma, C.; Hashimoto, M.; Soper, S. A. *Biomol. Eng.* **2006**, *23*, 213-231.

(134) Wabuyele, M. B.; Ford, S. M.; Stryjewski, W.; Barrow, J.; Soper, S. A. *Electrophoresis* **2001**, *22*, 3939-3948.

(135) Fister, J. C.; Jacobson, S. C.; Davis, L. M.; M, R. J. *Anal. Chem.* **1998**, *70*, 431-437.

(136) Effenhauser, C. S.; Bruin, G. J. M.; Paulus, A.; Ehrat, M. *Anal. Chem.* **1997**, *69*, 3451-3457.

(137) Ros, A.; Hellmich, W.; Duong, T.; Anselmetti, D. *J. Biotechnol.* **2004**, *112*, 65-72.

(138) Brewer, L. R.; Bianco, P. R. *Nature Methods* **2008**, *5*, 517-525.

(139) Haab, B. B.; Mathies, R. A. *Anal. Chem.* **1999**, *71*, 5137-5145.

(140) van Orden, A.; Keller, R. A.; Ambrose, W., P *Anal. Chem.* **2000**, *72*, 37-41.

(141) Emory, J. M.; Soper, S. A. *Anal. Chem.* **2008**, *80*, 3897-3903.

(142) Okagbare, P. I.; Emory, J. M.; Datta, P.; Soper, S. A. **In press**.

(143) Ishijima, A.; Yanagida, T. *Trends Biochem. Sci.* **2001**, *26*.

(144) Toprak, E.; Selvin, P. R. *Annu. Rev. Biophys. Biomol. Struct.* **2007**, *36*, 349-369.

(145) Sako, Y.; Minoguchi, S.; Yanagida, T. *Nat. Cell Biol.* **2000**, *2*, 168-172.

(146) Ha, T. *Biochemistry* **2004**, *43*, 4055-4063.

(147) Amitani, I.; Baskin, R. J.; Kowalczykowski, S. C. *Mol. Cell* **2006**, *23*, 143-148.

(148) Perkins, T. T.; Dalal, R. V.; Mitsis, P. G.; Block, S. M. *Science* **2003**, *301*, 1914-1918.

(149) Zhuang, X. *Annu. Rev. Biophys. Biomol. Struct.* **2005**, *34*, 399-414.

(150) Rueda, D.; Bokinsky, G.; Rhodes, M. M.; Rust, M. J.; Zhuang, X.; Walter, N. G. *Proc. Natl. Acad. Sci.* **2004**, *101*, 10066-10071.

(151) Mclure, W. R. *Annu. Rev. Biochem.* **1985**, *54*, 171-204.

(152) Harada, Y.; Funatsu, T.; Murakami, K.; Nonoyama, Y.; Ishihama, A.; Yanagida, T. *Biophys. J.* **1999**, *76*, 709-715.

(153) Rhoades, E.; Gussakovsky, E.; Haran, G. *Proc. Natl. Acad. Sci.* **2003**, *100*, 3197-3202.

(154) Lipman, E. A.; Schuler, B.; Bakajin, O.; Eaton, W. A. *Science* **2003**, *301*.

(155) Deniz, A. A.; Laurence, T. A.; Beligere, G. S.; Dahan, M.; Martin, A. B.; Chemla, D. S.; Dawson, P. E.; Schultz, P. G.; Weiss, S. *Proc. Natl. Acad. Sci.* **2000**, *97*, 5179-5184.

(156) Kinoshita, M.; Kamagata, K.; Maeda, A.; Goto, Y.; Komatsuzaki, T.; Takahashi, S. *Proc. Natl. Acad. Sci.* **2007**, *104*, 10453-10458.

(157) Lu, H. P.; Xun, L.; Xie, X. S. *Science* **1998**, *282*, 1877-1882.

(158) Edman, L.; Rigler, R. *Proc. Natl. Acad. Sci.* **2000**, *07*, 8266-8271.

(159) Velonia, K.; Flomenbom, O.; Loos, D.; Masuo, S.; Cotlet, M.; Engelborghs, Y.; Hofkens, J.; Rowan, A. E.; Klafter, J.; Nolte, R. J. M.; de Schryver, F. C. *Angew. Chem. Int. Ed.* **2005**, *44*, 560-564.

(160) Brender, J. R.; Dertouzos, J.; Ballou, D. P.; Massey, V.; Palfey, B. A.; Entsch, B.; Steel, D. G.; Gafni, A. *J. Am. Chem. Soc.* **2005**, *127*, 18171-18178.

(161) Antikainen, N. M.; Smiley, R. D.; Benkovic, S. J.; Hammes, G. G. *Biochemistry* **2005**, *44*, 16835-16843.

(162) Tokunaga, M.; Kitamura, K.; Saito, K.; Iwane, A. H.; Yanagida, T. *Biochem. Biophys. Res. Comm.* **1997**, *235*, 47-53.

(163) Cai, L.; Friedman, N.; Xie, X. S. *Nature* **2006**, *440*, 358-362.

(164) Wabuyele, M. B.; Farquar, H.; Stryjewski, W.; Hammer, R. P.; Soper, S. A.; Cheng, Y.-W.; Barany, F. *J. Am. Chem. Soc.* **2003**, *125*, 6937-6945.

(165) Chen, P.; Andoy, N. M. *Inorg. Chimi. Acta* **2008**, *361*, 809-819.

(166) Van Oijen, A. M. *Biopolymers* **2006**, *85*, 144-153.

(167) Forkey, J. N.; Quinlan, M. E.; Goldman, Y. E. *Prog. Biophys. Mol. Biol.* **2000**, *74*, 1-35.

(168) Xie, X. S. *Annu. Rev. Phys. Chem.* **1998**, *49*, 441-480.

(169) Kelso, D. M. *SPIE* **1997**, *2985*, 206-212.

(170) Dekker, C. *Nat. Nanotechnol.* **2007**, *2*, 209-215.

(171) ROSENBERG, S. A.; QUINLAN, M. E.; FORKEY, J. N.; GOLDMAN, Y. E. *Acc. Chem. Res.* **2005**, *38*, 583-593.

(172) Charvin, G.; Strick, T. R.; Bensimon, D.; Croquette, V. *Annu. Rev. Biophys. Biomol. Struct.* **2005**, *34*, 201-219.

(173) BARBARA, P. F.; GESQUIERE, A. J.; PARK, S.-J.; LEE, Y. J. *Acc. Chem. Res.* **2005**, *38*, 602-610.

(174) Bokinsky, G.; Zhuang, X. *Acc. Chem. Res.* **2005**, *38*, 566-573.

(175) Michalet, X.; Weiss, S.; Jger, M. *Chem. Rev.* **2006**, *106*, 1785-1813.

(176) Gribbon, P.; Schaertl, S.; Wickenden, M.; Williams, G.; Grimley, R.; Stuhmeier, F.; Preckel, H.; Eggeling, C.; Kraemer, J.; Everett, J.; Keighley, W. W.; Sewing, A. *Curr. Drug Discov. Technol.* **2004**, *1*, 27-35.

(177) www.evotec-technologies.com.

(178) Jager, S.; Garbow, N.; Kirsch, A.; Preckel, H.; Gandenberger, F. U.; Herrenknecht, K.; Rudiger, M.; Hutchinson, J. P.; Bingham, R. P.; Ramon, F.; Bardera, A.; Martin, J. *J. Biomol. Screen.* **2003**, *8*, 648-659.

(179) Rudiger, M.; Haupts, U.; Moore, K. J.; Pope, A. J. *J. Biomol. Screen.* **2001**, *6*, 29-37.

(180) Haupts, U.; Rudiger, M.; Ashman, S.; Turconi, S.; Bingham, R.; Wharton, C.; Hutchinson, J.; Carey, C.; Moore, K. J.; Pope, A. J. *J. Biomol. Screen.* **2003**, *8*, 19-33.

CHAPTER 2

HIGH THROUGHPUT SINGLE MOLECULE DETECTION FOR MONITORING BIOCHEMICAL REACTIONS*

2.1 Introduction

The ability to process large amounts of information for high throughput applications has become a primary ambition due in part to the large number of samples that must be interrogated and the complexity of those samples. An example where high throughput data processing is significant is in the drug discovery pipeline (*i.e.,* high throughput screening) where combinatorial libraries consisting of millions of potential small molecule drug candidates are screened for their interaction with therapeutic targets using fluorescence spectroscopy as the readout modality.[1-6]

An approach toward increasing the data production rate for processing biochemical reactions is to increase the number of reactions run in parallel, which allows for analyzing a large number of targets simultaneously. This parallel processing is commonly carried out in titer plates, with increases in the well density used to increase data throughput. For example, titer plates can be configured to run 96 to 9,600 reactions in parallel on a 3" x 5" plate.[7, 8] With increases in well density also comes reductions in well volume, placing severe demands on the readout hardware to provide parallel detection to further increase throughput while at the same time providing high detection sensitivity and favorable limits of detection in spite of the reduced well volume. Other applications that require the ability to transduce large numbers of targets quickly include capillary array electrophoresis,[9] DNA microarrays,[10] small-molecule arrays,[11, 12] and protein microarrays.[13] In addition, micro-Total Analysis Systems (μ-TAS) have been employed as a tool for increasing throughput in many applications due to their exquisite

63

characteristics conducive to high sampling rates brought about by reductions in analysis times and the parallelization of processing units. [14-17]

Another analytical technology, which facilitates the realization of high throughput biochemical data processing, is single molecule detection (SMD). SMD provides the ability to eliminate many sample processing steps associated with multi-step assays, significantly reducing assay time. This has recently been demonstrated by Wabuyele *et al.*, where the overhead processing time associated with PCR amplification of target DNAs was eliminated by detecting single nucleotide polymorphisms (SNPs) in genomic DNA using single-pair FRET (spFRET).[18] Using spFRET, the authors were able to detect SNPs in a processing time less than 5 min. Another advantage of SMD is the detailed information revealed when monitoring biochemical reactions. For example, it can yield insight into complex fluctuation phenomena and hidden heterogeneity that cannot be observed in ensemble techniques.[19]

However, the challenge associated with many SMD assays is their intrinsic low throughput, especially for flow-based SMD experiments where a laser focused to a diffraction limited spot is used to interrogate material as it traverses through the excitation volume.[20, 21] To realize the full processing potential of SMD for high throughput applications, the readout hardware needs to be configured in a parallel format without sacrificing sensitivity.

The common approach for realizing high single molecule sensitivity is, as stated above, the utilization of ultra-small probe volumes, which reduces background interferences resulting from the sample matrix emanating from autofluorescence or scattering.[22, 23] A common method for achieving ultra-small probe volumes is the use of confocal optics,[24-27] in which the laser beam is focused to a diffraction-limited area

producing sampling volumes in the sub-picoliter regime. However, these confocal sampling volumes are usually designed with single element detectors and thus, generate small sample processing throughput rates.

This limitation can be addressed by operating the readout system in a multi-channel configuration, such that single molecules are transported through a series of fluidic processors that are interrogated using wide-field illumination with the resulting fluorescence imaged onto an array detector for parallel readout. An array detector that can be employed for fluorescence imaging appropriate for single molecule high throughput processing is the charge coupled device (CCD).[28] Advancements in CCD technology has made available ultra-sensitive cameras appropriate for realizing detection of single fluorescence molecules in flow-based measurements where the signal is transitory in nature.[29-32] For example, Soper and coworkers[33] recently described a CCD-based single molecule analysis system in which a flowing sample composed of double stranded DNA molecules labeled with an intercalating dye (TOTO-3) were imaged onto a 1340 x 100 pixel CCD camera operated in a time-delayed integration (TDI) mode.[33] The TDI mode was used to collect photo-generated signal from single multiply-labeled DNA molecules into a potential well of the CCD array as the molecules traversed the field-of-view (FoV), thereby enhancing the SNR at the same time increasing the duty cycle of the detection system. Van Orden *et al.* also demonstrated the ability to image single DNA molecules labeled with an intercalating dye using a CCD operated in a snap-shot mode.[34]

While the aforementioned works are excellent examples of increasing the sample throughput for flow-based SMD experiments, the limitations are that the single molecules were double-stranded DNAs loaded with multiple flours. In the case of λ-DNA

(~48,500 bp), each DNA molecule had a load of approximately 9,700 dye molecules. Therefore, high throughput flow-based SMD systems have yet to demonstrate the ability to detect single fluorophore molecules.

Another viable operational modality for a CCD camera directed toward SMD is the frame transfer mode (FTM), which allows for high speed imaging.[35, 36] For example, Li and Yeung utilized a frame transfer electron amplifying CCD to monitor dynamic conformational changes of flavin adenine dinucleotides in different media on a cover slip in which the molecules were immobile. Their results demonstrated the ability to monitor the real-time dynamics of the photoproduct formation between FAD molecules at the single molecule level.[37]

The availability of FTM CCDs with on-chip gain has created the capability to study biochemical reactions at the single molecule level utilizing flow-based measurements in which the single molecules are dynamically transported through the illumination zone. These electron multiplying CCDs (EMCCDs) are equipped with a full frame storage region and a charge multiplication register that generates secondary electrons via an impact-ionization process. The net gain on these cameras can be greater than 1000-fold. Although, the resulting gain has a complex relationship with the applied voltage, it can be estimated using the expression;

$$G = (1+g)^N \qquad\qquad (2.1)$$

where G is the gain factor, g is the probability of generating secondary electrons in the multiplication register (typical value range from 0.01 to 0.016), and N is the number of pixels in the multiplication register. Thus, even with a fairly low probability of generating secondary electrons in the multiplication register, the cascade effect over the large number of stages is quite high. For example, a CCD with N equal to 500 and g = 0.012,

will produce an on-chip gain of ~389. The resulting signal (S_t), defined by the number of photoelectrons generated in each pixel, can be estimated using the following expression;

$$S_t = S*QE*G \qquad (2.2)$$

where S is the number of incident photons impinging on a pixel, QE is the quantum efficiency at the wavelength being monitored and G is the EMCCD gain (see eq. 2.1). The FTM allows continuous imaging with nearly 100% duty cycle and can track fluorescently labeled molecules at near video frame rates as they traverse through an interrogation zone while the on-chip gain provides adequate sensitivity for single fluorophore detection.

In this Chapter, we combined the advantages of microfluidics with a wide field fluorescence imaging system and present, for the first time, the ability to detect single chromophore molecules in a multi-channel flow-through configuration and monitor biochemical reactions at the single molecule/fluorophore level. The system reported herein provides high throughput single molecule processing capabilities using an ultra-sensitive epi-fluorescence imaging system consisting of a FTM EMCCD with on-chip multiplication gain. The system possessed a large FoV (200 μm, diameter, generated by a 40x/0.75 microscope objective) capable of imaging a series of parallel fluidic channels simultaneously. As an example of the utility of this system to monitor biomolecular reactions at the single molecule level at relatively high processing rates, a melt analysis of double-stranded DNA (dsDNA) using a resonance energy transfer reporting system was used. The dsDNA contained a construct labeled on the 5'-end of the sense strand with a dye and a quencher on the 3' end of the anti-sense strand. The number of photon

burst events arising from melted duplexes at different temperatures could be used to determine the melt profile of this double-stranded complex.

2.2 Experimental Details

2.2.1 Optical System

The optical set-up for the flow-based multi-channel SMD is shown in Figure 2.1a. An HL6535MG laser diode (Thorlabs, Newton, NJ, USA) provided excitation (660 nm) with a peak power of 30 mW. The laser diode was mounted on a LDM21 (Thorlabs) laser mount connected to a laser driver (LDC 205, Thorlabs) and a temperature controller unit (TED 200, Thorlabs). The laser output was collimated using an aspheric lens (C230TM-B, Thorlabs) and passed through a 660 nm laser line filter (660DF10, Omega Optical, Brattleboro, VT, USA) that was placed in the optical path of the excitation source. A dichroic mirror was used to direct the laser into a microscope objective (40x, 10x or 5x, Zeiss, Thornwood, NY, USA) and then, onto the sample after being shaped using a plano-convex lens (LA1509, Focal length = 100 mm, Thorlabs). The shaping lens was used to generate a collimated light output from the objective with a diameter determined by the aperture of the objective; the diameter of the collimated light, which determined the FoV of the imaging system, was different for each microscope objective used in our experiments (0.2 mm for a 40x, NA = 0.75 objective; 0.8 mm for a 10x, NA = 0.55 objective; and 1.6 mm for a 5x, NA = 0.12 objective). The fluorescence emission from the sample was collected with the same objective from a PMMA fluidic chip and directed through the dichroic filter, then a band pass filter (719AF40, Omega Optical), and finally a long pass filter (690ALP, Omega Optical) to spectrally isolate the emission from scattered radiation. The isolated emission was then directed onto a reflecting surface of a mirror, which was placed at a 45^0 angle of incidence with respect to the

optical path to direct the fluorescence onto the CCD camera. A plano-convex lens

(AC254-100, focal length = 100 mm) was placed between the mirror and EMCCD

camera, which generated a fluorescence image onto the CCD.

a

Figure 2.1 (a) Optical set-up of the imaging system using epi-illumination and employing a large FoV. The beam from the diode laser (λ = 660 nm) was isolated using a laser line filter (F1) and then shaped with a plano-convex lens (L1), which was used to focus the laser beam behind the input aperture of the microscope objective (OBJ). Following beam shaping, it was directed by a dichroic filter (DF) into the OBJ with the collimated laser beam impinging upon a multi-channel microchip. The fluorescence signal generated from the chip was collected by this same objective, passed through the DF and spectrally selected using a long pass filter (F2) and an interference band pass filter (F3). A mirror (M) was used to steer the fluorescence signal onto a CCD after passing it through a lens (L2), which focused the radiation onto the photoactive area of the CCD. The total magnification of the system was 40x. (b) An optical micrograph showing a section of the multi-channel microfluidic chip; the fluidic network consisted of microchannels with dimensions of 30 μm wide x 20 μm deep and a pitch of 25 μm. All channels had a common sample input reservoir. The driving electric field was applied at this reservoir and another on the opposite end of the fluidic network (not shown) to drive the sample electrokinetically through the imaging area. (c) Diagram showing the operation of the CCD in a frame transfer mode with image accumulation occurring during single molecule travel within the FoV of the microscope. The images of single molecules produced streaks on the CCD due to the molecular transit time being greater than the CCD exposure time and multiple frames summed to produce the final image. Continued on next page

b

**Fluidic Network for High
Throughput Detection of
Fluorescence Molecule using CCD**

**Common
Reservoir for
Sample input**

c
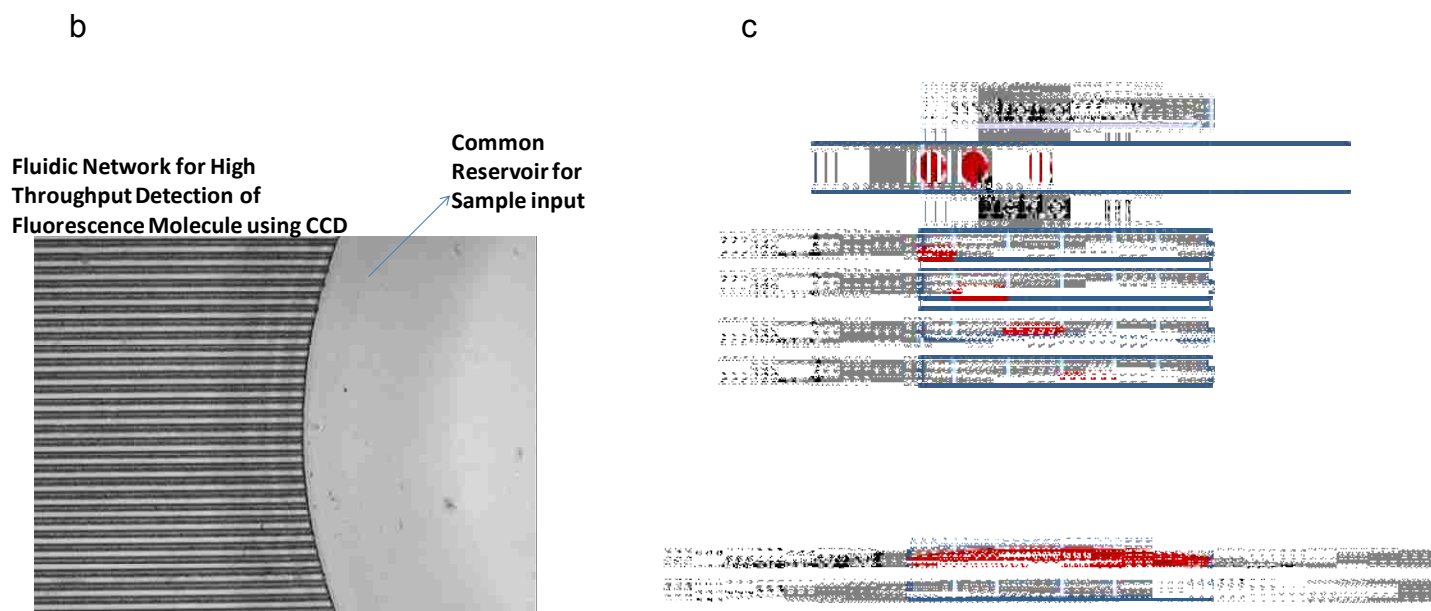
Figure 2.1 (B and C). See caption above.

The EMCCD camera (Cascade 1K, Photometrics, Tuscon, AZ, USA) was a frame transfer CCD equipped with signal enhancement via on-chip gain and possessed 8 μm x 8 μm pixels configured in a 1004 x 1002 front illumination format. The camera had a 10 MHz digital converter and a 16-bit digitization range. The frame transfer capability of the EMCCD allowed near 100% duty cycle when single molecules were tracked along their flow path within the illumination field. The CCD camera was thermoelectrically cooled to -30^{0}C to minimize dark noise and operated at the optimal gain to maximize the SNR in the measurement.

2.2.2 Multi-channel Illumination

The optical system was configured in an epi-illumination format (see Figure 2.1a) with beam shaping optics that generated a collimated output of the excitation source through the microscope objective for wide-field illumination. The collimated beam was used to irradiate a series of parallel microchannels. The system was operated with a

laser power of ~25 mW generating an irradiance of 1.9 x 10^{20} photons cm^{-2} s^{-1} for the 40x objective. For a dye such as AlexaFluor 660 that possesses an absorption cross section of 1.82 x 10^{-16} cm^2 (molar absorptivity = 110,000 $cm^{-1}M^{-1}$) and a fluorescence lifetime of ~1 ns, optical saturation occurs at an irradiance of ~5.4 x 10^{24}. Therefore, the system is currently being operated well below optical saturation.

2.2.3 Microfluidic Design

A PMMA microchip was designed for high throughput single molecule data processing that consisted of a series of flow channels tightly packed to provide the ability to image a number of single molecule experiments within the microscope's FoV. The microfluidic devices were fabricated via direct milling of the fluidic vias into a PMMA wafer using a Kern MMP2522 micromilling machine (KERN micro-und Feinwerktechnick, GmbH & CO, Murnau Westried, Germany). The device consisted of a series of microchannels with dimensions of 30 μm in width, 20 μm in depth and a pitch of 25 μm. All channels possessed a common sample reservoir (Figure 2.1b). Following micromilling, the device was sonicated for 1 min in IPA and rinsed thoroughly with deionized water. A PMMA cover plate (125 μm thickness) was placed on the device to enclose the microfluidic channels. The chip assembly was clamped between two glass plates and annealed in a GC oven at 107°C (slightly above the T_g of PMMA) for 22 min.

2.2.4 Chemicals and Reagents

Stock solutions of Tris-Taps-EDTA (TTE) buffer (10x) were diluted to obtain 1x TTE solutions (pH = 8.7) using nanopure water obtained from a Barnstead NANOpure System (Model D8991, Dubuque, IA). Fluorescence reagents used included AlexaFluor 660 and Syto-63 (Molecular Probes, Eugene, Oregon, USA). λ-DNA (48.5 kbp) was

obtained from Molecular Probes and diluted in 1x TTE buffer to the required concentration after being labeled with Syto-63 at a molar ratio of 5:1 (bp:dye). Single stranded DNA (ssDNA, 60 bases in length) were 5' labeled with AlexaFluor 660 (Molecular Probes) and a stock solution (80 nM) was prepared using a 1x TTE buffer. Double-stranded DNA (dsDNA, 15 bp in length) was obtained from Molecular Probes as well; the duplex had the sense strand labeled with AlexaFluor 660 at its 5' end while the complementary strand (anti-sense strand) was labeled with BHQ-3 at is 3' end. Stock solutions (0.4 µM) of the duplex were prepared in Tris/HCl buffer containing 20 mM Tris-HCl, 10 mM $MgCl_2$ and 10 mM KCl at pH 7.5. Dilutions from this stock solution to the desired concentrations required for the single molecule experiments was accomplished with the same buffer. In all cases, buffer solutions were filtered through 0.2 µm filters prior to sample preparation.

Stock solutions of λ-DNA molecules were labeled with an intercalating dye (Syto-63) and diluted in 1x TTE buffer to 10 pM. This concentration was selected to keep the single molecule occupancy probability low to reduce the double occupancy probability. With the system possessing a probe volume of 0.8 fL (CCD pixel size = 8 µm x 8 µm), a sample concentration of 100 pM produced a single molecule occupancy probability of 0.01 (probability of double occupancy = 0.0001).

2.2.5 Single Molecule Tracking via Frame Transfer EMCCD Operation

The system was optimized for its single molecule sensitivity when operated in the frame transfer mode using λ-DNA (48.5 kpb) labeled with Syto-63 and diluted in 1x TTE buffer. Single λ-DNA molecules were loaded into the common sample reservoir of the PMMA wafer and driven through the microfluidic channels by electrokinetic pumping

using a high voltage power source (Spellman CZE1000R, Hauppauge, NY, USA). The movement of the molecules through the illumination zone generated streak images for each single DNA molecule when the system was operated in the frame transfer mode and multiple images could be combined. A schematic representation of this process (frame transfer with image accumulation) is shown in Figure 2.1c. A streak image resulted from the collection of fluorescence signal from the same molecule into potential wells along a single column of the EMCCD as the molecule migrated through the FoV.

The single fluorophore detection capability of the system was evaluated using DNA molecules that were end-labeled with a single AlexaFluor 660 dye molecule. In this case, only a single image frame was used for the presented data due to the short bleaching lifetimes associated with single chromophore assemblies.

2.2.6 Bulk Fluorescence Measurements

Emission spectra of the duplexed DNA/AlexaFluor 660 constructs used for the bulk melt analyses were acquired using a FLUOROLOG-3 spectrofluorometer (Horiba Jobin Yvon, Edison, NJ). The spectrometer was equipped with a 450 W xenon lamp and a cooled Hamamatsu R928 extended-red photomultiplier that was operated at 900 V in the photon-counting mode. The cuvette was thermostatically controlled in order to provide the required temperatures for the melt analysis.

2.3 Results and Discussion

2.3.1 Multichannel Illumination and System Optimization

The optical system was operated using epi-illumination (see Figure 2.1a) with beam shaping of the laser source to generate a collimated light output from the microscope objective for wide-field illumination to provide the simultaneous excitation of

fluorophores traversing through a series of channels contained within the objective's FoV. The channel dimensions of the fluidic network were 30 μm (width) x 20 μm (depth), with the depth selected to provide sufficient single molecule sampling efficiency (*SE*), which was determined by the depth of focus of the microscope objective used for collecting the fluorescence (1.4 μm for 40x objective; 6.6 μm for 10x objective; and 60.1 μm for the 5x objective), and the percentage of molecules traveling through the illumination zone, which in this case is near 100%. The 40x objective (NA = 0.75) was used for single fluorophore measurements due to its high collection efficiency in spite of its smaller depth of focus. Therefore, the *SE* for our system for single fluorophores was approximately 7% (100% x 1.4/20). However, we are not using a pinhole aperture in the secondary image plane of the relay objective, which will allow for a larger depth of focus for the optical system than that calculated above and as such, the *SE* determined above should be considered a minimum estimation only.

The 40x objective generated a FoV of 200 μm, which allowed imaging 5 microchannels with the current fluidic architecture. Changing the imaging objective to a lower magnification would allow for the processing of more fluidic channels (see Table 2.1). For example, the use of a 5x objective would provide the ability to image 30 channels with the channel architecture used herein due to its larger FoV. However, the cost for this higher throughput is reductions in the collection efficiency of the resulting fluorescence emission, which could potentially reduce single molecule sensitivity. Clearly, reductions in the channel width and pitch could significantly improve the number of channels we could image. For example, using a microfluidic chip with a 1 μm wide channel and a pitch of 1 μm, which can be fabricated using optical lithography, would permit the ability to image 100 such channels for a FoV of 200 μm.

Table 2.1 System throughput and SMD signal-to-noise ratios for different FoVs.

Total Magnification (Magnification/Numerical Aperture)	Effective Field of View (FoV)	Number of channels within the FoV (30 µm x 20 µm; 25 µm pitch)	Single Molecule SNR for λ-DNA stained with Syto-63	Theoretical Single Molecule Throughput
40x/0.75	200 µm	5	810	6.7×10^4
10x/0.5	800 µm	17	510	2.28×10^5
5x/0.25	1.6 mm	30	314	4.02×10^5

2.3.2 Detection of Single λ-DNA Molecules

Experiments were first carried out at different electric field strengths to establish the transport velocity that would yield optimal signal-to-noise ratio (SNR) for the single molecules, which in this case were λ-DNA molecules stained with Syto-63, since the molecular transit time should be approximately equal to the photobleaching time to provide the highest SNR.[38] Results from 10 different measurements were averaged and plotted versus the applied field strength, which generated an optimal field strength of ~80 V/cm (see Figure 2.2a). At this field strength, the linear velocity was 0.01 cm/s, which was based on the applied field strength and the electrophoretic mobility of λ-DNA loaded with Syto-63. At this linear velocity and FoV, the molecular transit time was estimated to be ~1.6 s. We note that the processing rate is directly related to the flow velocity for flow-based measurements and as such, higher field strengths would result in higher system throughput. Even at field strengths of 300 V/cm (0.037 cm/s), we were able to generate sufficient SNR to detect single λ-DNA molecules.

a

b
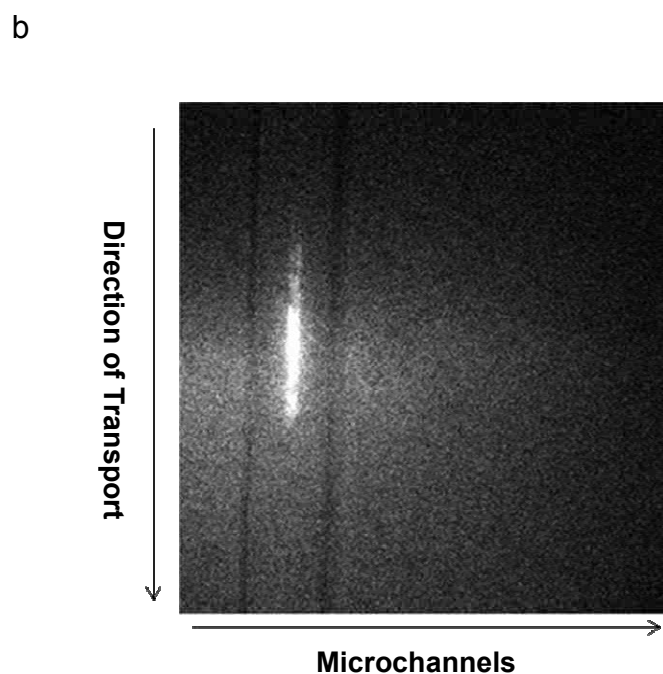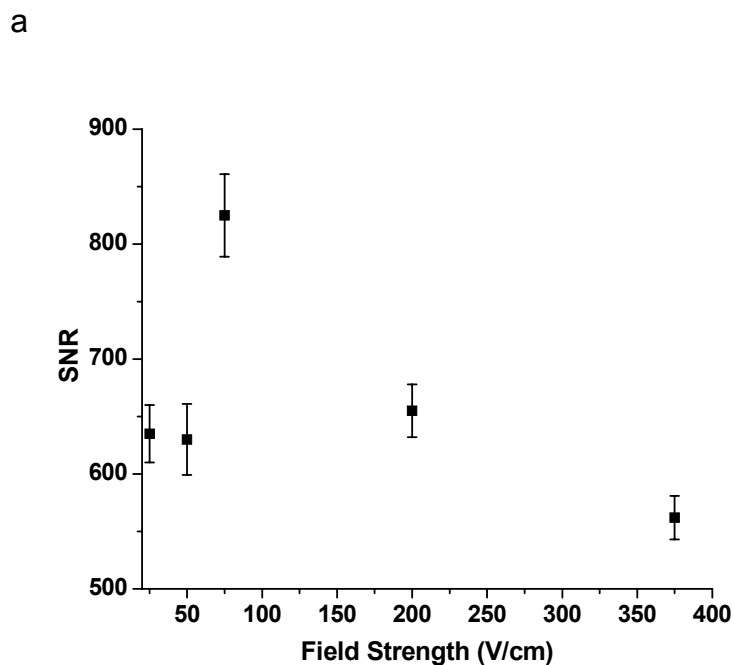
Figure 2.2 (a) Plot of the signal-to-noise ratio (SNR) at different field strengths used to transport single molecules through the irradiation zone of the imaging system. The SNR values were obtained from an average of 10 different measurements. (b) Fluorescence image from the CCD for a single molecule tracked along several pixels of the CCD, which was accumulated from two image frames that were acquired using 100 ms exposure time per frame with the fluorescence collected using a 40x objective (NA = 0.75).

To demonstrate the ability to track single dsDNA molecules traveling electrokinetically through the irradiation zone, experiments were carried out using single and multiple microchannels. Figure 2.2b shows a fluorescence image of a single DNA molecule tracked along the FoV of the imaging system by accumulating two image frames acquired using a 100 ms exposure time per frame. From the length of the streak (~60 μm) and the image accumulation time (2 frames at 100 ms per frame), we estimated the linear velocity to be 0.03 cm/s, very close to that determined above at a field strength of 300 V/cm.

To evaluate the sample throughput (*ST*) capabilities of the system, a 100 pM solution of λ-DNA was electrokinetically driven through the system at a field strength of 300 V/cm and the fluorescence image was collected using the 10x objective (NA = 0.5); the FoV of the system was 800 μm, which allowed imaging 17 channels. With the system operated in a frame transfer mode, the SMD sensitivity was improved by using 3x binning (3 x 3) with the multiplication gain of the EMCCD set at 3,700. Figure 3a shows one image frame from a series of images acquired for single λ-DNA molecules stained with Syto-63 traveling through the illumination zone. Each fluorescent streak represents an individual DNA molecule migrating through the chip due to the low probability of double occupancy per imaging pixel at this DNA concentration. The intensity distribution of this image was constructed by transforming the image in Figure 3a to a 3-D image (see Figure 2.3b).

To further demonstrate the ability to increase the throughput of the multi-channel fluidic device, a 5x objective (NA = 0.25) was incorporated into the imaging system and the same sample concentration of λ-DNA as that use above (100 pM) was analyzed. Figure 2.3c presents a single image frame showing photon bursts from single λ-DNA

a

Direction of Transport

Microchannels

b

Relative Intensity

400000
300000
200000
100000

1   50   100   150   200   250   300

Pixel Number (microchannels)
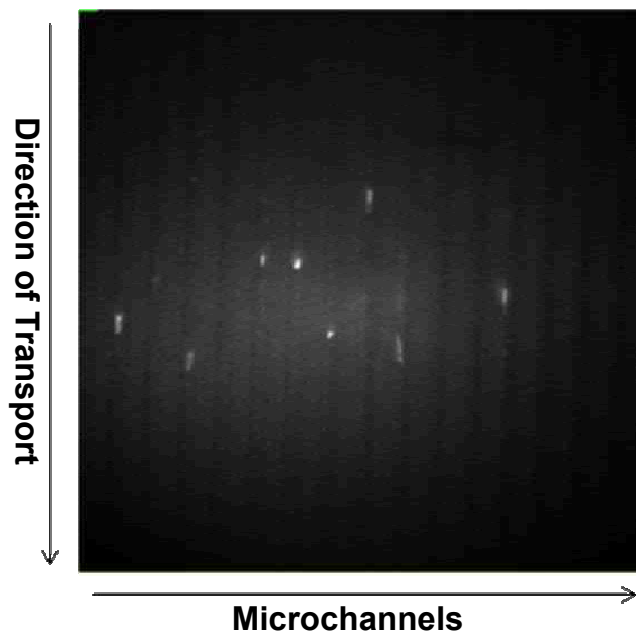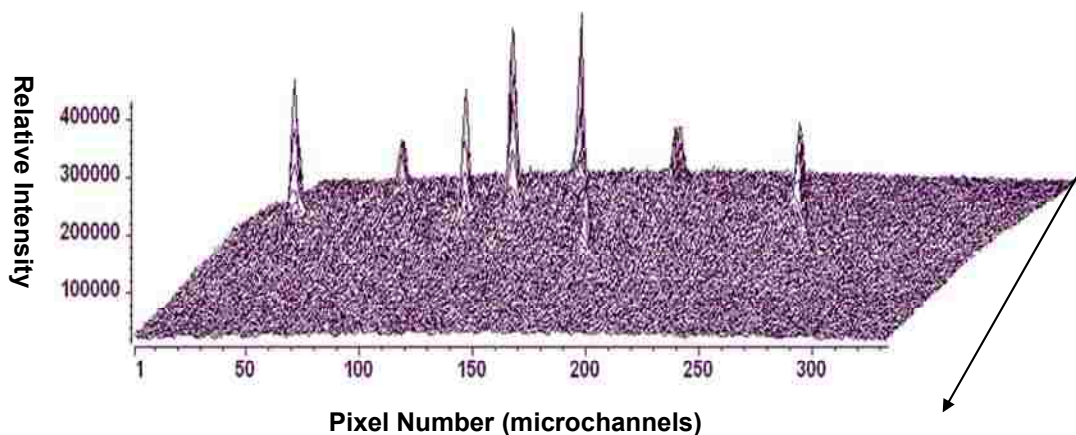
Figure 2.3 (a) Image of single λ-DNA molecules migrating through a series of microchannels (17-channels are shown). The image was acquired using a 10x (NA = 0.5) objective at an exposure time of 100 ms with the CCD multiplication gain set at 3,700 (controller gain set at 1). The sample solution (100 pM) was electrokinetically pumped through the fluidic channels with a field strength of 300 V/cm (linear velocity = 0.037 cm/s). Each fluorescent spot represents a single λ-DNA molecule. (b) 3-D image showing the intensity distribution of λ-DNA molecules shown in (a). (c) Single λ-DNA molecules migrating through series of 25 microchannels. Image was acquired using a 5x objective (NA=0.25). In all cases, the λ-DNA was stained with Syto-63 at a dye to base pair ratio of 5 to 1. Continued on next page

c
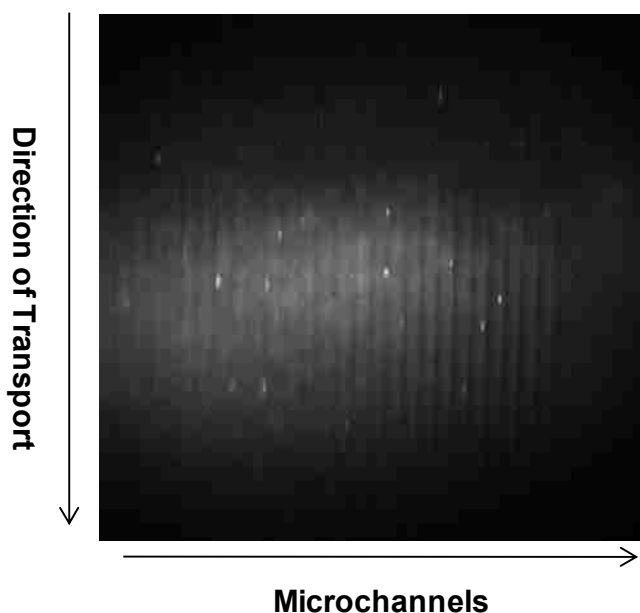
Figure 2.3 (C) see caption above.

molecules in 25 different microchannels. This objective generated a FoV of 1.6 mm, which allowed imaging 30 channels using our present fluidic architecture, but only 25 are shown in Figure 3c. Therefore, the single molecule processing throughput was increased by a factor of 6 compared to the 40X objective due to the higher FoV afforded by the lower power objective.

For flow-based single molecule detection experiments in which the single molecule events are dynamically transported through a fixed interrogation (sampling) zone, the sample throughput (*ST*) can be calculated from;[33]

$$ST = SE \times DE \times DR \times DC \qquad (2.3)$$

where *SE* represents the percentage of molecules that are sampled during the experimental run (1.0 for the 5x objective), *DR* is the delivery rate of molecules into the sampling volume, *DC* is the readout duty cycle (1.0) and *DE* is the detection efficiency. The *DR* can be calculated using;

$$DR = F_v \times C_b \qquad\qquad (2.4)$$

where F_v represents the volume flow rate (cm^3 s^{-1}) and C_b is the molecular concentration (molecules cm^{-3}). *DE* is basically the percentage of molecules detected above a threshold value, which is selected to minimize the number of false positive events registered during the experiment. For the present experiments, using a field strength of 300 V/cm and 100 pM concentration, the *DR* was determined to be 1.34 x 10^4 molecules s^{-1}. For *DE* = 1 and *SE* = 1.0, a *ST* of λ-DNA was estimated to be 13,400 molecules/s in each microchannel with a total system throughput of 4.02 x 10^5 molecules/s in the 30 channel network.

As noted above, scaling down the microchannel width and pitch can be used to further increase the *ST* of the present system. For example, reducing the channel width to 3 μm with a pitch of 3 μm and using the 10X objective to produce a reasonable collection efficiency (NA = 0.5), will increase the number of channels that can be imaged to 133 with a corresponding *ST* of 1.78 x 10^6. A further reduction in channel width to 1 μm with an inter-channel spacing of ~400 nm (diffraction limited resolution is ~λ/2) will allow the system to image 571 microchannels using the 10x objective increasing *ST* to 7.65 x 10^6 molecules/s. While this represents a significant increase in ST over our previous work [33], it also indicates exceptional increase in ST over previous research reports.[34, 39-46] For example, Van Orden *et al.* reported a ST of 2000 DNA fragments s^{-1} using a CCD operated in a snap-shot mode ,[34] while Ma *et al.* reported an ST of ~ 8500 molecules s^{-1} from their single molecule spectroscopy studies.[43] Recently, Chansin *et al.* speculated a throughput of ~1500 molecules s^{-1} using their synthetic nanopores to measure DNA translocation events.[46]

2.3.3 Detection of Single DNA/Fluorophore Conjugates

For these experiments, we utilized the 40x (NA = 0.75) objective and the optimized field strength (80 V/cm) for producing a high single molecule SNR to enhance sensitivity for the detection of single fluorophore molecules that were conjugated to ssDNAs. Solutions of ssDNAs labeled with AlexaFluor 660 were prepared in 1x TTE buffer and diluted to 750 pM in the same buffer. The samples were electrokinetically pumped through the microfluidic network and an exposure time of 100 ms was selected for the CCD per image frame when operated in FTM. With the 40x microscope objective, the laser excitation volume was calculated to be 0.12 nL, which in this case is not the sample probe volume due to the fact that the irradiation area was sub-divided into smaller elements defined by the pixels comprising the EMCCD camera. The probe volume was actually calculated from the size of each individual pixel of the EMCCD (8 μm x 8 μm) and the total magnification of the optical system (40x), producing a probe volume of 0.8 fL. Based on this probe volume size and the concentration used for these experiments (750 pM), the single molecule occupancy was 0.3 and the double occupancy probability was 0.09. Figure 2.4a shows a fluorescence image of individual ssDNA molecules end-labeled with AlexaFluor 660 migrating through the fluidic device. From this image, single molecule streaks were not observed as was seen in Figure 2.2b. This was a result of the binning operation performed on the image (3 x 3 bin), the relatively small linear velocity used and the data image shown in Figure 2.4a taken from a single frame. To enhance spot visualization of the single molecules, we acquired 10 images of the blank (1x TTE buffer) from which the standard deviation was calculated, which was found to be 42 units for an average background of 2,019 CCD units per pixel; a threshold value was selected as 3-times the standard deviation above the average

background (2,145), which was subtracted from a sample sub-frame (25 x 42 pixels) as indicated in Figure 2.4a. This also reduced false positive signals resulting from statistical variations in the background. Application of this threshold condition generated the sub-frame image shown in Figure 2.4a. This sub-frame represents approximately a 5 µm (wide) x 8.4 µm (length) area within a single microchannel. From this image, fluorescence from single molecules were clearly visible, which could be individually counted to extract quantitative information. This same operation was applied to an image acquired when there was only buffer in the microfluidic network with this image shown in Figure 2.4b. As can be seen from this image, there was no fluorescence registered as that observed in Figure 2.4a.
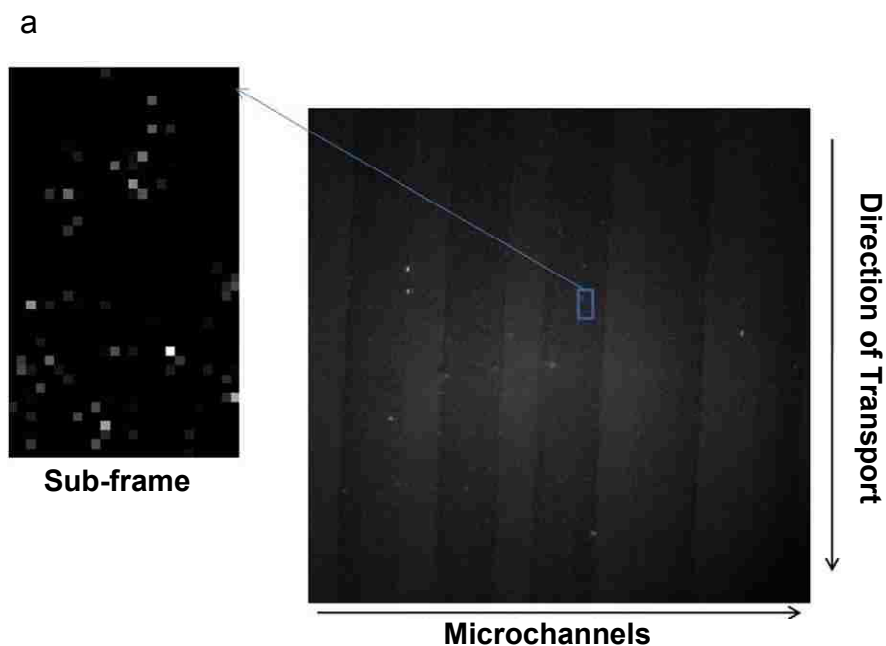
Figure 2.4 (a) Detection of individual dye molecules (AlexaFluor 660) end-labeled to a 60 base ssDNA distributed in different microfluidic channels (5 channels are shown) for a sample concentration of 750 pM. The dye/ssDNA conjugate was pumped through the fluidic channels using a field strength of 80 V/cm (linear velocity = 0.01 cm/s). To further visualize the fluorescent photon bursts in this image, a sub-frame (25 x 42 pixels) was expanded and quantitative information extracted by applying a threshold condition to this sub-frame (see text for details). (b) Image acquired when the fluidic channels were filled with buffer only, and the processed sub-frame with application of the threshold condition as described in the text. Continued on next page

b

Sub-frame

Direction of Transport

Microchannels
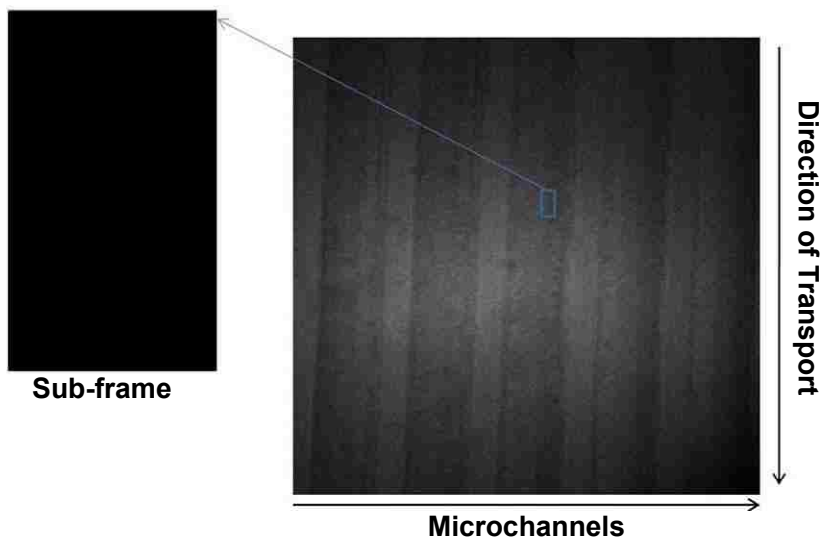
Figure 2.4(b) see caption above.

From careful inspection of the sub-frame image shown in Figure 2.4a, we were able to count 64 photon bursts generated from single ssDNA-AlexaFluor 660 conjugates. From the size of the image taken (5 x 8.4 x 1.4 μm^3, P_v) and the concentration of the conjugates used herein (750 pM, C_b), we could calculate the number of expected events (N_{ev}) from;

$$N_{ev} = C_b \, P_v \quad (2.5)$$

Insertion of the appropriate numbers into eq. 2.5 yielded a value of 26, which is somewhat smaller than the 64 events observed in the image sub-frame shown in Figure 2.4a. This can be reconciled considering that the probing volume was determined by the depth of focus of the microscope objective used here. Because there is no pinhole (confocal geometry) located in the secondary image plane of the objective, we are processing molecules outside of the 1.4 μm depth of focus of this 40x objective, making the observed event number higher than that calculated using eq. 2.5.

Different concentrations of ssDNA-AlexaFlour 660 conjugates were next evaluated using our multi-channel single molecule detector system and processed with the same threshold value as noted above. An average of eight images per dye concentration was plotted with the calibration plot constructed from the number of photon burst events versus the conjugate concentration. This analysis was performed on a sub-frame image with a size of 25 x 42 CCD pixels. The number of spots (single molecule events) observed was linear with the sample concentration yielding a correlation factor of 0.98 (data not shown).

2.3.4 Fluorescence Quenching Assay

We were next interested in evaluating the capability of our imaging system to monitor biochemical reactions using fluorescent probes to signal the extent of the reaction. We employed a model test case using an oligonucleotide duplex (15 bp) with one strand (sense strand) labeled with AlexaFluor 660 at its 5' end and the complementary strand (anti-sense strand) labeled with the Black Hole Quencher-3 (BHQ-3) at its 3' end to create sufficient proximity for resonance energy transfer quenching of the fluorescence from AlexaFluor 660 for the duplexed form of this construct (see Figure 2.5a). Melting of the duplex could be affected by introducing thermal energy into the system, producing ssDNAs that would result in the generation of fluorescence from the sense strand. Therefore, a melt analysis for this oligonucleotide could be generated by plotting the number of single molecule events observed from the sense strand versus the temperature.

For these experiments, the duplexed samples (750 pM) were prepared in Tris/HCl buffer containing 20 mM Tris-HCl, 10 mM $MgCl_2$ and 10 mM KCl at pH 7.5.

84

The microfluidic device was equipped with a strip heater, which was placed 200 µm upstream from the imaging area. The duplexes were electrokinetically driven through the fluidic device at the desired temperature using an 80 V/cm field strength. When operated at room temperature, there was no fluorescence signal registered on the detector. The absence of fluorescence photon bursts in the EMCCD image clearly indicated that the reporter dye was sufficiently quenched by BHQ-3 and no single stranded constructs could be seen (data not shown). This is in agreement with previous studies using this fluorophore-quencher pair with a reported 96% quenching efficiency.[47]

a

3'-CGCTTTTTAAAAAGC-5'-AF 660
5'-GCGAAAAATTTTTCG-3'-BHQ-3

Heat (67°C)

No Heat

3'-CGCTTTTTAAAAAGC-5'-AF 660

Fluorescence

3'-CGCTTTTTAAAAAGC-5'-AF 660
5'-GCGAAAAATTTTTCG-3'-BHQ-3

No Fluorescence

5'-GCGAAAAATTTTTCG-3'-BHQ-3

Figure 2.5 (a) Fluorescence single molecule quenching assay for determining duplex T_m using a 15-base pair oligonucleotide labeled with AlexaFluor 660 on its 5' end and its complement labeled with the Black Hole Quencher-3 (BHQ-3) on its 3' end. (b) Fluorescence single molecule image of the 15-bp oligonucleotide when the sample was heated to 67°C. Fluorescence from single DNA/AlexaFluor 660 molecules were visible as shown in this image due to duplex melting, producing ssDNAs. Also shown is the sub-frame of this image (37 x 67 pixels) that was processed as described in Figure 4. (c) Plot of number of single molecule events counted over a fixed interval of time at different sample temperatures (rectangles, concentration = 750 pM). Also shown is a plot of the normalized fluorescence intensity of the duplexed DNA at different temperatures using a bulk measurement (dsDNA concentration = 40 nM, circles; and 1 nM, triangles) measured using a conventional fluorometer (λ_{ex} = 675 nm). Continued on next page

b

Sub-frame   **Microchannels**

c

Figure 2.5 (b and c) See caption above.

To generate ssDNA in the flowing sample, the strip heater was then turned on

with the temperature set to 67°C. Figure 2.5b shows a single molecule fluorescence

image of photon bursts generated from the ssDNA constructs when imaged at this

temperature. To clearly visualize these spots and extract quantitative information by counting the single molecule events, the threshold condition was applied as discussed earlier. A sub-frame (37 x 67 pixels) was selected and processed (see Figure 2.5b). The presence of fluorescent photon bursts in the 67°C image versus that taken at room temperature is expected; the thermal energy introduced into the system produced a sufficient population of ssDNAs due to thermal denaturation of the duplexed DNA and thus, the energy transfer interaction between the two labels is eliminated because of proximity considerations.

A melt analysis was then conducted on the oligonucleotide duplex by taking images of single molecules traversing through the interrogation zone at different temperatures and counting the number of events (i.e., ssDNAs) at each temperature investigated. This analysis generated a sigmoidally-shaped plot (see Figure 2.5c) with a sharp rise in the number of single molecule events between 30°C and 50°C with a midpoint at ~40°C. This midpoint represents the melting temperature (T_m) of the duplex, which is defined as the temperature in which 50% of the DNA is in its double-stranded form and 50% in its single-stranded form. This value agrees favorably with that obtained from a theoretical prediction (T_m = 41.7°C) using oligonucleotide analysis software.[48, 49] The melting temperature of the duplex was also estimated by measuring fluorescence from a bulk sample of the duplex (1 nM) as a function of temperature using a standard fluorometer (λ_{ex} = 675 nm). Figure 2.5c shows the resulting plot of fluorescence intensity obtained at various temperatures, which generated a T_m value of 43°C. The slight deviation of this value (43°C) compared to the single molecule result could be attributed to the slightly higher concentration of the duplex used in the bulk solution since the inter-strand duplex T_m depends on concentration.[48] This supposition was further

supported by the experimental T_m (50^oC) obtained for a 40 nM solution of this same duplex (see Figure 2.5c).

As an example of the necessity for high throughput processing required to perform this measurement, we were able to reduced the processing time by a factor directly related to the number of channels imaged during the single molecule measurement, which in this case yielded a 5-fold reduction in processing time compared to a single point SMD flow-based scenario. Implementation of a smaller microchannel width and pitch producing a higher packing density of channels would significantly increase the data processing rate. For 1 µm wide channels and a pitch of 400 nm, the number of channels that could be effectively imaged using a 200 µm FoV would be 143 channels, reducing the processing time by 143-fold.

2.4 Conclusion

We have demonstrated the ability to detect single molecules using a frame transfer EMCCD in a high throughput format using a series of microchannels packed into the FoV of our imaging system. The system was configured in an epi-illumination format with beam shaping optics to generate a collimated output adequate for wide field illumination and providing adequate irradiance and SNR to observe photon bursts from single fluorophore molecules. The present design allowed imaging 30 microchannels when λ-DNAs were stained with an intercalating dye. This represents a 12-fold increase in the sample throughput (4.02 x 10^5 molecules/s) over our previous work, which employed a CCD operated in a time-delayed integration mode.[33] The reported optical system also provided, for the first time, single fluorophore sensitivity for a multi-channel flow-based single molecule experiment as demonstrated by the photon burst detection of ssDNAs end-labeled with AlexaFluor 660. However, in this case, a 40X objective with

its high NA was required to collect sufficient numbers of fluorescent photons to produce adequate SNR for detection of these single fluorophore molecules. This resulted in a decrease in the system sample processing throughput due to the reduced FoV (200 µm vs. 1,600 µm for a 5X objective), which permitted the simultaneous interrogation of 5 channels (40x objective) versus 30 channels (5x objective). However, reducing the microchannel width and pitch can significantly improve the sampling throughput for the 40x objective using optical lithography to produce a molding tool for micro-replicating high density fluidic networks in polymers, such as PMMA.

The results obtained from a fluorescence quenching assay associated with DNA duplex melting demonstrated the ability of our system to generate high throughput data processing appropriate for evaluating the fate of a biochemical reaction by monitoring population differences between reactants and/or products in a single molecule approach. The appealing aspect of the single molecule approach is the ability to use low concentrations of precious biological reactants and enzymes, the exquisite sensitivity associated with single molecule detection to record subtle changes in the reaction profile and the ability to monitor reactions efficiently in ultra-small volumes. This will be particularly attractive for high throughput screening applications, where the effects of elements from a large combinatorial library must be screened against a therapeutic target (*i.e.,* bioenzyme). Due to the large size of most combinatorial libraries ($>10^6$ elements), high throughput processing is critical.

2.5 References

(1)   Sklar, L. A.; Edwards, B. S.; Larson, R. S.; Prossnitz, E.; Andrejewski, B.; Bennett, T.; Buranda, T.; Chigaev, A.; Foutz, T.; Jackson, C.; Key, A.; Kuckuck, F.; Potter, R.; Ramirez, S.; Simons, P.; Young, S.; Lopez, G. *Clinic. Canc. Res.* **2001**, *7*, 3701S-3701S.

(2)   Ehret, R.; Baumann, W.; Brischwein, M.; Lehmann, M.; Henning, T.; Freund, I.; Drechsler, S.; Friedrich, U.; Hubert, M. L.; Motrescu, E.; Kob, A.; Palzer, H.; Grothe, H.; Wolf, B. *Fres. J. Anal. Chem.* **2001**, *369*, 30-35.

(3)   Aherne, G. W.; McDonald, E.; Workman, P. *Breast Canc. Res.* **2002**, *4*, 148-154.

(4)   Zheng, W.; Spencer, R. H.; Kiss, L. *Assay Drug Dev. Techn.* **2004**, 2, 543-552.

(5)   Posner, B. A. *Curr. Opin. Drug Disc. & Dev.* **2005**, *8*, 487-494.

(6)   Wesche, H.; Xiao, S. H.; Young, S. W. *Combin. Chem. & High Throughput Screen.* **2005**, *8*, 181-195.

(7)   Sundberg, S. A. *Curr. Opin. Biotechn.* **2000**, *11*, 47-53.

(8)   Oldenburg, K. R.; Zhang, J. H.; Chen, T. M.; Maffia, A.; Blom, K. F.; Combs, A. P.; Chung, T. D. Y. *J. Biomol. Screen.* **1998**, *3*, 55-62.

(9)   Huang, C. X.; Quesada, M. A.; Mathies, R. A *Anal. Chem.* **1992**, *64*, 967-972.

(10)   Lockhart D.J., Moerner, W. E. *Nature* **2000**, *405*, 827-836.

(11)   MacBeath, G.; Koehler, A. N.; Schreiber, S. L. *J. Am. Chem. Soc.* **1999**, *121*, 7967-7968.

(12)   MacBeath, G. *Gen. Biol.* **2001**, *2*, 2005.

(13)   MacBeath, G.; Schreiber, L. S. *Science* **2000**, *289*, 1760-1763.

(14)   West, J.; Becker, M.; Tombrink, S.; Manz, A. *Anal. Chem.* **2008**, *80*, 4403-4419.

(15)   Dittrich, S. P.; Tachikawa, K.; Manz, A. *Anal. Chem.* **2006**, *78*, 3887-3907.

(16)   Whitesides, M. G. *Nature* **2006**, *442*, 368-373.

(17)   Vilkner, T.; Janasek, D.; Manz, A. *Anal. Chem.* **2004**, *76*, 3373-3386.

(18)   Wabuyele, M. B.; Farquar, H.; Stryjewski, W.; Harmer, R. P.; Soper, S. A.; Cheng, Y. W.; Barany, F. *J. Am. Chem. Soc.* **2003**, *80*, 6937-6945.

(19)   Barkai, E.; Jung, Y.; Silbey, R. *Ann. Rev. Phys. Chem.* **2004**, *55*, 457-507.

(20)   Shera, E. B.; Seitzinger, N. K.; Davis, L. M.; Keller, R. A.; Soper, S. A. *Chem. Phys. Lett.* **1990**, *174*, 553-557.

(21)   Soper, S. A.; Mattingly, Q. L.; Vegunta, P. *Ana. Chem.* **1993**, *65*, 740-747.

(22) Moerner, W. E.; David P. *Rev. Sci. Instr.* **2003**, *74*, 3597-3619.

(23) Zander, C. *J. Anal. Chem.* **2000**, *366*, 745-751.

(24) Haab, B. B.; Mathies, R. A *Anal. Chem.* **1999**, *71*, 5137-5145.

(25) Byassee, T. A.; Chan, W. C.; Nie, S. *Anal. Chem.* **2000**, *72*, 5606-5611.

(26) Wabuyele, M. B.; Ford, S. M.; Stryjewski, W.; Barrow, J.; Soper, S. A. *Electrophoresis* **2001**, *22*, 3939-3948.

(27) Nie, S.; Chiu, D. T.; Zare, R. N. *Anal. Chem.* **1995**, *67*, 2849-2857.

(28) Sweedler, J. *Critic. Rev. Anal. Chem.* **1993**, *24*, 59-98.

(29) Bernard, O.; Coates, C. *Laser Focus World* **2005**, *41*, 133-134.

(30) Petty, R. H. *Microsc. Res. Techn.* **2007**, *70*, 687-709.

(31) Denvir, J. D.; Coates, G.; Collin, C. *Proc. SPIE* **2002**, *4626*, 502-512.

(32) O'Grady, A. *Proc. SPIE* **2006**, *6093*, 60930S.

(33) Emory, M. J.; Soper, S. A. *Anal. Chem.* **2008**, *80*, 3897 - 3903.

(34) Van Orden, A.; Keller, R. A.; Ambrose, P. W. *Anal. Chem.* **2000**, *72*, 37-41.

(35) Christenson, M. *Single Mol.* **2000**, *1*, 177-179.

(36) Hiller, W. J.; Kowalewski, T. A.; Tatarczyk, T. *Proc. SPIE* **1992**, *1801*, 595-601.

(37) Li, H.-W.; Yeung, E. S. *J. Photochem. Photobiol. A* **2004**, *172*, 73-79.

(38) Mathies, R. A.; Peck, K. *Biophysical J.l* **1990**, *57*, A189-A189.

(39) Castro, A.; Fairfeild, F. R.; Shera, E. B. *Anal. Chem.* **1993**, *65*, 849 - 852.

(40) Petty, J. T.; Johnson, M. E.; Goodwin, P. M.; Martin, J. C.; Jett, J. H.; Keller, R. A. *Anal. Chem.* **1995**, *67*, 1755-1761.

(41) Huang, Z. P.; Petty, J. T.; O'Quinn, B.; Longmire, J. L.; Brown, N. C.; Jett, J. H.; Keller, R. A. *Nucl. Acids Res.* **1996**, *24*, 4202-4209.

(42) Chou, H. P.; Spence, C.; Scherer, A.; Quake, S. *Proc. Natl. Acad. Sci.* **1999**, *96*, 11-13.

(43) Ma, Y. F.; Shortreed, M. R.; Yeung, E. S. *Anal. Chem.* **2000**, *72*, 4640-4645.

(44)   Anazawa, T.; Matsunaga, H.; Yeung, E. S. *Anal. Chem.* **2002**, *74*, 5033 - 5038.

(45)   Krogmeier, J. R.; Schaefer, I.; Seward, G.; Yantz G. R.; Larson, J. W. *Lab Chip* **2007**, *7*, 1767 - 1774.

(46)   Chansin, G. A. T.; Mulero, R.; Hong, J.; Kim, M. J.; Demello, A. J.; Edel, J. B. *Nano Lett.* **2007**, *7*, 2901-2906.

(47)   Marras, S. A. E.; Kramer, R. F.; Tyagi, S. *Nucl. Acids Res.* **2002**, *30*, e122.

(48)   Santa Lucia, J. *Proc. Natl. Acad. Sci.* **1998**, *95*, 1460-1465.

(49)   Owczarzy, R.; Behlke, M. *Mol. Gen. Biophys., Integrated DNA Techn.* **2005**, 1-4.

CHAPTER 3

CYCLIC OLEFIN COPOLYMER PLANAR WAVEGUIDE EMBEDDED IN A MULTI-CHANNEL POLY (METHYL METHACRYLATE) FLUIDIC CHIP FOR EVANESCENCE EXCITATION

3.1 Introduction

Lab-on-a-chip (LOC) systems offer a number of compelling advantages compared to conventional bench-top systems, including the ability to process large amounts of chemical/biochemical information due to the ability to build chips in a highly parallel fashion.[1-6] A major challenge associated with these miniaturized systems is the associated reduced sample and reagent volume requirements, which place a high demand on the detection system to provide the required sensitivity for interrogating a few molecules present in the resulting detection volume. Whilst several detection methods exist for microfluidic systems,[7,8] laser-induced fluorescence (LIF) has been widely adopted due to the high sensitivity, selectivity and extremely low limits-of-detection obtainable.[9,10]

Classical optical configurations for LIF are often based on epi-illumination or trans-illumination formats,[11,12] in which both excitation and fluorescence light propagate in the same optical path with spectral sorting accomplished using dichroic filters. Another optical configuration, which has found applications in LIF detection, is total internal reflection (TIR) fluorescence,[13-15] in which fluorescent samples are excited using a surface-confined excitation field. Several reports have documented the use of TIR optics which use prisms,[16-18] microscope objectives,[19,20] and optical fibers.[21,22] In all cases, fluorescence excitation utilized the evanescent field generated by TIR at a high refractive index to a low refractive index boundary.

The penetration depth of the evanescent field is usually fairly small (<750 nm) with the absolute value dependent upon the excitation wavelength, the refractive indices of the waveguiding material and substrate and the launch angle of the incident light. The intensity of the evanescent field, which is proportional to the square of the electric field amplitude,[23] normally drops off exponentially into the lower index medium, thus enabling the realization of small excitation volumes.

A common class of materials used for TIR fluorescence is optical waveguides,[24,25] which offer a number of advantages, such as the realization of compact sensing elements suitable for LOC applications and the potential for fabricating multiple sensors on a single chip.[26] Planar waveguides for biosensing applications have been made using a variety of materials such as metal films,[27] metal oxide films,[28] photonic crystals,[29,30] and silicon oxynitride.[31] While glass remains the most commonly used material for waveguide applications,[15,32] its incorporation into other sample processing units required for LOC sensing is a challenge due to its limited and sometimes costly fabrication modalities. As a result, polymer-based waveguides[33,34] have attracted much interest in many LOC applications because of their simple fabrication characteristics and in some cases, their favorable optical properties.[35] Also, the ease of integrating these materials into instruments suitable for point of care (POC) applications is of great value.

Several polymer materials have been employed for waveguiding, including poly(dimethylsiloxane), PDMS,[36,37] SU-8,[26,38-40] and poly(methyl methacrylate), PMMA.[41] As an example, Xu *et al.*[41] recently demonstrated the use of a PMMA-based air-embedded planar waveguide for reading DNA microarrays. This waveguide was fabricated in a single step using double-sided hot embossing from metal mold masters.

Another polymeric material, which holds great promise as a waveguide material, is cyclic olefin copolymer (COC). This class of polymers has properties that can be tailored within a wide range of characteristics during polymerization.[42] COC is a copolymer of ethylene and norbornene produced via a metallocene catalyst-mediated polymerization with glass transition temperatures (T_g) that range from 75°C to 180°C and depends on the amount of norbornene in the copolymer. COC possesses high optical transparency, excellent electric properties, high rigidity, excellent biocompatibility, very good resistance to acids and alkalis and good thermal properties.[42,43] Several works have reported on the microfabrication of COC substrates,[44-49] which have created avenues for expanding the utility of this polymer especially as a waveguide material due to its exquisite optical properties.[50]

Although much progress has been made toward integrating waveguides to microfluidic systems,[14,51-53] effective propagation of light through a single planar waveguide for evanescent excitation in multiple fluidic channels suitable for high throughput biochemical analysis has not been reported. In this Chapter, we present for the first time the fabrication of a COC waveguide that was embedded in a PMMA substrate serving as a cover plate for a PMMA substrate that contained a series of fluidic vias. The COC waveguide was situated orthogonal to the microfluidic channels to provide parallel evanescent excitation of the material moving through the fluidic vias. The fluidic channels were hot embossed from a metal master on a 250 μm thick PMMA sheet, which was thermally fusion bonded to the PMMA cover plate containing the embedded COC waveguide. To carefully control the laser launch angle into the waveguide to near the critical angle, which is defined by the refractive index of COC (n = 1.53) and PMMA (n = 1.48), a monolithic prism was integrated to the COC waveguide

in a single fabrication step, eliminating the need for an external prism and index matching oil. In another design, laser light was coupled to the embedded waveguide through an optical fiber (N.A. = 0.12), which minimized light loss due to scattering.

3.2 Experimental

3.2.1 Materials and Reagents

COC sheets (grade: 5010L; T_g = 110°C; n = 1.53) were obtained from Topas (Topas Advanced Polymer, USA); the molecular structure of Topas COC is shown in Figure 3.1a with the monomer units represented as x and y. Toluene was obtained from Fisher Scientific (Fisher Chemicals, USA) and used as supplied to make a polymer solution of COC. The COC solution was obtained by dissolving pieces of COC in toluene, which made a clear solution of the polymer in 24 h. A PDMS base and curing agents were obtained from Dow Corning (Dow Corning Corporation, Midland, USA.). Optical fibers (NA = 0.12) were obtained from Thorlabs (Thorlabs, Newton, NJ, USA) with the blunt bare fiber end created using a fiber optic cutting tool (Precision Tool kit, 698-STK-100). AlexaFluor 647 was obtained from Molecular Probes (Eugene, Oregon, USA) with the stock and sample solutions made in 1X Tris-Taps-EDTA (TTE) buffer (pH = 8.7).

3.2.2 Image Acquisition

All fluorescence images were acquired using a Roper Scientific (Trenton, NJ) Spec-10 charge-coupled device (CCD) camera that was thermally cooled to -90°C and contain a 1 MHz digital converter. The CCD had 20 μm pixel sizes that were configured in a 1340 x 100 back-illuminated format. Scanning electron micrograph (SEMs) images were acquired using a Cambridge S-260 SEM (Cambridge instruments Ltd. Cambridge, UK) interfaced with Video Wave 5 program (Real Networks Inc. Washington, USA).

Atomic force microscopy (AFM) images were acquired using a Nanoscope III instrument (Digital Instruments, CA).
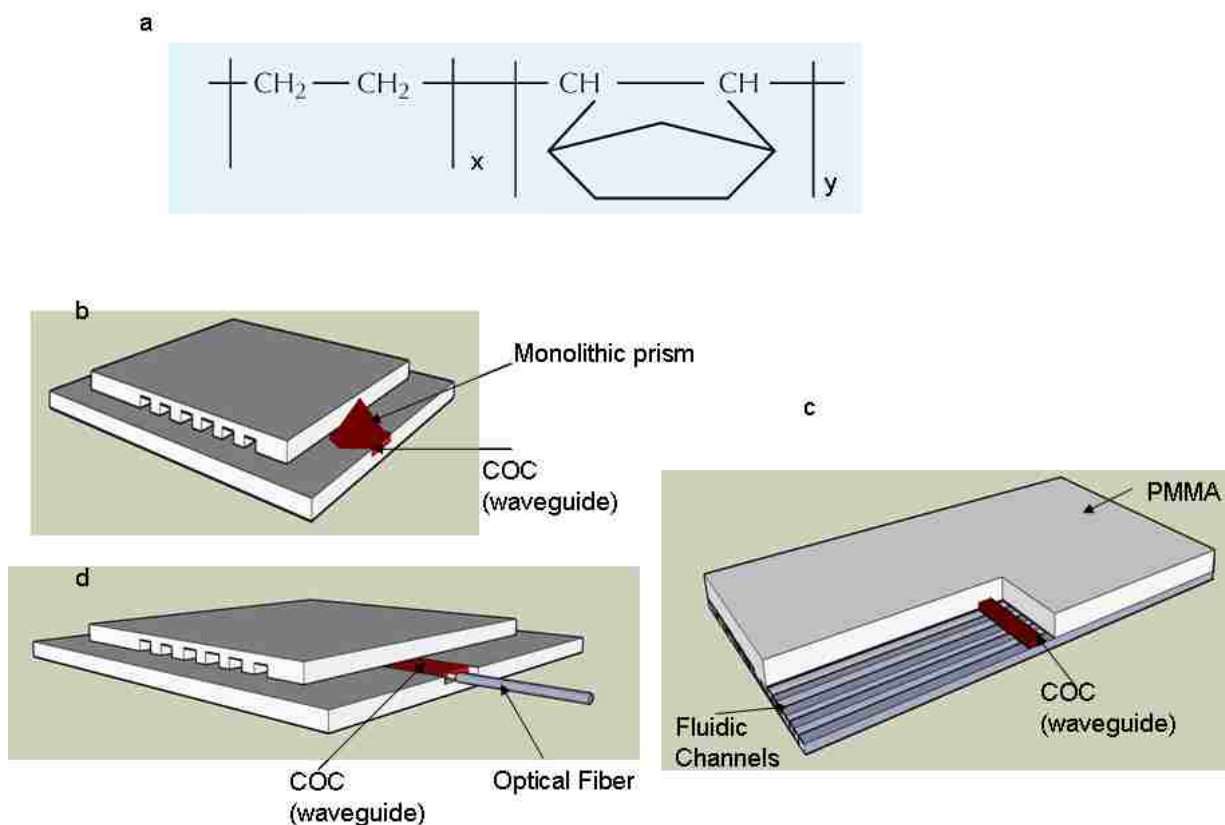
Figure 3.1 (a) Molecular structure of Topas COC, x and y represent the monomer units, which are polymerized by metallocene catalyzed polymerization; the T_g can be modified by increasing or decreasing the amount of norbornene (y) in the monomer mixture during polymerization. (b) Schematic representation of the fluidic device with embedded COC core waveguide fabricated with a monolithic prism. (c) Schematic of a dissected portion of the device showing the multi-channel fluidic architecture and waveguide geometry. (d) Diagram showing the launching of laser light into the waveguide using an optical fiber.

3.2.3 Layout of the Integrated System

Figure 3.1b shows a schematic diagram of the multi-channel fluidic device with an embedded COC core waveguide and monolithic prism. The device consisted of two

layers; a PMMA cover plate (refractive index, n, = 1.48, T_g = 107°C) into which the COC

core waveguide (refractive index, n = 1.53) was embedded and a PMMA substrate,

which contained the fluidic channels that were replicated/embossed from a metal mold

master (see Figure 3.1c). The waveguide was situated orthogonal to the longitudinal

axis of the fluidic channels along the width of the PMMA cover plate, the size of which

defined the excitation volume in each fluidic channel along with the penetration depth of

the evanescent field. The monolithic prism (see Figure 3.1b) facilitated coupling of light

into the waveguide without the need for an external prism or index matching oil. Figure

3.1d is a schematic of the optical fiber coupled COC core waveguide. The use of the

optical fiber in this design eliminated the need for a prism.

3.2.4 Fabrication of the Embedded Waveguide

The stepwise fabrication process for creating the embedded COC core

orthogonal planar waveguide and monolithic prism is shown in Figure 3.2a. The first

step involved the generation of a PDMS stencil, which was used to form the waveguide

and coupling prism and was produced using a relief made from PMMA. The PMMA

relief consisted of a prism-shaped structure that was aligned to a 1 mm diameter pole

structure (height of structure = 2.0 mm) used to create an access reservoir. The PMMA

relief was replicated from a brass mold master fabricated by high precision micromilling

(using Kern MMP micromilling and drilling machine).[54,55] A PDMS pre-polymer solution

was obtained by mixing the PDMS base and the curing agent at a ratio of 10:1 by mass.

This solution was degassed and loaded through the injection port of a molding frame

containing the PMMA relief to completely fill the mold cavity. Curing of the PDMS pre-

polymer solution was achieved in 1.5 h using a vacuum oven set at 70°C. The resulting

PDMS stencil containing the prism-shaped recess and a 1 mm diameter reservoir (created by the 1 mm diameter pole) was peeled from the PMMA relief.

The PDMS stencil was then placed onto a sheet of PMMA containing a pre-fabricated waveguide channel (200 µm x 200 µm). The waveguide channel was replicated onto the sheet PMMA from a brass mold master that was fabricated by high precision micromilling. The prism-shaped recess on the PDMS stencil and the reservoir were carefully aligned with both ends of the waveguide channel under a microscope. A COC solution (melt) was then introduced into the waveguide channel through the reservoir to fill the channel and the prism-shaped recess. This assembly was placed on a dry glass plate and allowed to cure in a vacuum oven for 24 h at room temperature. Following curing of the COC, the PDMS stencil was carefully peeled from the PMMA sheet, which formed the embedded COC core waveguide and the monolithic coupling prism. Figure 3.2b shows an image of the embedded COC waveguide with monolithic prism.

3.2.5 Fabrication of the Optical-Fiber-Coupled (OFC) Waveguide

The OFC waveguide was fabricated following the procedure outlined in Figure 3.2a with slight modifications. In this case, the prism-shaped structure in the mold (see Figure 3.2a (i)) was replaced with a second pole (1 mm diameter and 2 mm tall), which allowed the generation of a PDMS stencil with two aligned reservoirs (each situated at both ends of the PDMS stencil). An optical fiber (OD = 125 µm, core diameter = 62 µm) was cleaned with acetone and inserted into the waveguide channel with the tip of the fiber situated 5 mm from the insertion end of the channel. The optical fiber was kept in place using the fabricated PDMS stencil, which was placed on the PMMA wafer with the

reservoirs aligned to the ends of the waveguide channel and subsequently clamped to a

glass plate. The COC melt was introduced into the waveguide channel through the

(a)
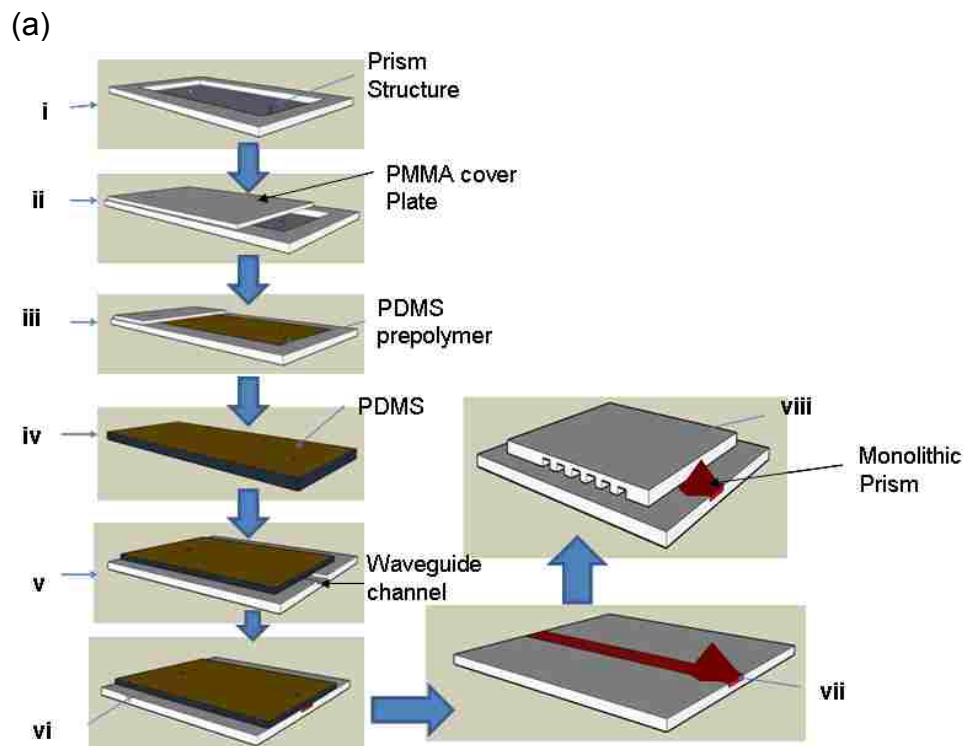
Figure 3.2 (a) Schematic representation of the stepwise process for the fabrication of the embedded COC core orthogonal waveguide. In the first step, the mold structures were fabricated in PMMA wafer via hot embossing from a mold master made using high precision micromilling (i). The mold was assembled for PDMS casting using a pre-aligned cover plate containing injection reservoirs (ii) for the introduction of the PDMS prepolymer (PDMS + Curing agent at 10:1 ratio) (iii).The PDMS stencil was peeled from the mold after curing at 70^oC for 90 min (iv) and placed on the surface of a PMMA sheet containing a pre-fabricated waveguide channel (waveguide channel was embossed from a mold master fabricated using high precision micromilling), the injection reservoir and prism recess for launching light into the waveguide were aligned with respect to the waveguide channel (v). The COC melt (prepared using toluene as a solvent) was introduced through the reservoir to fill the entire waveguide channel and the prism recess (vi). This created the embedded waveguide with the monolithic prism in a single casting step (vii). The waveguide assembly was further integrated to multiple fluidic channels (viii) that were prepared using hot embossing into PMMA. The fluidic substrate and PMMA sheet containing the waveguide, which served as the cover plate for the fluidic network, were thermally fusion bonded at approximately 105^oC, near the T_g of the polymeric materials. (b) Photographs of the PMMA sheet showing the embedded waveguide (i) with the integrated monolithic prism (to the right is the SEM of a section of the prism). (c) Photograph of the OFC waveguide (i) showing the fiber-coupling point (to the right is an optical micrograph of the coupling site) and the optical fiber (ii). Continued on the next page

(b)
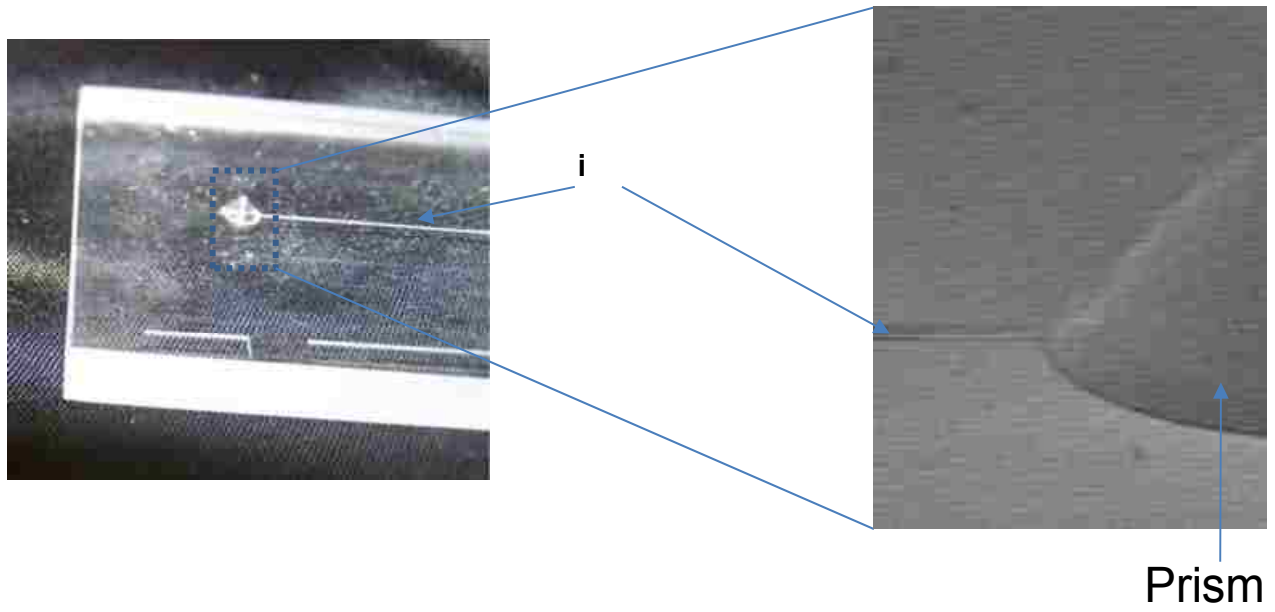
(c)
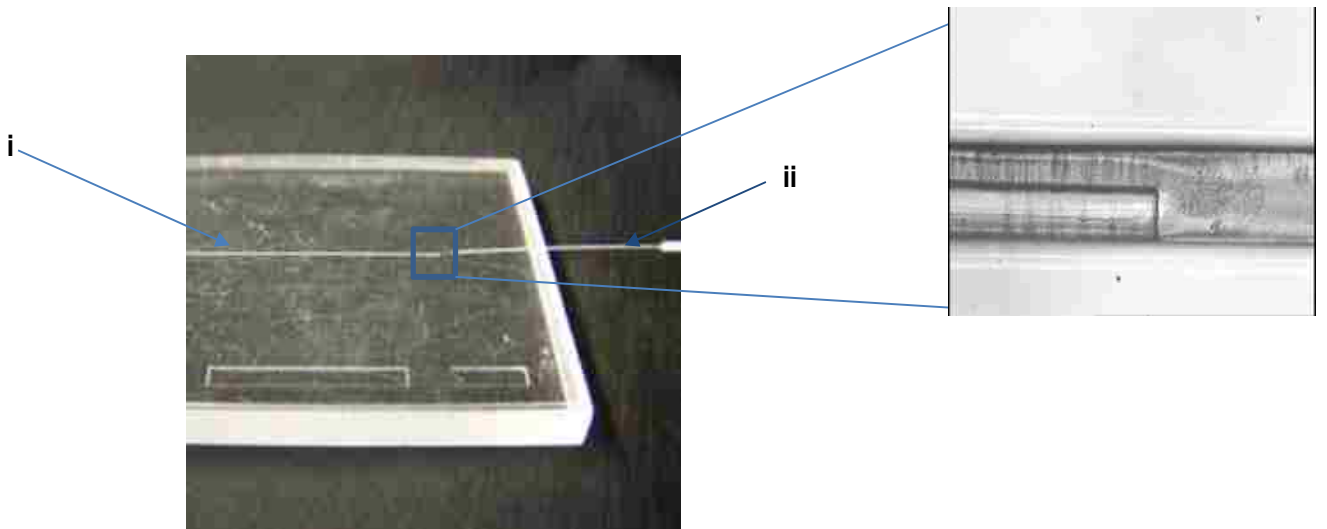
Figure 3.2 (b and c) see caption above

access reservoir to fill the waveguide-defining channel, which spanned a length of 3 cm.

This assembly was placed on a dry glass plate and allowed to cure in a vacuum oven

for 24 h. At the end of the curing period, the PDMS stencil was carefully peeled from the PMMA sheet to obtain the optical-fiber-coupled COC core embedded waveguide (see Figure 3.2c).

3.2.6 Integration of the Embedded Waveguide with the Multi-channel Substrate

The fluidic channels were replicated into a PMMA substrate (thickness = 250 µm) via hot embossing from a brass mold master, which was fabricated by high precision micromilling.[54,55] This PMMA wafer contained channels with dimensions of 100 µm width x 30 µm depth and was thermally fusion bonded to the waveguide-bearing PMMA sheet in an orthogonal configuration with the waveguide spanning the length of the entire array of fluidic channels. In this case, the PMMA sheet containing the embedded waveguide served as the cover plate for the fluidic network and also defined the illumination cross sectional area for each fluidic channel. Figure 3.3a shows an optical micrograph of the waveguide and the fluidic channel when thermally assembled.

3.2.7 Coupling of Light into the Waveguide

To minimize light lose at the entrance to the waveguide, a collimated laser beam was passed through a beam expander that was used in the reverse mode to reduce the beam diameter from 2 mm to ~200 µm. The resulting beam was launched through the monolithic prism into the waveguide with a launch angle adjusted to 76° (critical angle θ_c = 75°) using a goniometer. The critical angle here (θ_c = $\sin^{-1} 1.48/1.53$) was defined by the refractive indices of the PMMA cladding (n = 1.48) and the COC core (n = 1.53).

In the case of the OFC waveguide, the laser light was first coupled into an optical fiber, which was latter coupled into the OFC waveguide using a fiber-fiber coupler (see Figure 3.3b).

a
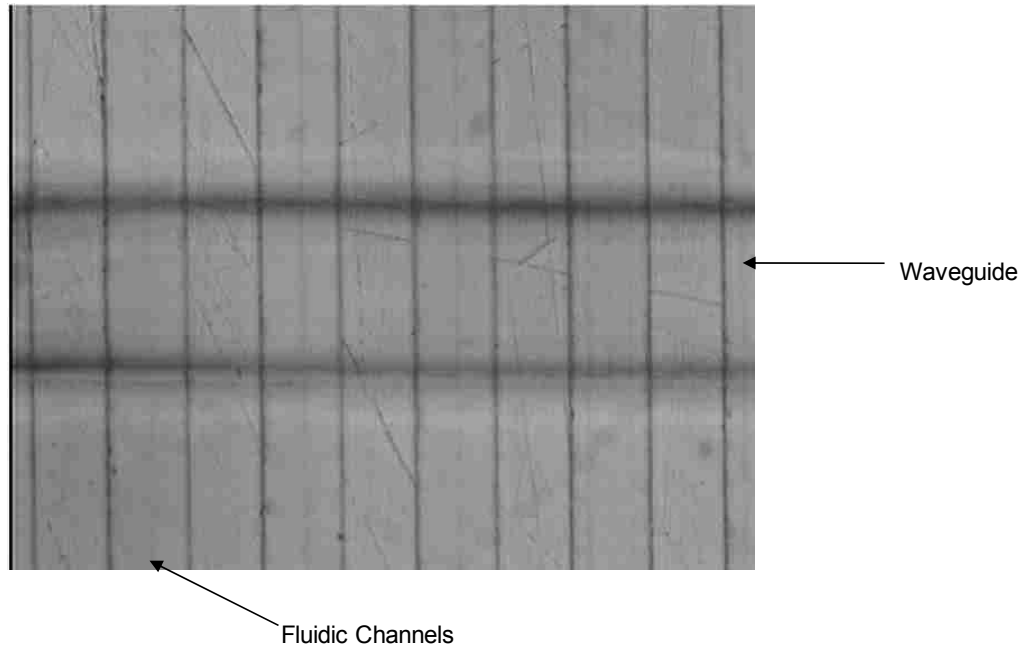
b
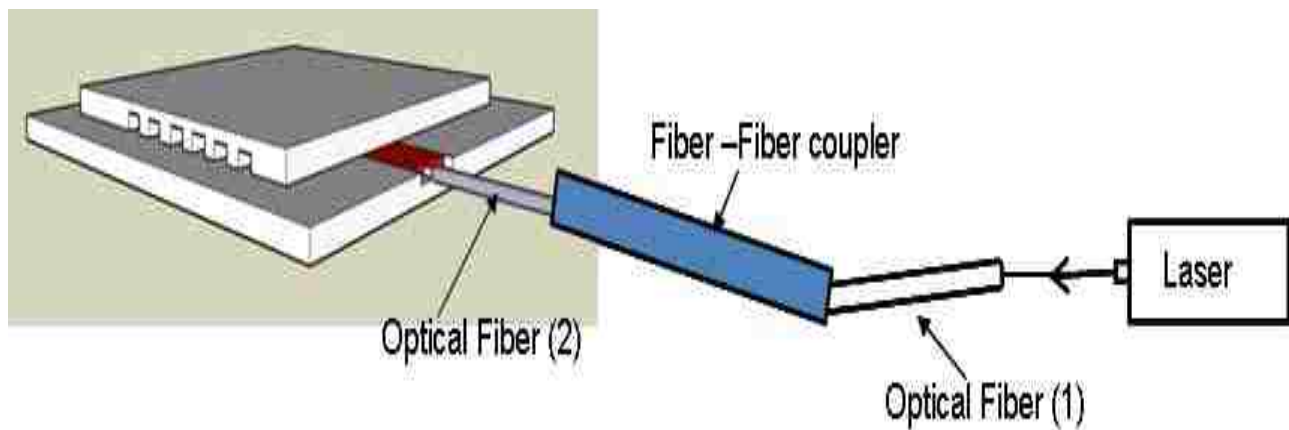
Figure 3.3 (a) Optical micrograph of the embedded waveguide integrated to the fluidic channels. (b) Schematic representation of laser coupling into the OFC waveguide. The light was first coupled into an optical fiber (labeled 1), followed by another coupling to the second optical fiber (labeled 2, which is the fiber coupled to the waveguide) using a fiber-fiber coupler, which send the input light to the waveguide. (c) The photograph shows the guiding of light (532 nm) through the length of the waveguide (i) when an optical fiber was used to couple light into the waveguide; and the scattering of the light when there was poor coupling between the optical fiber and waveguide (ii). Continued on the next page

c

i

Fiber to Waveguide
Coupling point

ii

Fiber to Waveguide
Coupling points

Air-space between
Fiber and Waveguide
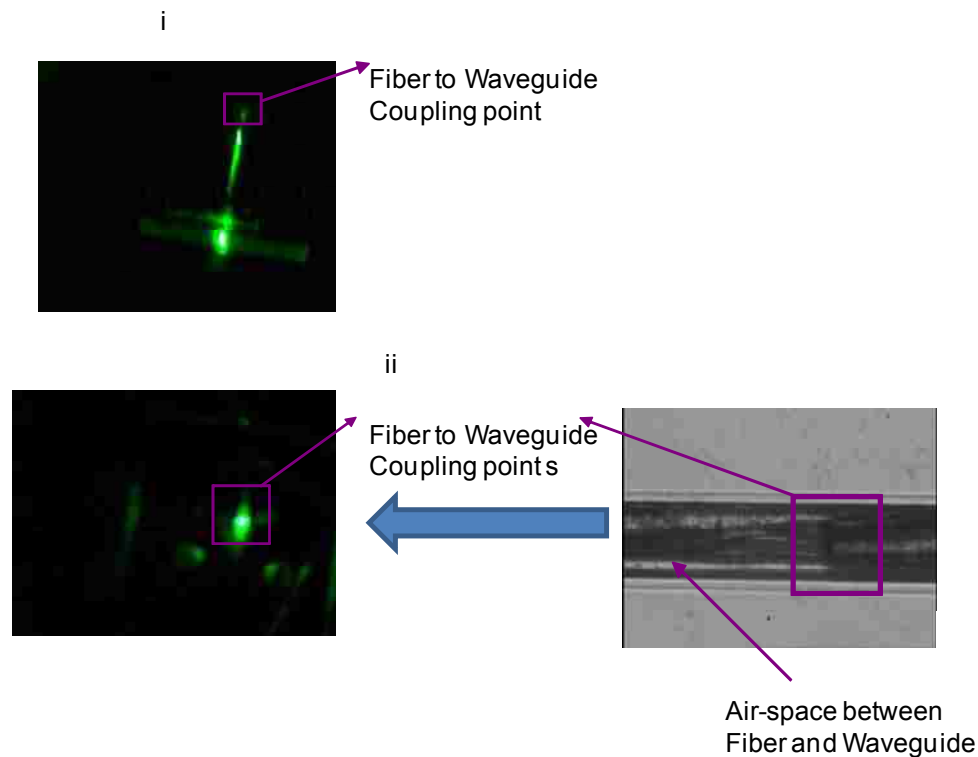
Figure 3.3 (c) See caption above

This generated continuous guiding of the light through the waveguide. To demonstrate the waveguiding capabilities of the OFC waveguide, a 532 nm laser (20 mW) was coupled into the optical fiber. In Figure 3.3c is shown a photograph of the OFC waveguide with the 532 nm laser coupled into it (i). The bottom panel of Figure 3.3c (ii) shows an optical micrograph of the waveguide with the optical fiber not properly coupled to the waveguide (air space between waveguide and optical fiber). The emerging bright laser spot in Figure 3.3c (top panel) is a clear indication of continuous light guiding through the waveguide, whereas the unguided laser (bottom panel) resulted in significant amounts of scattered light at the optical fiber tip, which indicated improper coupling to the waveguide.

3.3 Results and Discussion

3.3.1 Evaluation and Characterization of the Embedded COC Waveguide

To confirm that loading of the waveguide channel with the COC melt generated an optically homogeneous interface between the COC core and PMMA after curing of the COC, a scanning electron micrograph (SEM) of the empty waveguide channel and the COC filled channel were obtained (data not shown). In addition, we also inspected the COC core for inhomogeneity, for example resulting from air bubbles that may create speckle patterns in the waveguide due to refractive index changes. Close examination revealed a highly uniform interface between the COC/PMMA waveguide with no imperfections at the top of the COC core. These results were further supported by AFM images (see Figure 3.4) of the surface of the embedded waveguide. As can be seen in this image, the COC core surface was very smooth showing no evidence of large pits arising from air bubbles or other materials during its production, which could generate light propagation losses.

a   b

X = 20.00 µm/div
Y = 4104 nm/div

RMS = 61.248 nm
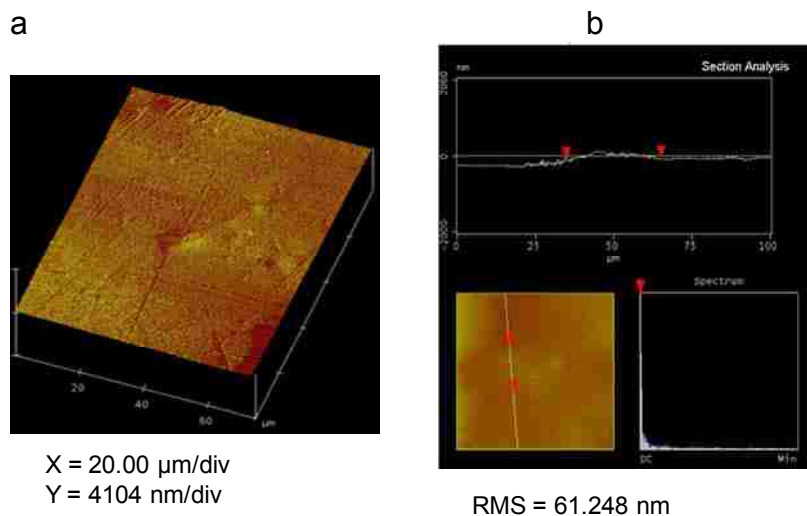
Figure 3.4 (a) AFM image of the surface of the cured COC planar polymer waveguide embedded in sheet PMMA; z-scale is 4104 nm/div., x-scale is 20 µm/div. (b) Section analysis of the waveguide surface, top panel shows the surface roughness with RMS = 61.284 nm.

a
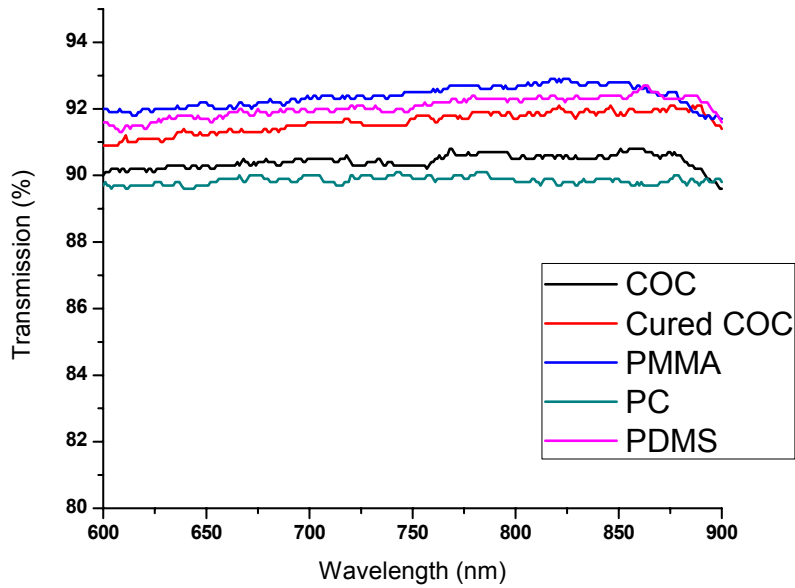
b
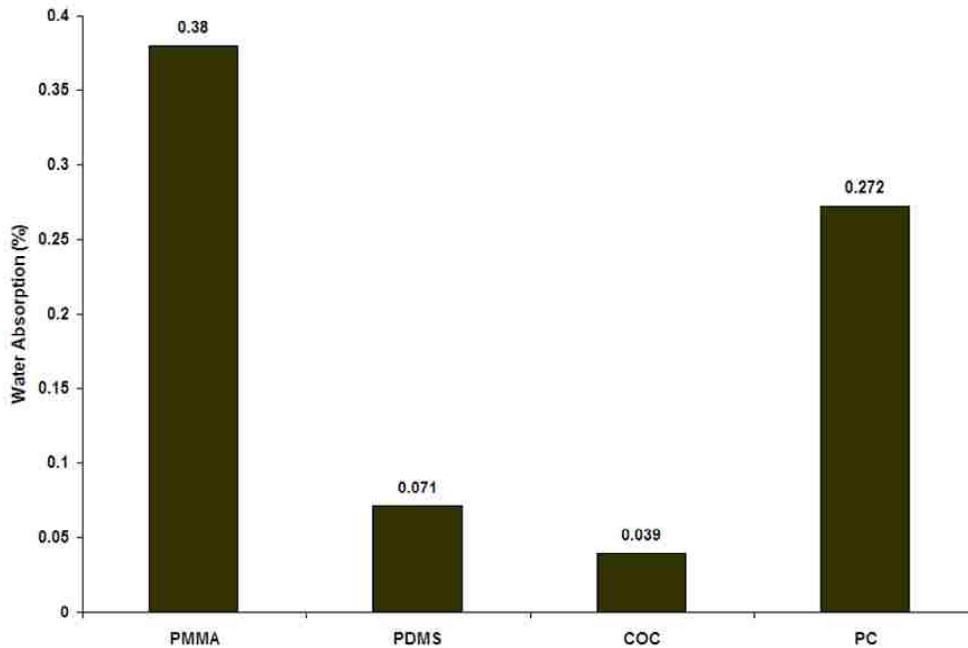
Figure 3.5 (a) Optical transmission spectra (600 nm – 900 nm) of COC (black), cured COC waveguide (red), PMMA (blue), PC (green) and PDMS (purple). (b) Moisture resistance of COC compared to other polymer waveguide materials.

Amongst the properties of waveguides that defines their suitability for efficient light transmission is their optical transmittance at different wavelengths. This is particularly important for fluorescence applications, because transmission losses not only introduces propagation losses, but can also give rise to autofluorescence that can degrade the signal-to-noise ratio in any sensitive fluorescence measurement.[35] Therefore, optical transmission spectra were collected between 600 and 900 nm for both the COC sheet and the cured COC core waveguide material using Ultrospec 4000 UV/VIS Spectrophotometer. A comparison of the optical transmission properties were made for other potential polymeric waveguiding materials, such as PC, PMMA, and PDMS. As can be seen in Figure 3.5a, COC showed high optical transparency of ~91% across the wavelength range scanned, which compared favorably with those of PMMA, PC and PDMS. In addition, there was no significant difference in the transmission spectrum obtained for a COC sheet and the cured COC waveguide.

Water absorption is also a critical issue in selecting proper waveguide materials because water absorption can change the refractive index of the waveguide material inducing light loss or specularly scattered radiation increasing the background in the fluorescence measurement. Therefore, an investigation of the moisture resistance of the embedded COC core waveguide was carried out. A portion of the COC melt was coated onto a glass slide to a thickness of 200 μm and cured as discussed earlier. Films of other polymers were also made in a similar fashion but using a solvent in which each particular polymer showed high solubility. The polymer films were heated to 95°C for 50 min and subsequently weighed. The sample was then immersed into water for 24 h at room temperature and re-weighed following drying under a constant flow of N_2 to remove surface moisture. The difference in weight was calculated in order to establish

the percentage of water absorption.[50] Figure 3.5b shows the water absorption characteristics of COC and other polymer films with COC giving the highest moisture resistance. This result could be related to the more hydrophobic nature of COC, compared to the other materials.

Another important optical characteristic of waveguides is their transmission efficiency as a function of waveguide length. We measured light attenuation in decibels (dB) per unit length (cm) using the equation below;

$$A = -10\log (P_{out}/P_{in}) \times 1/L \qquad (3.1)$$

where A is the attenuation in decibels (dB), P_{in} is the input laser power (in mW), P_{out} is the output power (in mW) and L is the length of the waveguide (cm). Light was launched into the waveguide (launch angle = 76°) near the critical angle (to maximize the penetration depth) when a plain PMMA sheet (n = 1.48) was thermally fusion bonded to the COC/PMMA waveguide. Using an input laser power of 4.2 mW, an output power of 1.3 mW was measured resulting in an attenuation of 1.69 dB/cm. From our observation, the actual light loss was primarily from scattering of the exiting beam from the distal end of the waveguide before reaching the light sensor.

3.3.2 Waveguide Functionality

As mentioned earlier, propagation of light through a planar waveguide generates an evanescent electromagnetic field, which penetrates into the surrounding medium with an amplitude that decays exponentially with distance from the interface. The penetration depth (at 1/e intensity) of the evanescent field is estimated with respect to the launch angle using the following expression;[56]

$$d_{\mathrm{p}} = \frac{\lambda}{2\pi(n_1^2 \sin^2\theta - n_2^2)^{1/2}} \qquad (3.2)$$

where θ is the launch angle, n_1 is the refractive index of the waveguide and n_2 is the refractive index of the medium (cladding). For example, if the laser light (λ = 635 nm) is launched at 76^0, which is near the critical angle of the waveguide system (n for COC = 1.53, n for PMMA = 1.48), the corresponding penetration depth is ~870 nm, whereas if the launch angle is increased by 1^0, the corresponding penetration depth is only 564 nm. Therefore, the appropriate launch angle must be selected in order to obtain the maximum penetration depth of the evanescent field into the adjacent solution layer to maximize the amount of sample excited by the evanescent field.

We evaluated the ability of our embedded polymer waveguide for fluorescence excitation into the adjacent solution by depositing 20 µL of a 1 µM solution of AlexaFluor 647 on the embedded waveguide and placing a thin cover slip on the surface to provide a uniform thickness of fluid above the waveguide. A 635 nm laser was launched into the embedded waveguide through the prism and fluorescent signals were collected at different launch angles using a 2x microscope objective to image the entire length (3 cm) of the waveguide onto a CCD camera (exposure time = 1 s). Figure 3.6a shows a plot of the fluorescence intensity as a function of launch angle. As can be seen, the highest fluorescence intensity was obtained at a launch angle of 76°, which is close to the critical angle of this waveguide. This is expected based on equation 3.2, which corresponds to the maximum penetration depth of the evanescent field into the adjoining solution layer.

To test the ability to generate evanescent excitation with the OFC embedded waveguide, laser light (635 nm) was coupled into the optical fiber that fed the COC embedded waveguide. The same Alexafluor 647 solution was sandwiched between the waveguide and cover slip as described above. Figure 3.6b shows a typical fluorescence image acquired with the CCD using the OFC waveguide (CCD exposure time = 1 s).These results demonstrate the utility of the OFC waveguide for fluorescence measurements without beam shaping optics and careful launch angle adjustments, which are required for prism coupling.

The ability to utilize the waveguide and fluidic architecture after assenbly for fluorescence measurements in a multi-channel format was also demonstrated by filling the fluidic channels (see Figure 3.3a) with a 100 nM solution of AlexaFluor 647 and reading the fluorescence signal from each fluidic channel using the CCD with a 10x relay objective (NA = 0.5), the results of which are shown in Figure 3.7.

In Figure 3.7a, the fluorescence image from eleven (11) parallel microchannels (100 μm wide x 30 μm deep with a 100 μm pitch) is shown with a clear demarcation between the dye-filled channels (fluorescence signal present with a fairly uniform intensity) and the inter-channel space showing negligible fluorescence signal. To clearly visualize the waveguide geometry while collecting fluorescence from the fluidic channels, a low magnification objective (2x, NA = 0.1) was used to acquire a second image. Figure 3.7b gives the fluorescence image from each fluidic channel with the region outside the waveguide region showing a dark background. This indicated that fluorescence excitation was confined to the waveguide area.

a

Launch Angle (Degree)
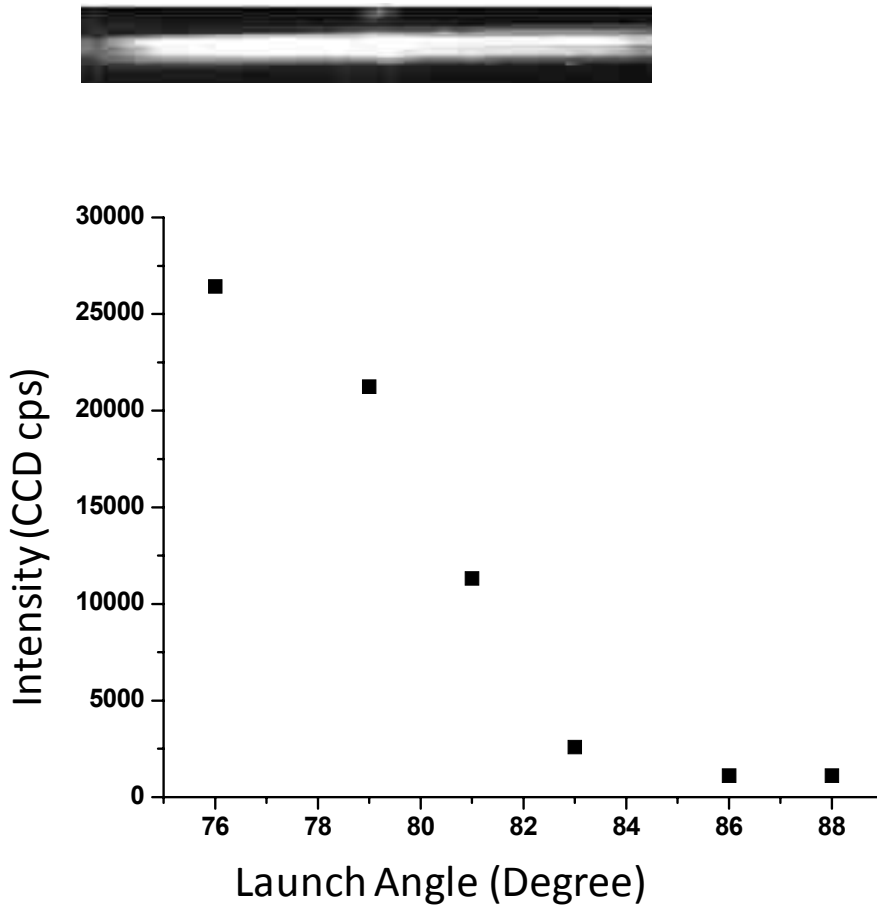
b

Figure 3.6 (a) Top pane is a typical fluorescence image acquired with CCD when light was launched into the waveguide with fluorescence solution sandwiched on the surface. Bottom pane is the plot of fluorescence intensity at different launch angles. (b) Typical fluorescence image acquired with CCD when laser (light) was coupled into the OFC waveguide with fluorescence solution sandwiched on the surface with PMMA cover plate.

a
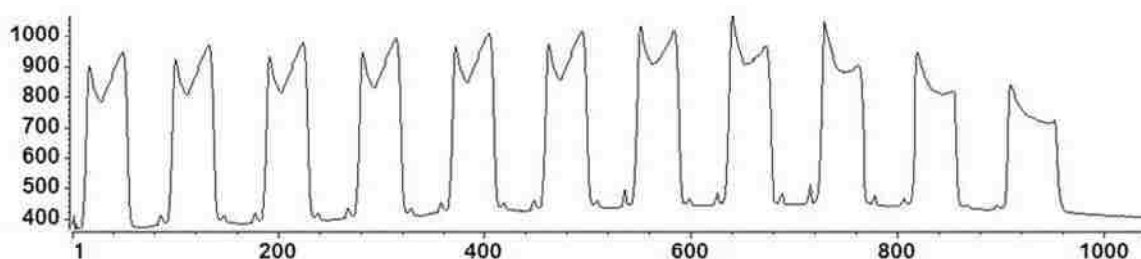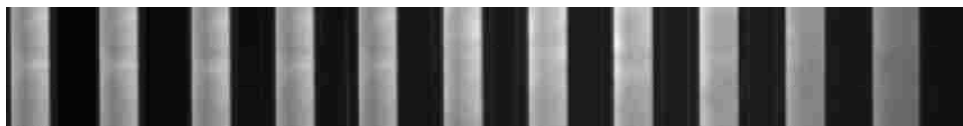
b

Figure 3.7(a) Fluorescence image acquired from multiple fluidic channels (11 micro-channels shown) filled with 100 nM AlexaFluor 647 when light was launched into the COC core embedded waveguide through the monolithic prism; there was a clear distinction between channels (with sample) showing fluorescence signal with fairly uniform intensity (bottom pane) and inter-channel spacing showing dark background, image was acquired with a 10x microscope objective (NA = 0.5) (b) Fluorescence image from the same device acquired with a 2x microscope objective (NA = 0.1) to clearly reveal the waveguide geometry.

3.4 Conclusion

We have fabricated and evaluated a novel COC core waveguide embedded in

PMMA that was situated orthogonal to multiple fluidic channels along the width of a

112

PMMA wafer. This design allowed for fluorescence detection from multiple fluidic channels using evanescent excitation and a CCD camera for parallel readout. We have presented and evaluated two methods of launching light into the embedded waveguide; the use of monolithic prism for effective laser launch into the waveguide and the use of an optical fiber coupled to the waveguide. The two designs generated an evanescent field for the wide field excitation of fluorescent dyes traveling above the waveguide in fluidic channels, which enabled reading fluorescence signal from multiple fluidic channels in a parallel format. This technology may be particularly attractive for high throughput or multiplexed sample analyses. In the near future, the waveguide system will be integrated to a high density fluidic network possessing multiple vias for high throughput screening of biochemical reactions for drug discovery applications.

3.5 References

(1)   Reyes, D. R.; Iossifidis, D.; Auroux, P. A.; Manz, A. *Anal. Chem.* **2002**, *74*, 2623-2636.

(2)   Auroux, P. A.; Iossifidis, D.; Reyes, D. R.; Manz, A. *Anal. Chem.* **2002**, *74*, 2637-2652.

(3)   Vilkner, T.; Janasek, D.; Manz, A. *Anal. Chem.* **2004**, *76*, 3373-3385.

(4)   Whitesides, M. G. *Nature* **2006**, *442*, 368-373.

(5)   Dittrich, S. P.; Tachikawa, K.; Manz, A. *Anal. Chem.* **2006**, *78*, 3887-3907.

(6)   West, J.; Becker, M.; Tombrink, S.; Manz, A. *Anal. Chem.* **2008**, *80*, 4403-4419.

(7)   Vandaveer, W. R.; Pasas-Farmer, S. A.; Fischer, D. J.; Frankenfeld, C. N.; Lunte, S. M. *Electrophoresis* **2004**, *25*, 3528-3549.

(8)   Mogensen, K. B.; Klank, H.; Kutter, J. P. *Electrophoresis* **2004**, *25*, 3498-3512.

(9)   Tao, L.; Kennedy, T. R. *Trends Anal. Chem.* **1998**, *17*, 484-491.

(10)   Gooijer, C.; Kok, S. J.; Ariese, F. *ANALUSIS* **2000**, *28*, 679-685.

(11)   Duveneck, L. G.; Abel, P. A.; Bopp, A. M.; Kresbach, M. G.; Ehrat, M. *Anal. Chimica Acta* **2002**, *469*, 49-61.

(12)   Bermini, R.; Cennamo, N.; Minardo, A.; Zeni, L. *IEEE Sens. J.* **2006**, *6*, 1218-1226.

(13)   Kronick, M. N.; Little, W. A. *J. Immunol. Methods* **1975**, *8*, 235-240.

(14)   Sapdford, K. E.; Shubin, Y. S.; Delehanty, J. B.; Golden, J. P.; Taitt, C. R.; Shriver-Lake, L. C.; Ligler, F. S. *J. Appl. Microbiol.* **2004**, *96*, 47-58.

(15)   Taitt, C. R.; Anderson, G. P.; Ligler, F. S. *Biosens. Bioelectron.* **2005**, *20*, 2470-2487.

(16)   Moerner, W. E.; Peterman, E. J. G.; Brasselet, S.; Kummer, S.; Dickson, R. M. *Cytometry* **1999**, *36*, 232-238.

(17)   Xu, N. X.-H.; Edward, S. Y. *Science* **1998**, *281*, 1650-1653.

(18)   Xu, X.-H.; Edward, S. Y. *Science* **1997**, *275*, 1106 - 1109.

(19)   Paige, M. F.; Bjerneld, E. J.; Moerner, W. E. *Single Mol.* **2001**, *2*, 191-201.

(20)   Ambrose, W. P.; Goodwin, P. M.; Nolan, J. P. *Cytometry* **1999**, *36*, 224-231.

(21)   Mehrvar, M.; Bis, C.; Scharer, J. M.; Moo-Young, M.; Luong, J. H. *Anal. Sci.* **2000**, *16*, 677-692.

(22)   Fang, X.; Tan, W. *Anal. Chem.* **1999**, *71*, 3101 - 3105.

(23)   Moerner, W. E.; Fromm, D. P. *Rev. Sci. Instrum.* **2003**, *74*, 3597-3619.

(24)   Potyrailo, A. R.; Hobbs, E. S.; Hieftje, M. G. *Fresenius J. Anal. Chem.* **1998**, *362*, 349-373.

(25)   Grandin, H. M.; Stadler, B.; Textor, M.; Voros, J. *Biosens. Bioelectron.* **2006**, *21*, 1476-1482.

(26)   Ong, B. H.; Yuan, X.; Tan, Y. Y.; Irawan, R.; Fang, X.; Zhang, L.; Tjin, S. C. *Lab Chip* **2007**, *7*, 506-512.

(27)   Barnes, W. L.; Dereux, A.; Ebbesen, T. W. *Nature* **2003**, *424*, 824-830.

(28)   Budach, W.; Abel, P. A.; Bruno, E. A.; Neuschafer, D. *Anal. Chem.* **1999**, *71*, 3347-3355.

(29) Pawlak, M.; Schick, E.; Bopp, M. A.; Schneider, M. J.; Oroszlan, P.; Ehrat, M. *Proteomics* **2002**, *2*, 383-393.

(30) Arentoft, J.; Sondergaard, T.; Kristensen, M.; Boltasseva, A.; Thorhauge, M.; Frandsen, L. *Electron. Lett.* **2002**, *38*, 274-275.

(31) Plowman, T. E.; Durstchi, J. D.; Wang, H. K.; Christensen, D. A.; Herron, J. N.; Reichert, W. M. *Anal. Chem.* **1999**, *71*, 4344-4352.

(32) Rowe, C. A.; Tender, L. M.; Feldstein, M. J.; Golden, J. P.; Scruggs, S. B.; MacCraith, B. D.; Cras, J. J.; Ligler, F. S. *Anal. Chem.* **1999**, *71*, 3846-3852.

(33) Ives, J. T.; Reichert, W. M. *Appl. Spect.* **1988**, *42*, 68-72.

(34) Reichert, W. M.; Ives, J. T.; Suci, P. A.; Hlady, V. *Appl. Spect.* **1987**, *41*, 636-640.

(35) Shadpour, H.; Musyimi, H.; Chen, J. F.; Soper, S. A. *J. Chrom.* **2006**, *1111*, 238-251.

(36) Bliss, C. L.; McMullin, J. N.; Backhouse, C. J. *Lab Chip* **2007**, *7*, 1280-1287.

(37) Chang-Yen, A. D.; Eich, K. R.; Gale, K. B. *J. Lightwave Technol.* **2005**, *23*, 2088-2093.

(38) Powers, M. A.; Koev, S. T.; Schleunitz, A.; Yi, H. M.; Hodzic, V.; Bentley, W. E.; Payne, G. F.; Rubloff, G. W.; Ghodssi, R. *Lab Chip* **2005**, *5*, 583-586.

(39) Huang, S. H.; Tseng, F. G. *J. Micromech. Microeng.* **2005**, *15*, 2235-2242.

(40) Balslev, S.; Jorgensen, A. M.; Bilenberg, B.; Mogensen, K. B.; Snakenborg, D.; Geschke, O.; Kutter, J. P.; Kristensen, A. *Lab Chip* **2006**, *6*, 213-217.

(41) Xu, F.; Datta, P.; Wang, H.; Gurung, S.; Hashimoto, M.; Wei, S.; Goettert, J.; McCarley, R. L.; Soper, S. A. *Anal. Chem.* **2007**, *79*, 9007-9013.

(42) Huang, W. J.; Chang, F. C.; Chu, P. P. J. *Polymer* **2000**, *41*, 6095-6101.

(43) Khanarian, G.; Celanese, H. *Opt. Eng.* **2001**, *40*, 1024-1029.

(44) Fredrickson, K. C. *J. Microelectro. Sys.* **2006**, *15*, 1060-1068.

(45) Esch, B. M.; Kapur, S.; Irizarry, G.; Genova, V. *Lab Chip* **2003**, *3*, 121-127.

(46) Mela, P.; Berg van den, A.; Cummings, B. E.; Simmons, A. B.; Kirby, J. B. *Electrophoresis* **2005**, *26*, 1792-1799.

(47)   Koh, G. C.; Tan, W.; Zhao, M.-q.; Ricco, J. A.; Hugh, F. Z. *Anal. Chem.* **2003**, *75*, 4591-4598.

(48)   Pu, Q.; Oyesanya, O.; Thompson, B.; Liu, S.; Alvarez, C. J. *Langmuir* **2007**, *23*, 1577-1583.

(49)   Stachowiak, B. T.; Mair, A. D.; Holden, G. T.; Lee, J. L.; Svec, F.; Frechet, M. J. J. *J. Sep. Sci.* **2007**, *30*, 1088 - 1093.

(50)   Hwang, S. J.; Yu, H. H. *Japanese J. Appl. Phys. part 1* **2005**, *44*, 2541-2545.

(51)   Schmidt, H.; Hawkins, A. R. *Microfluid. Nanofluid.* **2008**, *4*, 3 - 16.

(52)   Mogensen, K. B.; Petersen, N. J.; Hubner, J.; Kutter, J. P. *Electrophoresis* **2001**, *22*, 3930-3938.

(53)   Mogensen, K. B.; El-Ali, J.; Wolff, A.; Kutter, J. P. *Appl. Optics* **2003**, *42*, 4072-4079.

(54)   Hupert, M. L.; Guy, J. W.; Llopis, S. D.; Situma, C.; Rani, S.; Nikitopoulos, D. E.; Soper, S. A. *Proc. SPIE* **2006**, *6112*, 61120B-61121 - 61120B-61112.

(55)   Hupert, M. L.; Guy, J. W.; Llopis, S. D.; Shadpour, H.; Rani, S.; Nikitopoulos, D. E.; Soper, S. A. *Microfluid. Nanofluid* **2007**, *3*, 1-11.

(56)   Ahmad, M.; Hench, L. L. *Biosens. Bioelectron.* **2005**, *20*, 1312-1319.

CHAPTER 4

POLYMER-BASED DENSE FLUIDIC NETWORK FOR HIGH THROUGHPUT SCREENING WITH ULTRASENSITIVE FLUORESCENCE

4.1 Introduction

High Throughput Screening (HTS) is the process of selecting a potential drug candidate from a pool of diverse chemical elements, and it represents an integral part of the drug discovery process, which is constantly desiring improved efficiency by emerging scientific advances and increasing pressure to reduce drug development cost.[1-5] The number of potential therapeutic targets are rapidly increasing due to a better understanding of the genetic basis of disease. Also, combinatorial chemical synthesis has generated large compound libraries for screening against the growing number of targets. These advancements have placed high demand on drug discovery screening technologies to provide a suitable platform/system that will enhance throughput in the screening process. Such screening systems must be able to sustain assay processing rates of several thousands per run without sacrificing data quality. In addition, screening platforms must be robust and reliable, cost-effective, simple and user-friendly, and should be amenable to rapid implementation, standardization and automation to provide competitive advantages for the operator.[6]

The primary approach toward providing for this demand and to shorten the time scale for all aspects of drug discovery has been the adoption of high-density plate systems characterized by small well volumes capable of screening ~100,000 assays per day.[3,7-9] These systems require sophisticated and highly sensitive detection techniques to generate high quality assay results due to the small well volume. To provide for this sensitivity requirement, fluorescence-based detection techniques have become

increasingly popular in designing miniaturized HTS system due to the inherent sensitivity advantage of fluorescence measurements. For example, Modern HTS technology, such as the Evotec robotic micro-plate systems (EVOscreen Mark-II and EVOscreen Mark-III)[10] employs confocal fluorescence readers to serially address assay results, and are capable of screening over 100,000 assays/day.[10-12] Unfortunately, the serial strategy associated with the confocal fluorescence scanner places a severe limitation on the capability of the system to enhance assay throughput. Furthermore, the implementation of higher density micro-plates with reduced well volumes is faced with a number of other hurdles. These include, evaporation problems resulting from the high surface-to-volume ratio (i.e. quick evaporation of dispensed liquid), and the sophistication required for liquid dispensing. Although, some of these challenges can be addressed through concerted efforts in engineering of automated micro-plate workstations for HTS (e.g. the Evotec second generation screening platform, EVOscreen Mark-III, which utilizes four parallel confocal readers in four detection channels),[10] it comes with enormous price tags, which could be up to several millions of dollars.

Advances in microfabrication technology has created opportunities for exploring the potential of microfluidics for HTS.[13] These microfabricated devices are capable of manipulating and processing miniature volumes (10^{-9} to 10^{-18} Liter) of fluids in microchannels with dimensions of a few micrometers, which makes them suitable for performing continuous flow assays in a miniaturized format. In addition, several processing units can be configured in a small footprint suitable for optical imaging, which provides the opportunity for massively parallel experimentation. Furthermore, microfluidic devices are characterized by their small size and employ hydrodynamic

118

pressures or electrokinetic pumping for fluid transportation (fluidflow),[14-18] which facilitates integration to sample detection systems without complex engineering designs. These unique features of microfluidics make them viable platforms for HTS.[19,20] Employing microfluidics for HTS technology provides several other advantages, including, reduction in solvent evaporation problems associated with micro-plates,[21] low consumption of samples and reagents, short time of analysis and the ability to automate fluid handling.[22-25] Another key feature of microfluidics is the ability to integrate several processing steps into a single system, which simplifies routine operations and also eliminates sample cross-contamination. For example, it can integrate functions such as sampling, sample transport, biochemical reactions, analyte separation, product isolation and detection within a microchannel network.[26-28] Consequently, microfluidics provides the ability for serial sample processing and analysis in a single fluidic element and in addition, can accomplish massive parallelization brought about by the configuration of multiple processors in a single device.[29]

The utility of microfluidics for throughput enhancement in different types of assays have been demonstrated.[30-35] The potential of microfluidics for large-scale biochemical screening was demonstrated through the use of microfabricated microchannel array systems with automatic sample loading from microtiter plates, to screen 96 samples in less than 90 s.[36] Other examples of reports that employed microfluidics for high throughput assays includes on-chip immunoassays for screening fluorescently labeled antibodies,[37] continuous-flow sandwich hybridization assay for pathogen detection,[38] integrated microfluidics and bead-based assays for high throughput detection of gene expression,[39] detection of low-affinity transient binding events in biomolecular interactions,[40] parallel screening of in-situ click chemistry,[41] kinase assays based on

separation of reaction products from substrates and cell-based assays.[3,42-44] Therefore, the application of microfluidics in HTS can provide a way to resolve current challenges in drug screening and significantly increase throughput with minimal operation cost in drug discovery projects.[29]

Fabrication of microfluidic devices have been traditionally done in glass and silicon using technology borrowed from the microelectronics sector.[45,46] The attractiveness of glass as materials for microfluidic fabrication includes their well-defined surface chemistry, and good electroosmotic properties, which make them compatible with many biochemical and flow-based assays. Also, the excellent optical properties of glass make them suitable for ultra-sensitive fluorescence measurements. However, the fabrication modalities are time-consuming, challenging and relatively expensive.

Polymers offer important advantages and have attracted much interest in microfluidic device production due to their simple fabrication characteristics, and in some cases their favorable optical properties. In addition, they are generally low-cost materials, which allows for inexpensive mass production of microfluidic devices.[47]

While microfluidics provide a suitable platform for HTS by generating high number of sample processing units over a small footprint, a suitable detection system is required for parallel interrogation of the fluidic processors using wide-field illumination, such that the resulting fluorescence is imaged onto an array detector possessing the prerequisite sensitivity for parallel readout. An array detector that can be employed for ultra-sensitive fluorescence detection is the electron multiplying charge-coupled device (EMCCD) with frame transfer capabilities to provide for high speed imaging in near video frame rates, which allows monitoring of biochemical reactions with high efficiency.[48-50] Throughput in this case is directly related to the number of fluidic processors that can be imaged onto

the detector; therefore, the configuration of the fluidic processors in a high density format is important to provide increased throughput and to realize the full potential of microfluidics in HTS.[51]

In this Chapter, we present a high density fluidic device with a series of individual sample processors configured in a small footprint suitable for optical imaging. The device was fabricated using UV-LiGA to first produce the required fluidic structures on a metal mold (Ni mold master), which was transferred onto a polymer substrate during replication. The polymer microchip possessed multiple fluidic processors with an individual input reservoir. An ultrasensitive fluorescence detection system with a large field-of-view (FoV) was used to transduce fluorescence signals simultaneously from each fluidic processor onto the active area of an EMCCD. The utility of the multichannel network for HTS with an optical system for providing the prerequisite sensitivity was demonstrated by parallel monitoring of fluorescence signal from AlexaFluor 660 labeled oligonucleotides that were hydrodynamically pumped through individual fluidic channels. Evaluation of the fluidic system using blank and dye samples indicated the absence of cross talk between fluidic channels, and thus, indicating the apparent capability for simultaneous monitoring of multiple biochemical assays as appropriate for HTS.

4.2 Experimental Procedure

4.2.1 Fabrication of the Fluidic Network

The fluidic structures were fabricated using UV-LiGA to produce Ni electroforms (mold master) according to standard lithography procedures already reported (see also Chapter 1, Section 1.4.2).[52, 53] To achieve a precise depth of 1 µm for the fluidic channels, SU-8 photoresist was spin coated (3500 rpm; 30 s) on a silicon disc to a thickness of 1 µm and baked for 1 min at 95°C on a hot plate. A UV mask containing the
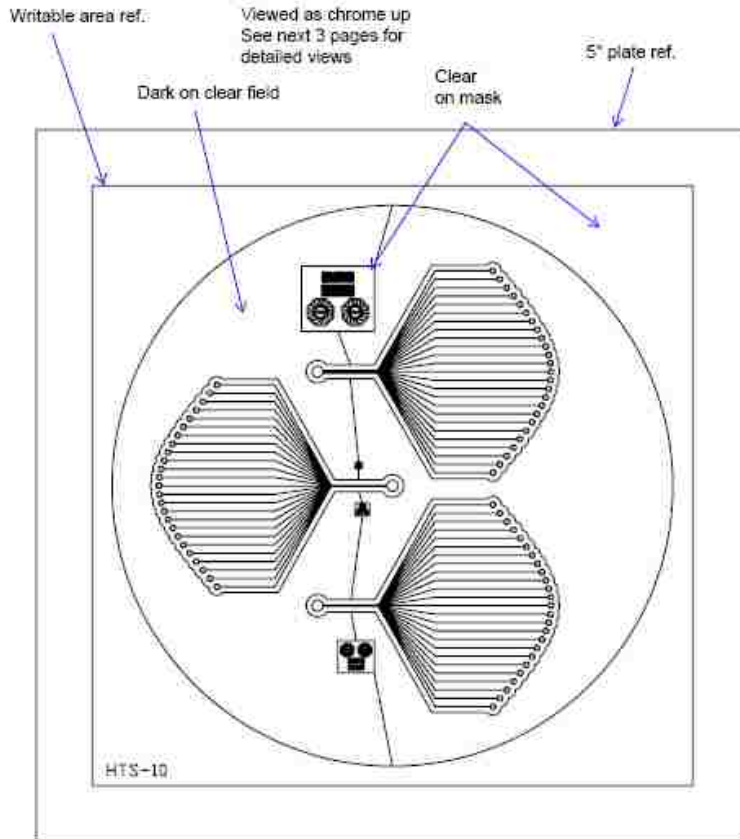
Figure 4.1 The design of the UV mask containing the fluidic patterns. Three different patterns were poised on the mask; from top to bottom. 10 μm wide (pitch = 10 μm), 5 μm wide (pitch = 2 μm) and 1 μm wide (pitch = 1 μm) patterns.

fluidic patterns was designed (see Figure 4.1) and used for the UV exposure prior to development and electroplating steps to make the master mold. The UV mask (see Figure 4.1) consisted of three different device designs: *(1)* a 10 μm width (pitch = 10 μm), *(2)* a 5 μm width (pitch = 2 μm) and *(3)* a 1 μm width (pitch = 1 μm) patterns, that could be used interchangeably to make any of the three different structures (See Qu *et al.* for specific details on UV-LiGA procedures[52]). Hot embossing was used in the molding step to transfer the fluidic pattern from the mold master onto PMMA substrates by employing a JenOptik HEX02 high-precision hot embossing system to create high fidelity in the features over large areas. The fluidic architecture of the high density model

microchip is shown in Figure 4.2. The device consisted of 25 fluidic processors with dimensions of 5 μm width, 1 μm depth and a pitch of 2 μm configured in a footprint of ~180 μm in the high density region for optical detection. Figures 4.3a and 4.3b present SEM images of sections of the molded parts made in PMMA. A PMMA cover plate (Thickness = 125 μm) was placed on the device to create the fluidic channels and subsequently fusion bonded to the substrate in a GC oven at 107°C (slightly above the T$_g$ of PMMA) after being clamped between two glass plates to render uniform pressure (see Figure 4.3c). Each fluidic processor possessed an individual sample input reservoir (see Figure 4.3b) for introduction of reactants (enzyme and substrate) and also a reaction zone equipped with a strip heater for incubation of the enzyme and substrate and thermal perturbation of the reaction products (see Figure 4.2). The fluidic channels gradually fan-out (see Figure 4.3 a and c) from the high density region to connect with the individual sample reservoirs (see Figure 4.3b). The spread of the fluidic channels provides two advantages: *(1)* Each fluidic channel serves as an independent sample processor, which allows for multi-sample interrogation; and (2) generation of adequate reaction zone (reactors) with sufficient room for incubating enzyme and substrate (see Figure 4.2) via integration with small heating elements, such as a strip heater to supply thermal energy to the fluidic processors without negatively impacting the fidelity of the fluidic channels. The width of the channel is 22 μm at each individual reservoir (see Figure 4.3b) and tapers to 14 μm at the reaction zone (see Figure 4.3a) and then to 5 μm at the high density (detection) region. All fluidic processors have equal lengths (3 cm) and equal depths (1 μm) from the sample input reservoir to the common reservoir. This was important to maintain uniform hydrodynamic pressure in all the fluidic processors. The volume capacity of each individual fluidic processor is ~0.15 nL, which
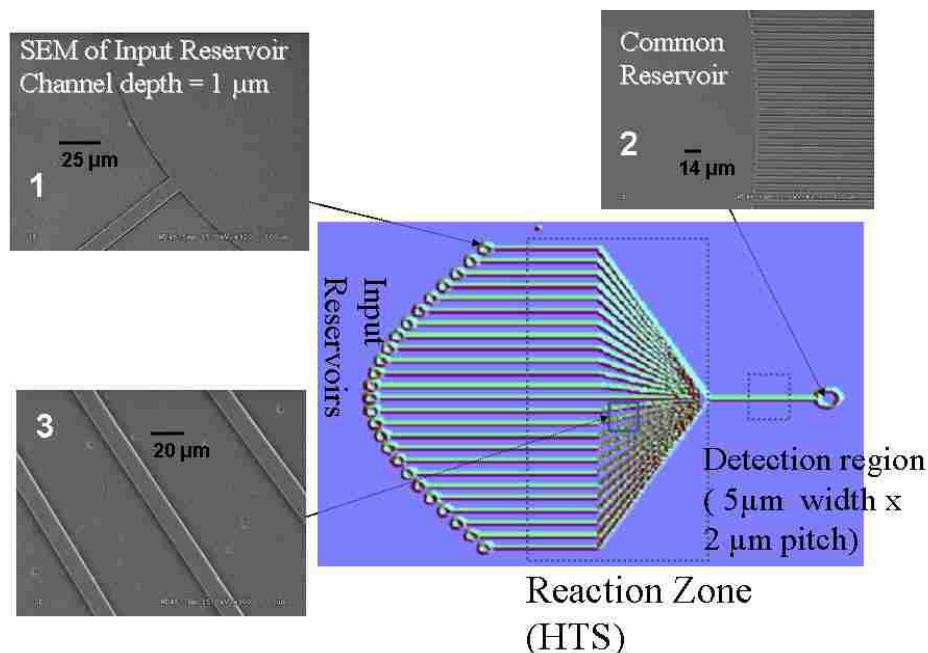
Figure 4.2 Schematic of the fluidic network for HTS (1, 2 & 3 are SEMs of a Ni electroform related to the indicated sections of the device) possessing reactor channels for incubating the enzyme target with the substrate and potential drug inhibitor. The dense network of channels for imaging evaluates the efficiency of drug inhibition by measuring fluorescent signal. The device has a total of 25 fluidic processors configured in a 180 μm wide footprint.
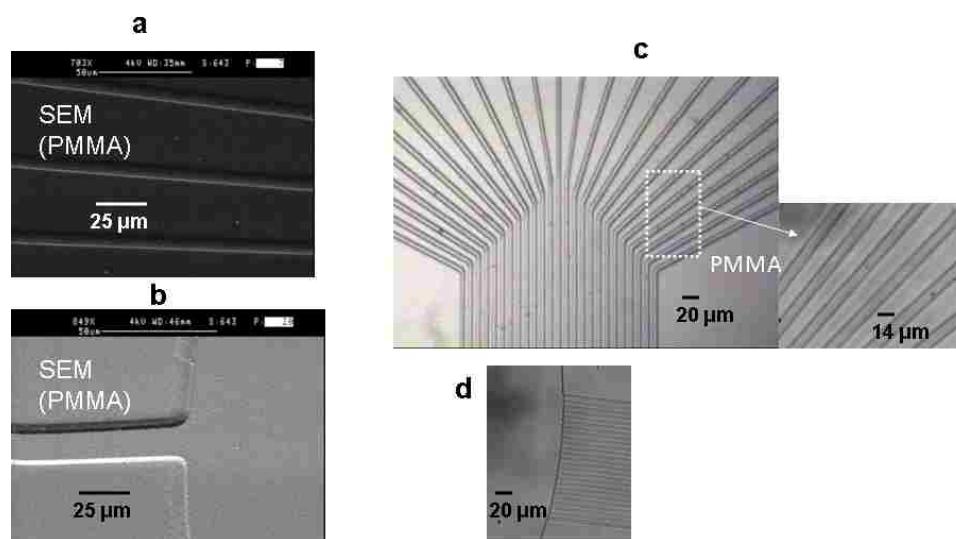
Figure 4.3 (a) SEM of a section of the molded device in PMMA using hot embossing. The section shown is where the channels spread out to accommodate individual sample input reservoirs (b) SEM of one of the channels showing the individual sample input reservoir. (c) Optical micrograph of a section of the sealed device showing the geometry of the fluidic network. (d) Optical micrograph of the microchip showing the fluidic network and the common reservoir.

provides advantages in terms of reagents economy. All channels possessed a common output reservoir (see Figure 4.3d) for collection of waste following each assay. A replica device was also made through the same process but having a width of 10 µm and pitch of 10 µm (depth = 1 µm).

4.2.2 Optical Set-up and Multichannel Illumination

A wide field-of-view (FoV) fluorescence detection system (details presented in Chapter 2) was used to monitor fluorescent signals from the fluidic vias using a highly sensitive EMCCD operated in a frame transfer mode. The optical system was configured in an epi-illumination format with beam shaping optics and employed a 40x microscope objective (Numerical Aperture, NA = 0.75) to generate a collimated light output with a diameter of ~200 µm. At this magnification, the system possessed a FoV of ~200 µm, which allows interrogation of all 25 fluidic processors simultaneously. The system is not limited by magnification of the objective and thus accommodates other microscope objectives with the appropriate NA to expand the FoV. For example a 20x microscope objective (NA = 0.75) generated a FoV of 400 µm.

4.2.3 Chemicals and Reagents

Tris-Taps-EDTA (TTE) buffer was used for all measurements; 1x TTE buffer solution (pH = 8.7) was prepared from a stock solution of the buffer (10x) using nanopure water obtained from a Barnstead NANOpure System (Model D8991, Dubuque, IA). AlexaFluor 660 was obtained from Molecular Probes (Eugene, Oregon, USA) and working solution samples were diluted from a stock solution (80 nM) using 1x TTE buffer. Buffer solutions were filtered through a 0.2 µm filter prior to sample preparation.

4.3 Results and Discussion

4.3.1 Parallel Fluorescence Measurements in the Multichannel Device

Hydrodynamic pumping was used to drive fluid through the device. This was achieved by connecting a syringe pump to the common reservoir while each fluidic channel fed with a prepared sample at its appropriate reservoir. The syringe pump was operated in the refilling mode, which transported the liquid sample from its reservoir through each fluidic channel at a constant flow rate (linear velocity = 0.03 cm/s). Using this set-up, a 2.0 nM solution of AlexaFluor 660 was hydrodynamically pumped through each fluidic channel of the device and a fluorescent signal was acquired simultaneously from all the fluidic processors. Figure 4.4a is a fluorescence image obtained with the CCD showing fluorescent signal from all 25 microchannels. With these channel dimensions (5 µm width, 2 µm pitch), a 20x objective with the same numerical aperture (NA) as the 40x (NA = 0.75) will generate a FoV of 400 µm, which will allow the simultaneous fluorescence detection from 50 microchannels. We also investigated sample throughput with a 10 µm wide channel (pitch = 10 µm) because it was easier to drive fluid through these larger channels due to lower pressure drop. The fluorophore was driven through the fluidic channels in the same manner and fluorescent signal measured. Figure 4.4b shows a fluorescence image from 15 microchannels. This means that if the 20x objective is used, 30 channels can be imaged using these channel dimensions.

4.3.2 Investigation of Cross Talk Between Channels

To investigate potential cross talk between the fluidic channels, blank samples (buffer) and dye samples (AlexaFluor 660) were loaded into the individual sample reservoirs

and a fluorescence image was acquired. Figure 4.5a shows an image when some

channels were loaded with dye and others loaded with buffer. The channels loaded with

dye gave fluorescent signal while those loaded with the buffer (marked x in Figure 4.5a)

gave no fluorescent signal. Thus, the system could monitor multiple biochemical assays

without cross contamination. This was further explicitly indicated by generating a 3D

image of Figure 4.5a (see Figure 4.5b) to show fluorescent signal profile from channels

loaded with dye samples.

a **b**
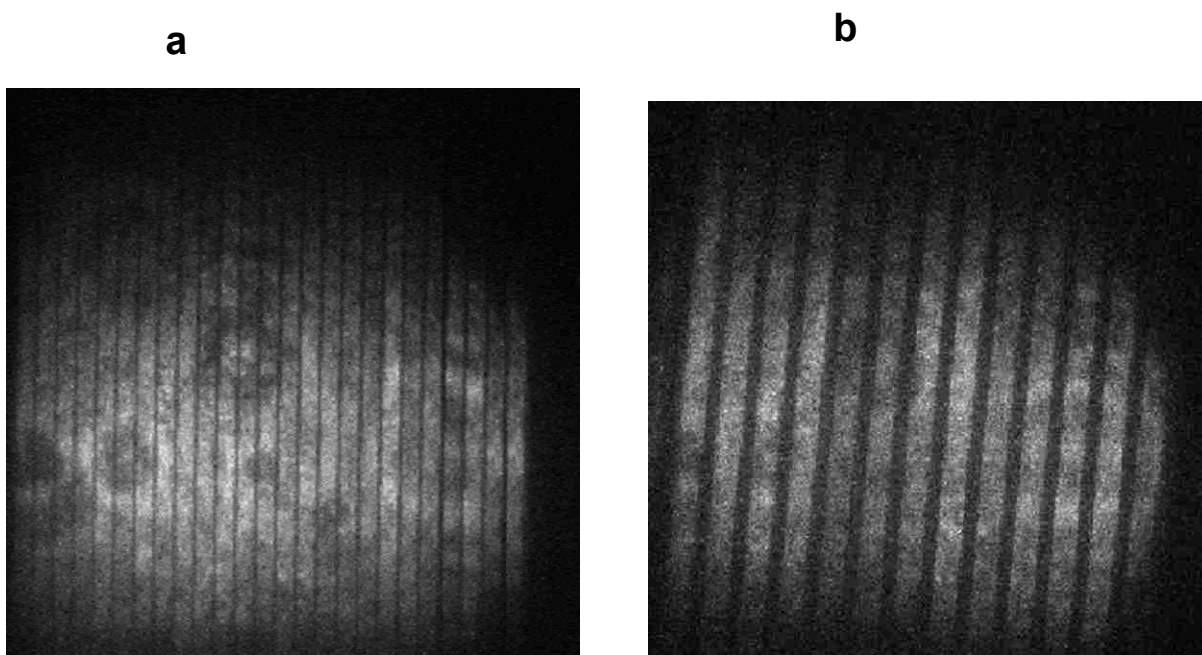
Figure 4.4 (a) CCD image of fluorescent molecules (AlexaFluor 660) migrating through the high density chip (channel dimension = 5 µm x 1 µm (pitch = 2 µm). The fluorescence was collected with a 40x/0.75 objective using a 200 ms CCD exposure time (25-fluidic channels were imaged (b) CCD image acquired using the same condition in a wider channel (dimension: 10 µm x 1 µm, pitch = 10 µm); 15 fluidic channels were imaged.

4.4 Conclusion and Future Work

A novel microfluidic system was fabricated suitable for high throughput screening of

combinatorial libraries for a specific target. The fluidic channels were configured in a

high density format that could also be optical imaged. We have demonstrated the ability

to carry out simultaneous fluorescence measurements in multiple fluidic channels,

which will allow for multiple assays to be analyzed in a massively parallel fashion. Whilst

a

x x   x x   x x x   x x   x x x x x

b
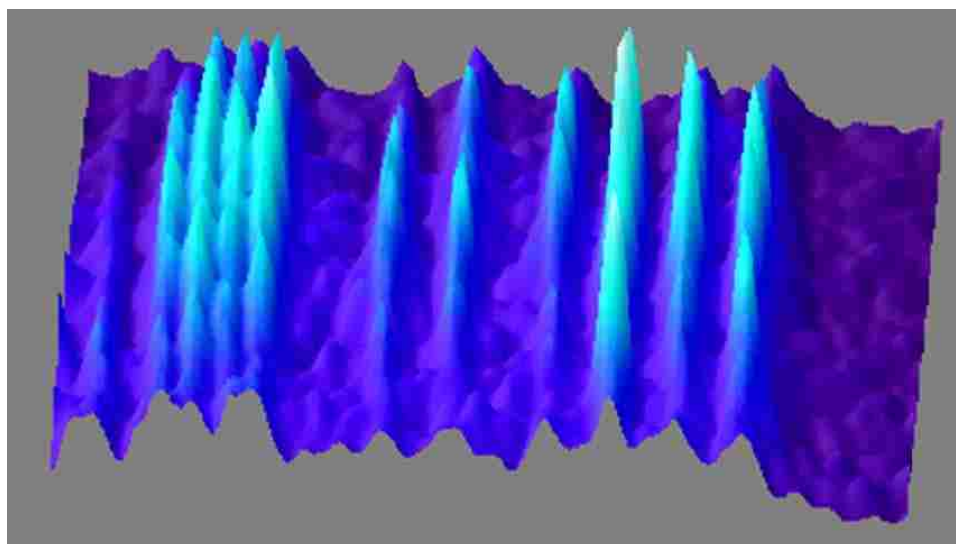
Figure 4.5 (a) CCD Image acquired when fluidic channels were filled with buffer or dye (AlexaFluor 660) samples; the locations marked 'x' are buffer-filled channels. (b) 3D image showing the fluorescence intensity profile in channels loaded with AlexaFluor 660; the channels marked x in (a) appeared as a dark background also in (b)

the present fluidic design yielded a theoretical 50-fold increase in sample throughput compared to serial strategies for HTS, this throughput can be significantly increased simply by reducing the channel width. For example, with a channel width of 1 μm (pitch = 1 μm), 100 fluidic processors can be imaged in an ~200 μm field-of-view. Further reduction in channel width to 500 nm with a pitch of 500 nm would allow the ability to image a total of 200 fluidic processors simultaneously using a 40x microscope objective. The introduction of a 20x microscope objective with high numerical aperture (NA = 0.75) in this case would generate a throughput of 200-fold for a 1 μm wide channel design and 400-fold for the 500 nm channel design. The fluidic device will be further evaluated by screening a small library of compounds against a specific target. For example, L1 endonuclease (L1-EN) is an enzyme responsible for double strand breaks in genomic DNA and is associated with 45 different diseases, including aging and cancer.[54] Also APE1 is another important target which causes radio- and chemo-resistance in human tumors.[55] A small library of potential therapeutic agents for these important targets will
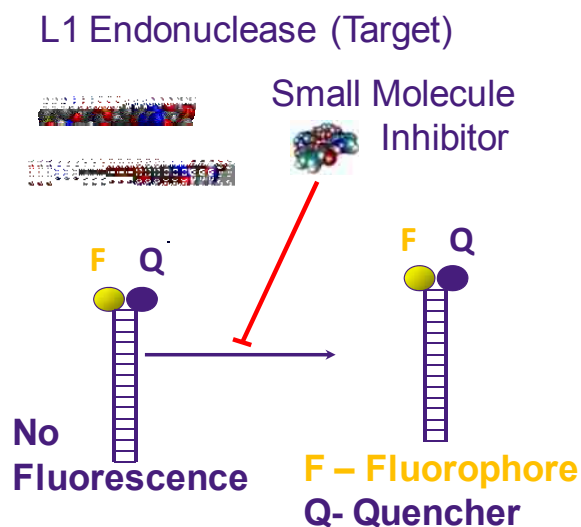
Figure 4.6 A pictorial depiction of a model assay for screening a combinatorial library for L1-EN and APE1.

be screened to register drug candidates for clinical trials. The pictorial depiction of a model screening assay for these targets is shown in Figure 4.6. The small molecule inhibitor (drug candidate) will be incubated with the enzyme in the presence of an appropriate substrate containing the action site of the enzyme. The substrate (double stranded DNA) will be labeled with a fluorophore and a quencher and fluorescence monitored with proximity considerations to determine the extent of double strand breaks induced by the enzyme activity. Whilst L1-EN which is a 6-base cutter recognizes AATTTT motif, APE1 recognizes the apurinic (AP) site in genomic DNA and these sites will be incorporated in the designed substrate for the screening experiments.

4.5 References

(1)   Aherne, G. Y.; McDonald, E.; Workman, P. *Breast Canc. Res.* **2002**, *4*, 148-154.

(2)   Olsen, M.; Iverson, B.; Georgiou, G. *Curr. Opin. Biotechnol.* **2000**, *11*, 331-337.

(3)   Sundberg, S. A. *Curr. Opin. Biotechnol.* **2000**, *11*, 47-53.

(4)   Sittampalam, G. S.; Kahl, S. D.; Janzen, W. P. *Curr. Opin. Chem. Biol.* **1997**, *1*, 384-391.

(5)   Zheng, W.; Spencer, R. H.; Kiss, L. *Assay Drug Dev. Technol.* **2004**, *2*, 543-552.

(6)   Major, J. *J. Biomol. Screen.* **1998**, *3*, 13-17.

(7)   Maffia, A. M.; Kariv, I.; Oldenburg, K. R. *J. Biomol. Screen.* **1999**, *4*, 137-142.

(8)   Oldenburg, K. R.; Zhang, J. H.; Chen, T. M.; Maffia, A.; Blom, K. F.; Combs, A. P.; Chung, T. D. Y. *J. Biomol. Screen.* **1998**, *3*, 55-62.

(9)   Mere, L.; Bennett, T.; Coassin, P.; England, P.; Hamman, B.; Rink, T.; Zimmerman, S.; Negulescu, P. *Drug Discov. Today* **1999**, *4*, 363-369.

(10)   www.evotec-technologies.com.

(11)   Gribbon, P.; Schaertl, S.; Wickenden, M.; Williams, G.; Grimley, R.; Stuhmeier, F.; Preckel, H.; Eggeling, C.; Kraemer, J.; Everett, J.; Keighley, W. W.; Sewing, A. *Curr. Drug Discov. Technol.* **2004**, *1*, 27-35.

(12) Jager, S.; Garbow, N.; Kirsch, A.; Preckel, H.; Gandenberger, F. U.; Herrenknecht, K.; Rudiger, M.; Hutchinson, J. P.; Bingham, R. P.; Ramon, F.; Bardera, A.; Martin, J. *J. Biomol. Screen.* **2003**, *8*, 648-659.

(13) Breslauer, D. N.; Lee, P. J.; Lee, L. P. *Mol. BioSyst.* **2006**, *2*, 97-112.

(14) Whitesides, G. M. *Nature* **2006**, *442*, 368-373.

(15) Gunther, A.; Jensen, K. F. *Lab Chip* **2006**, *6*, 1487-1503.

(16) Stone, H. A.; Stroock, A. D.; Ajdari, A. *Annu. Rev. Fluid Mech.* **2004**, *36*, 381-411.

(17) Shui, L. L.; Eijkel, J. C. T.; van den Berg, A. *Sens. Actuat. B-Chem.* **2007**, *121*, 263-276.

(18) Hong, J. *Biochip J.* **2008**, *2*, 12-26.

(19) Thorsen, T. *BioTechniques* **2004**, *36*, 197-199.

(20) Khandurina, G.; Guttman, A. *Curr. Opin. Chem. Biol.* **2002**, *6*, 359-366.

(21) Litborn, E.; Roeraade, J. *J. Chromatogr.* **2000**, *745*, 137-147.

(22) Melin, J.; Quake, S. R. *Annu. Rev. Biophys. Biomol. Struct.* **2007**, *36*, 213-231.

(23) Dittrich, P. S.; Manz, A. *Nature Rev. Drug Discov.* **2006**, *5*, 210-218.

(24) Yager, P.; Edwards, T.; Fu, E.; Helton, K.; Nelson, K.; Tam, M. R.; Weigl, B. H. *Nature* **2006**, *442*, 412-418.

(25) Craighead, H. *Nature* **2006**, *442*, 387-393.

(26) West, J.; Becker, M.; Tombrink, S.; Manz, A. *Anal. Chem.* **2008**, *80*, 4403-4419.

(27) Hong, J. W.; Quake, S. R. *Nature Biotechnol.* **2003**, *21*, 1179-1183.

(28) Thorsen, T.; Maerkl, S. J.; Quake, S. R. *Science* **2002**, *298*, 580-584.

(29) Brenan, C. J.; Morrison, T.; Stone, K.; Heitner, T.; Katz, A.; Kanigan, T. S.; Hess, R.; Kwon, S.-J.; Jung, H.-C.; Pan, J.-G. *Proc. SPIE* **2002**, *4626*, 560-569.

(30) Hadd, A. G.; Jacobson, S. C.; Ramsey, J. M. *Anal. Chem.* **1999**, *71*, 5206-5212.

(31) Cohen, C. B.; Chin-Dixon, E.; Jeong, S.; Nikiforov, T. T. *Anal. Biochem.* **1999**, *273*, 89-97.

(32)   Chiem, N. H.; Harrison, D. J. *Clin. Chem.* **1998**, *44*, 591-598.

(33)   Hadd, A. G.; Raymond, D. E.; Halliwell, J. W.; Jacobson, S. C.; Ramsey, J. M. *Anal. Chem.* **1997**, *69*, 3407-3412.

(34)   Li, P. C. H.; Harrison, D. J. *Anal. Chem.* **1997**, *69*, 1564-1568.

(35)   Khandurina, J.; Guttman, A. *J. Chromatogr. A* **2002**, *943*, 159-183.

(36)   Shi, Y. N.; Simpson, P. C.; Scherer, J. R.; Wexler, D.; Skibola, C.; Smith, M. T.; Mathies, R. A. *Anal. Chem.* **1999**, *71*, 5354-5361.

(37)   Yang, T. L.; Jung, S. Y.; Mao, H. B.; Cremer, P. S. *Anal. Chem.* **2001**, *73*, 165-169.

(38)   Erch, M. B.; Locascio, L. E.; Tarlov, M. J.; Durst, R. A. *Anal. Chem.* **2001**, *73*, 2952-2958.

(39)   Yang, L.; Tran, D. K.; Wang, X. *Genome Res.* **2001**, *11*, 1888-1898.

(40)   Maerkl, S. J.; Quake, S. R. *Science* **2007**, *315*, 233-237.

(41)   Wang, J.; Sui, G.; Mocharla, V. P.; Lin, R. J.; Phelps, M. E.; Kolb, H. C.; Tseng, H.-R. *Angew. Chem. Int. Ed.* **2006**, *45*, 5276-5281.

(42)   Hung, P. J.; Lee, P. J.; Sabounchi, P.; Lin, R.; Lee, L. P. *Biotechnol. Bioeng.* **2005**, *89*, 1-8.

(43)   Wolff, A.; Perch-Nielsen, I. R.; Larsen, U. D.; Friis, P.; Goranovic, G.; Poulsen, C. R.; Kutter, J. P.; Telleman, P. *Lab Chip* **2003**, *3*, 22-27.

(44)   Ye, N. N.; Qin, J. H.; Shi, W. W.; Liu, X.; Lin, B. C. *Lab Chip* **2007**, *7*, 1696-1704.

(45)   Li, J.; Thibault, P.; Bings, N. H.; Skinner, C. D.; Wang, C.; Colyer, C.; Harrison, J. *Anal. Chem.* **1999** *71*, 3036-3045.

(46)   McClain, M. A.; Culbertson, A. T.; Jacobson, S. C.; Allbritton, N. L.; Sims, C. E.; Ramsey, J. M. *Anal. Chem.* **2003**, *75*, 5646-5655.

(47)   Becker, H.; Locascio, L. E. *Talanta* **2002**, *56*, 267-287.

(48)   Christenson, M. *Single Mol.* **2000**, *1*, 177-179.

(49)   Hiller, W. J.; Kowalewski, T. A.; Tatarczyk, T. *Proc. SPIE* **1992**, *1801*, 595-601.

(50)   Okagbare, P. I.; Soper, S. A. *Analyst* **2009**, *134*, 97-106.

(51)   Wen, Y.; Yang, S. T. *Expert Opin. Drug Discov.* **2008**, *3*, 1237-1253.

(52)   Qu, W.; Wenzel, C.; Jahn, A.; Zeidler, D. *IEEE: Optoelectron. Microelectron. Mat. Devic.* **1999**, *Dec. 14-16*, 380-383.

(53)   Ford, S. M.; Davies, J.; Kar, B.; Qi, S. D.; McWhorter, S.; Soper, S. A.; Malek, C. K. *J. Biomech. Eng.-Transact. Asme* **1999**, *121*, 13-21.

(54)   Gasior, S. L.; Wakeman, T. P.; Xu, B.; Deininger, P. L. *J.Molc. Biol.* **2006**, *357*, 1383-1393.

(55)   Madhusudan, S.; Smart, F.; Shrimpton, P.; Parsons, J. L.; Gardiner, L.; Houlbrook, S.; Talbot, D. C.; Hammonds, T.; Freemont, P. A.; Sternberg, M. J. E.; Dianov, G. L.; Hickson, I. D. *Nucl. Acids Res.* **2005**, *33*, 4711-4724.

CHAPTER 5

MICROFLUIDIC DEVICE WITH INTEGRATED CONDUCTIVITY SENSOR FOR QUANTITATIVE ENUMERATION OF CIRCULATING TUMOR CELLS (CTCS): AN APPROACH TO CLINICAL EVALUATION OF DRUG EFFICACY

5.1 Introduction

Hematogenous spread of metastatic carcinomas is the reason for most cancer-related mortalities.[1] For Breast cancer, the death rate is estimated to be ~45,000 deaths per year in women.[2] Therefore, intensified research effort is required to develop simple techniques that can monitor the effectiveness of cancer therapies, and at the same time could support the successful search for suitable therapeutic agents, as well as promote early diagnosis of the disease to enhance survival rate of cancer patients. Whilst tumors, such as breast cancer have been traditionally diagnosed using a combination of radiological, surgical biopsy, as well as pathological assessment of tissue samples based on morphological and immunohistochemical characteristics, requiring evaluation of tissue samples under a microscope, the process has proved to be invasive and time consuming and is also accompanied with high rates of false positive results, which range from 20 – 50%.[3,4] A clear understanding of the stages in tumor metastases could provide an avenue for developing new tools for early tumor diagnosis which will allow for appropriate and timely administration of cancer therapies. Classical views envisioned metastasis as a late process in tumor progression; however, it has been shown that dissemination of cancer cells to distant organs is an early process in tumorigenesis, especially in breast cancer.[5-7] There are two main routes for cancer cell dissemination to distant organs; these are the bone marrow (BM) and peripheral blood of cancer patients. While there is evidence that the BM serves as a homing reservoir for tumor cells of many types of carcinomas, the peripheral blood

serves as a transportation medium through which distant sites are effectively accessed by tumor cells.[8-11] This indicates that the number of tumor cells in peripheral blood and also in BM can reflect tumor burden at all stages of cancer progression. Therefore, the detection and characterization of tumor cells in BM and in circulating peripheral blood has gained significant attention in cancer research.[12] Disseminated tumor cells (DTCs) and circulating tumor cells (CTCs) are two nomenclatures used to describe tumor cells in bone marrow and peripheral blood, respectively, and both present clinical significance in cancer management.[9]

Quantitative assessment of DTCs and CTCs can facilitate early detection of cancer and its successful treatment, as well as indicating survival probability of cancer patients.[13] In addition, it can be used for real-time monitoring of systemic anticancer therapies in clinical management of several cancer-related diseases to provide information such as the success or failure of therapeutic agents.[14] Furthermore, it can serve as an indicator to guide the development and clinical evaluation of new cancer drugs,[12,15,16] for example in the search for suitable therapeutic agents for L1-Endonuclease and APE1 (see chapter 3).

Although, the detection of DTCs in BM has been hypothesized to be of superior clinical significance compared to CTCs in blood,[17,18] sampling BM for DTCs enumeration during routine procedures in clinical management of cancer patients is invasive, time consuming, and uncomfortable for the patients. Moreover, sampling modality of BM is difficult to perform in certain situations, such as during control visits at outpatient centers, which can hamper repeated analysis. As a result, efforts have been concentrated on CTC enumeration in peripheral blood,[12,19] which has also assumed a

leading role in cases such as gastrointerstinal cancer, where dissemination of cancer cells to BM is rare.[20]

The major challenge with quantitative enumeration of CTCs is the ability to make determination of the extremely low abundance of these cells among high numbers of co-existing cells, such as erythrocytes and leukocytes. For example, 1 mL of whole blood may harbor < 10 CTCs but have $>10^9$ erythrocytes and $>10^6$ leukocytes.[13]

There are two main approaches to CTC detection; these are, immunological assays (immunocytochemistry) that employ monoclonal antibodies directed against certain membrane protein targets specifically expressed in cancer cells (e.g. cytokeratins), and the other being PCR-based molecular assays, such as reverse transcriptase (RT)-PCR and quantitative PCR (qPCR), which target tissue specific gene expression,[21-23] and utilize detection methods, such as fluorescence in-situ hybridization (FISH) to identify gene aberrations and measure tumor-associated gene expression.[24] Unfortunately, these methods are usually preceded by an enrichment procedure, such as immunomagnetic bead techniques,[25,26] and are associated with poor quantitative results,[27] long preparation times, expensive experimental equipment and lack of methodological standardization. Thus, developing CTC detection methods that are more sensitive, and highly reproducible are still required.

Several research findings have shown that cells of different types or in distinct biological states have different dielectric properties,[28-30] and this difference in dielectric nature has been used to select certain biological cells from mixed populations based on differential dielectrophoretic (DEP) forces.[31-33] Wang *et al.*[34] used this principle in combination with field-flow-fractionation to separate human breast cancer cells from T-lymphocytes and hematopoietic stem cells. Becker *et al.*[35] also demonstrated that the

dielectric properties of metastatic human breast cancer cells are significantly different from those of erythrocytes and T-lymphocytes, and they used a dielectric affinity column to remove tumor cells from dilute blood. These approaches are based on the fact that biological cells become electrically polarized when subjected to an alternating electric field,[31] and the degree of polarization of these cells depends strongly on their composition, morphology, and phenotype and is also highly dependent on the frequency of the applied electrical field, thereby enabling the selection of these cells.[36] This results in cells of different types and in different physiological states having distinctly different dielectric properties. [37]

Information secured from electrical impedance spectroscopy (EIS) techniques opened up another venue for characterizing biological cells based on their electrical properties.[38-40] Han *et al.*[3] employed micro-impedance spectroscopy (μ-EIS) to discriminate human breast cancer cell lines of different pathological stages from normal human breast tissue cell lines.

While μ-EIS and DEP have been widely employed for cell characterization, they are not adept at selecting rare tumor cells from mixed populations due to the low throughput of these sampling techniques. Therefore, a more reliable method that provides high-speed quantitative detection and enumeration of cancer cells is needed. For example, simple electrical conductivity measurements can be configured in high flow rate systems to transduce cellular and molecular species traveling through an electrode pair. This was demonstrated by Galloway *et al.*[41] and McWhorter *et al.*[42] in the analysis of mono- and poly-anionic molecules and in the detection of polymerase chain reaction products.

The fundamental morphology of tumor cells indicates that they possess very low membrane potential and low impedance, resulting from the migration of the extracellular sodium ion (Na^+) in compensation for the depleted potassium ion concentration (K^+) of the intracellular fluid.[43,44] Consequently, these cells are characterized with high intracellular Na^+ concentration.[44] This sustained elevation of intracellular sodium acts as a mitotic trigger causing cells to divide rapidly.[45] In the resting phase, normal cells maintain a high membrane potential at around 60 mV to 100 mV, but when mitosis and DNA synthesis begin, the membrane potential falls to around 15 mV.[46] Thus, an increased rate of cell division associated with tumor cells constantly keeps them at a low membrane potential. In addition, tumor cells have different lipid and sterol contents in their membrane when compared to normal cells.[47] This altered membrane composition disrupts the membrane permeability, which results in the movement of potassium, magnesium and calcium out of the cell while accumulating sodium and water in the cell.[48] Also, the alteration in the cell membrane content with respect to the types of glycoproteins and antigens that tumor cells express result in an increase in the number of negatively charged sialic acid molecules that cap the tips of glycoproteins and glycolipids that extend outward from the cell membrane.[49,50] The inability of tumor cells to produce cellular energy: adenosine tri-phosphate (ATP) is another factor responsible for the high rate of transmembrane movement of the mineral contents of the cell. A steady supply of cellular energy is required to maintain a normal concentration of intracellular minerals and a healthy membrane potential. These phenomena, which result in changes in the mineral contents of the cell, increase the intracellular concentration of positively-charged sodium ions and also generate an increase in negative charges on the cell coat (glycocalyx),[51,52] which are the major factors causing

cancer cells to have lower membrane potentials compared to healthy cells.[53] This makes tumor cells highly conductive amidst normal erythrocytes and leukocytes, thus prompting the design of appropriate conductivity systems for their selective quantification.

Conductivity detection is an electrochemical technique with the ability of detecting small changes in ionic composition of tiny amount of solution, which could result from the presence of minute species in a miniaturized system and thus, has found utility in micro-fluidic applications,[41,42,54] in which fluidic channels can be configured to closely parallel the size of molecular species. The effectiveness of this detection technique is highly dependent on the electronic design of the conductivity system to provide optimal sensitivity appropriate for interrogating single cells, such as CTCs.[55,56] The conductivity response (G) is defined with the following expression:

$$G = (\lambda_+ + \lambda_-)C/1000K \qquad (5.1)$$

where λ_+ and λ_- (S cm^2 equiv^{-1}; S = Siemens) are the limiting ionic conductances of cations and anions in solution, C is the solution concentration and K is the cell constant (K = L/A, where L is the distance between the electrode pair and A is the area of the electrode). Reducing the spacing between the electrodes and/or increasing the area of the electrodes will increase the magnitude of G (by reducing K) and consequently improve the detection limit of the conductivity measurement.

In this study, we designed a simple but very sensitive microfluidic-based conductivity detection system, which was constructed with platinum (Pt) wires that were integrated into a PMMA-based microfluidic device fabricated by hot-embossing and high precision micromilling. The fluidic channel and the cell constant (defined by the

electrode geometry) were carefully scaled to nearly parallel the size of tumor cells. The detection system demonstrated high efficiency enumeration of tumor cells in seeded samples that were hydrodynamically transported through the fluidic channels and the electrode pair. Smaller cells with different electrical properties, such as red blood cells, were not detected using the present conductivity cell configuration due to low signal-to-noise ratio for this cell type. The ability of the detection system to selectively detect CTCs in blood samples was demonstrated via its integration with a microfluidic-based, high throughput micro sampling unit for CTC isolation and subsequent label-free enumeration without interference from erythrocytes and leucocytes.

5.2 Experimental

5.2.1 Reagents and Materials

Human breast cancer cell line, MCF-7 was used as a model for CTC detection which was studied along with other co-existing cells in blood: the white blood cells (WBC) and red blood cells (RBC). The Jurkad E6 cell line was used as a model for white blood cells in this study.

MCF-7 and WBC were purchased from ATCC cultures, USA. RBC, tris(hydroxylmethyl)aminomethane (TRIS), glycine, trypsin (proteomic grade) and Tween-20 detergent were purchased from SIGMA ALDRICH, USA. The measurement buffer was prepared from TRIS, glycine and Tween-20 detergent using nanopure water obtained from a Barnstead NANOpure system (Model D8991, Dubuque, IA).

5.2.2 Microscopy

Axiovat 200M (Zeiss) fitted with a CCD video camera (JAI CV 252) was used for cell visualization and to acquire real time video microscopy information during conductivity measurement. The video camera was operated at a frame rate of 30 fps.

5.2.3 Cell Culturing and Sample Preparation

MCF-7 cells were cultured in Dubelco modified Eagle's medium for 2 days at $37^{\circ}C$, then harvested using 0.25% trypsin and resuspended in the same medium. Prior to conductivity measurements, a portion of the cell suspension was centrifuged for 2 min at 300 rcf, then washed twice with Tris-glycine buffer (0.18 mM Tris, 47 mM Glycine and 0.05 % Tween 20) to completely eliminate residual growth medium. The resulting cells were re-suspended in the same buffer and counted using a hemocytometer to obtain working samples. WBCs were grown under the same condition as those used for MCF-7 cells, harvested from the culture plate with slight agitation and re-suspended in the measurement buffer (Tris-glycine buffer with Tween-20) from which working samples were obtained as described earlier. A suspension of the RBCs (0.3 mL) was centrifuged and washed in the buffer (Tris-glycine, Tween-20), then re-suspended in the same buffer to obtain a stock sample from which dilutions were made and counted with the hemocytometer to obtain the required cell density.

5.2.4 Design of the Conductivity Detector

The design and electronic layout of the conductivity detector is shown in Figure 5.1. To reduce the effects of parasitic capacitance, C_p, due to wiring and electrode configuration, a synthetic inductor, L, of 132 mH was designed using a Gyrator circuit. Gyrators, for a given bandwidth, allow the creation of a high quality factor (Q) of inductors from resistance and capacitance (RC) components. Q is defined as;

$$Q = \omega L/R \qquad (5.2)$$

where ω is the angular frequency and R is the series resistance of the inductor, which represents energy lost by the inductor; Inductors of the size and Q needed would be

impossible to construct utilizing coils wound on ferrite materials. This inductance was placed in parallel with the capacitance C_p (produced by the electrical wiring), and the frequency varied to locate the resonance voltage across L and C_p. Once this resonance point was found, the voltage across the sample cell would be directly sensitive to changes in the solution conductivity, G_s. The equation for the impedance of the equivalent circuit consisting of the sample cell in parallel with the inductor is a third-order polynomial that makes the analytical determination of impedance difficult. But for typical circuit values near resonance, the absolute value of impedance is approximated with the expression:

$$/Z/ = 1/G_s \qquad (5.3)$$

where /Z/ is the absolute value of the impedance. The sine wave generator produced a waveform that could be adjusted from 0 to ±1 V in amplitude and 25–50 kHz in frequency. A target frequency of 40 kHz was chosen to minimize the impedance due to the double layer capacitance, C_d, and also hold the inductance to a reasonable value. This signal was fed to a transconductance amplifier, G_1, which converted the sinusoidal voltage to a current. The gain of G_1 was set to 10 µA/V. A current source was needed to drive the sample cell since a voltage source, with its low output impedance, would negatively impact the circuit's Q. For the experiments performed in this study, the current was set to ±5 µA. The required resonance frequency (f) could be approximated by the standard parallel resonance equation;

$$f = 1/2\pi(LC_p)^{1/2} \qquad (5.4)$$
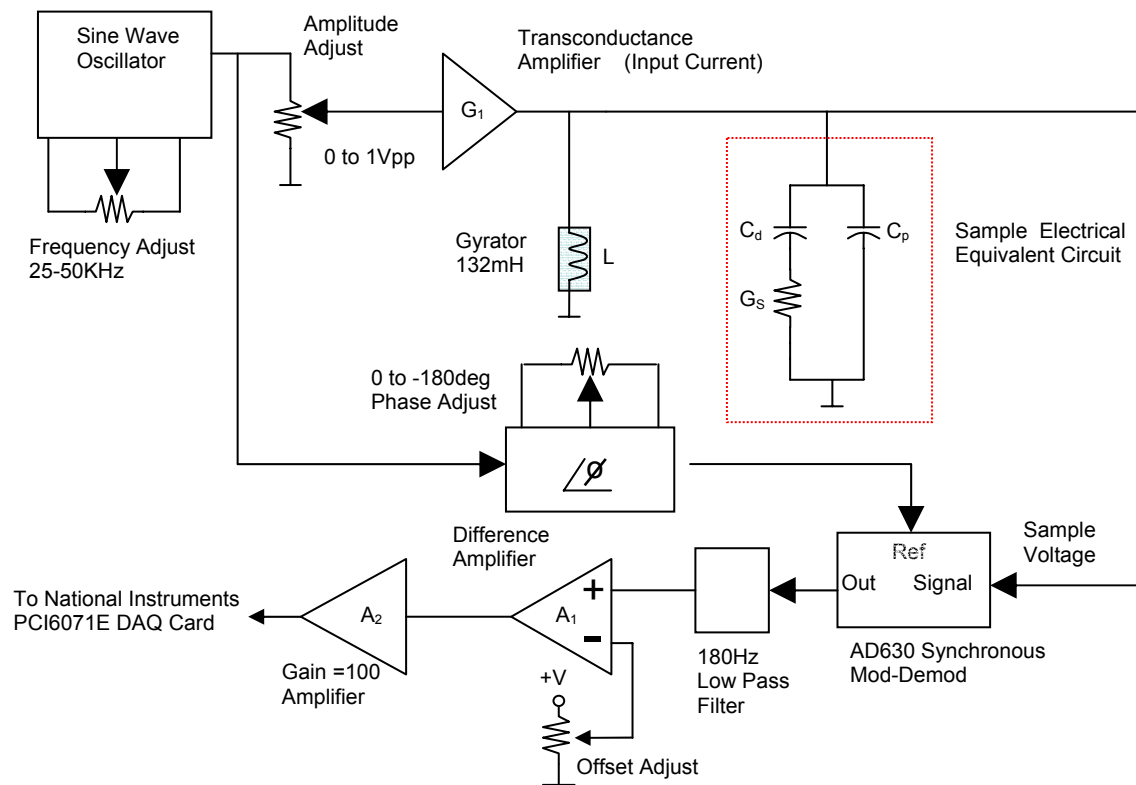
Figure 5.1 Electronic circuit diagram of the detector system. The bipolar waveform (±0.5V) was supplied by the sine wave oscillator, which was converted to AC current (±5µA) by the transconductance amplifier. The inductor L (132mH) was configured parallel to the sample equivalent circuit to cancel out the effect of parasitic capacitance C_p. The phase adjust was used to compensate for delay signal through the sample cell while the AD630 delivers phase synchronized signal through the low pass filter (180 Hz) and offset filter to the amplifier.

The voltage across the sample cell was fed to an analog device (AD630 synchronous modulator/demodulator, Norwood, MA) that was configured as a phase-sensitive detector. The AD630's reference input was driven from the phase-delayed sine wave oscillator output. This phase adjustment was needed to compensate for phase lags in the detected sample voltage. This voltage was then fed to a low-pass filter with a cut-off frequency of 180 Hz. The filter produced an averaged direct current (DC) signal that

was sent to a differencing amplifier, A_1. The difference amplifier serves to null the output to 0 V, such that any output other than 0 V provided, will be due solely to changes in the solution capacitance. A high gain amplifier, A_2, could amplify small changes in solution conductivity without saturation of the voltage produced by the buffer itself. A National Instruments PCI6071E, 12 bit A/D acquisition card was used to convert the analog signal to 12-bit data.

5.2.5 Fabrication of the Microfluidic Device with Integrated Electrodes for Conductivity Detection

Figure 5.2A shows the design of the microfluidic device with integrated Pt electrodes. The device was fabricated by a combination of hot embossing and high precision micro-milling as outlined in Figure 5.2B. The Pt wire (76 µm) was perfectly positioned on the surface of a PMMA wafer and tacked down at both ends with transparent adhesive tape (see Figure 5.2B). This was followed with embossing of the wire into the PMMA wafer using hot embossing technology (1200 psi for 4 min at 160°C). Prior to micro-milling, the PMMA chip with embossed Pt wire was flattened in a GC oven at 107°C for 12 min after being clamped between a pair of glass plates. A microchannel with dimension of 50 µm (width) x 80 µm (depth) was then constructed on the PMMA chip by micro-milling across the Pt wires to generate a pair of electrodes aligned with the wall of the channel. The distance between the electrodes paralleled the width of the channel (50 µm), thus generating a cell constant, $K = 110$ cm^{-1}. The micro-milled channel with the electrode assembly was sonicated for 2 min in water, dried and cleaned in isopropyl alcohol prior to being enclosed with a PMMA cover plate (125 µm thick PMMA) by thermal annealing at 107°C for 22 min to create the fluidic channel and the integrated Pt electrodes. The detection system possessed a probe volume of 226 pL which was adequate to

interrogate a single tumor cell traversing the micro electrodes based on size consideration.

a   b
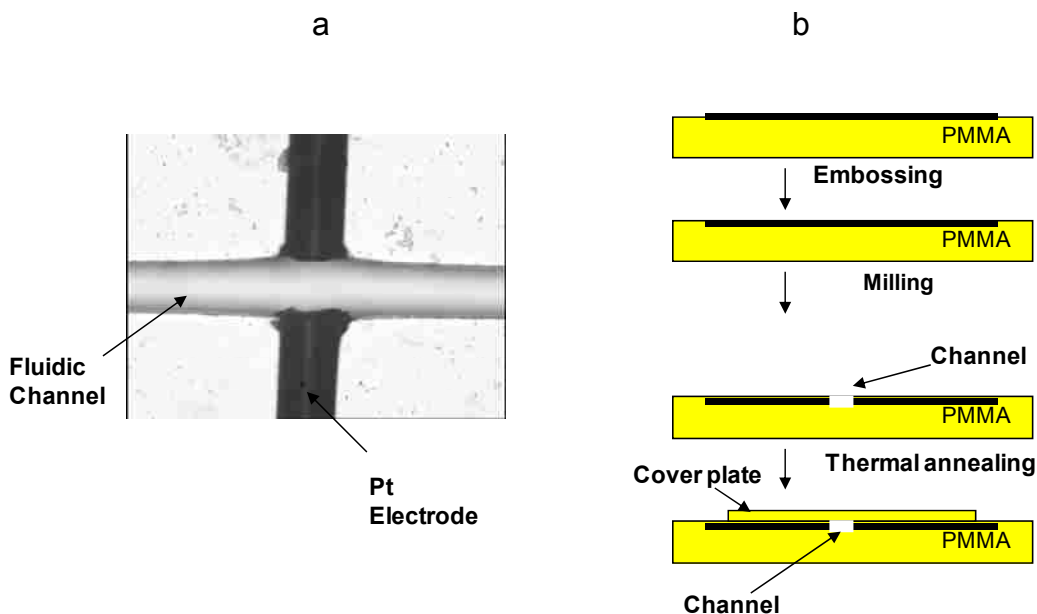
Figure 5.2 (a) Optical micrograph of the microfluidic device with integrated Pt electrodes. (b) Schematic presentation of the fabrication process for generating the microfluidic device with the integrated Pt electrodes. The Pt wire possessed a diameter of 76 µm.

5.2.6 Conductivity Measurements

All experiments were carried out using Tris-glycine buffer containing 0.18 mM Tris, 47 mM glycine and 0.05% vol/vol Tween-20 detergent as earlier mentioned. This buffer was chosen due to its very low conductivity (~50 µS/cm, pH 7.2) and the fact that it was able to prevent intercellular adhesion and non-specific adsorption of the cells to the surfaces of the fluidic chip. The experimental set-up for the conductivity measurement is shown in Figure 5.3. The integrated electrode pair (sensor) was connected to the conductivity detection box that housed the conductivity circuit (see section 5.2.4) which was used to generate the conductivity signal. Prior to the introduction of cell suspension into the integrated device, the buffer was

hydrodynamically pumped through the micro-channel using a syringe pump (see set-up in Figure 5.3), and the signal from the buffer was normalized to 0 (see also section 5.3.1). This was then followed with the cell suspensions (samples) prepared in the same buffer, which were hydrodynamically pumped through the channel at different flow rates (0.05 µl/min and 0.02 µl/min) in order to measure conductivity changes as single cells traversed through the detector. These flow rates were chosen based on the minimum sampling time (0.1 s) of the data acquisition software and to allow enough detection time (T_d) for a single cell traversing the electrodes. This time was calculated to be 0.3 s at 0.02 µl/min flow rate and 0.7 s at 0.05 µl/min flow rate. Thus, at higher flow rates, a cell spending less than 0.1 s in the detection volume (226 pL) will not be detected, and at lower flow rates, there will be peak broadening due to increased T_d and consequently increasing the length of the experiment. In addition, cell densities were chosen in agreement with these flow rates so as to keep the probability (P_c) of finding a single cell in the detection volume low (i.e. $P_c < 1$).
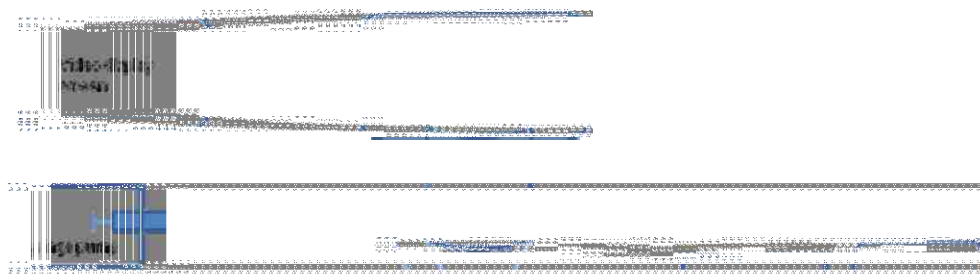
Figure 5.3 Schematic presentation of the experiment set-up for conductivity detection of cells and visualization with video microscopy. The fluidic channel was connected to the syringe pump via a capillary (OD =0.75 µm) and stabilized on a motorized stage of the video microscope. The video microscope was operated with a 20x microscope objective to acquire image at a frame rate of 30 fps. The electrode pair was connected to the detector which supplied the bipolar wave form for interrogating the cells.

5.3 Results and Discussion

5.3.1 Background Stabilization

The detection system herein reported for single-cell detection was characterized with a double-layer capacitance C_d and parasitic capacitance C_p (see Figure 5.1) that could generate high background signals which can mask the small signals generated from the single cells. To reduce such unwanted interference from the background signals, the offset filter (see Figure 1) was adjusted to bring the background signal to 0 when only buffer was introduced into the microchannel. The low-pass filter (180Hz) was used to minimize the random noise resulting from the AC components of the system's electronics to further improve the signal-to-noise ratio. Figure 5.4 shows a background adjusted conductivity plot of Tris-glycine buffer pumped through the microchannel. The absence of signal perturbations clearly indicates the stability of the generated signal and the conductivity electronics. In addition, no evidence of Faradaic reactions can be seen from this plot, which would generate "spikes" in the trace due to gas evolution. The absence of Faradaic reactions results from the bipolar pulse voltage waveform used at a frequency of 40KHz, which prevents double layer formation within the cell.[41]

5.3.2 Conductivity Measurement of Cell Suspensions

Conductivity measurements were performed using different cell densities and various flow rates (0.02 µL/min and 0.05 µL/min). Figure 5.5 shows the results obtained when MCF-7 cells at a concentration of 150 cells/µL (cell suspension prepared in buffer and counted with hemocytometer) was hydrodynamically transported through the device at a flow rate of 0.02 µL/min. Fifty-eight signals were registered (counted) from the volume (0.33 µL) processed, which indicated the presence of 58 cells with each signal
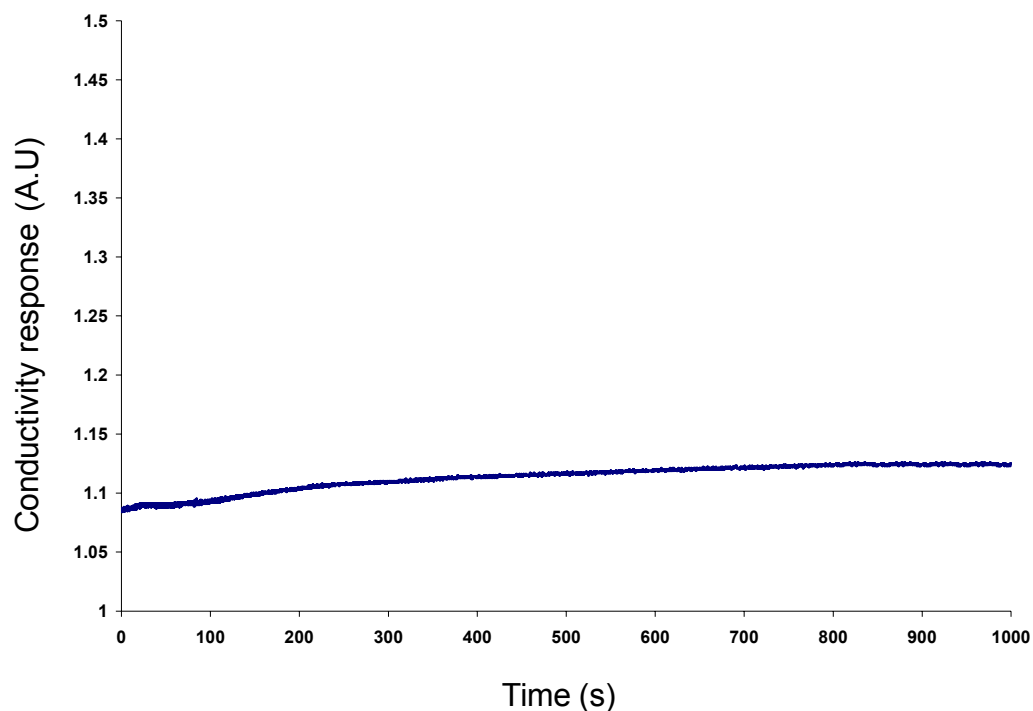
Figure 5.4 Background-adjusted conductivity plot with only the measurement buffer (Tris-glycine buffer) contained in microchannel. Experiment conditions used were; 40 KHz frequency, ±0.5V bipolar voltage, ±5µA alternating current (AC current), and a flow rate of 0.02µl/min

representing a single tumor cell as confirmed by video microscopy. With these values, the concentration measured was calculated to be 175 cells/µL, which agrees favorably to the input concentration. Figure 5.6 is the result obtained from MCF-7 cells using a concentration of 146 cells/µl and a flow rate of 0.05 µL/min. At these conditions, the number of cells registered was 122 cells and the total volume processed was 0.83 µL, providing a measured cell concentration of 147 cells/µL, again agreeing favorably to input concentration. Based on these observations, the detection and sampling efficiency of the detection system was estimated as ~100%.

Conductivity signals were verified with video microscopy (see Figure 5.3) acquired in real time with the conductivity measurement to confirm that each signal resulted from a single tumor cell traversing the electrodes. A video frame image of such

real time video acquisition is shown in Figure 5.7. The peak width obtained using 0.05

µl/min flow rate (see Figure 5.6) appeared smaller than those obtained using 0.02

µl/min flow rate (see Figure 5.5), which agrees with our expectations due to differences

in transit time (i.e T_d) of the cells in the detection volume at the different flow rates. The

cell densities (or cell concentration) of 146 cells/µL and 150 cells/µL were used with
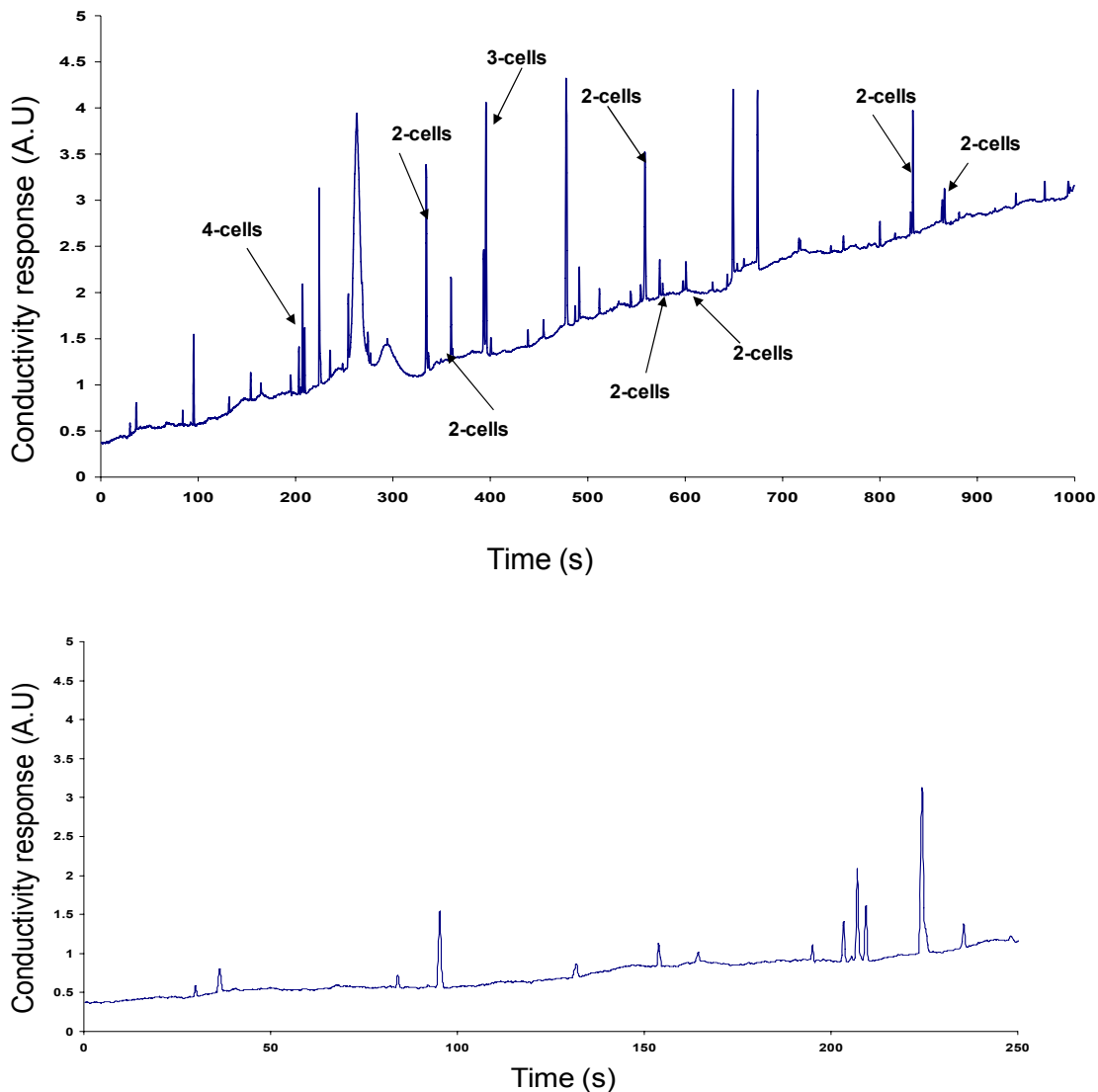
Figure 5.5 Conductivity response from MCF-7 cells ([cell] = 150 cells/µL) using tris-glycine buffer as the suspension medium and at a flow rate of 0.02 µl/min. Upper panel shows signal obtained over 1000s with a total of 58-cells registered from the volume processed (0.33 µL), the lower panel shows the signal over the first 300s. Experiments were run at a sampling time of 0.1s using ±5µA AC current, ±0.5 bipolar voltage, and 40KHz frequency.

these flow rates to keep the probability of finding a single cell in the detection volume per second at ~0.12 and ~0.05 respectively. This is important to avoid double occupancy during signal acquisition.

Because the goal of this project was to transduce and enumerate the presence of CTCs selected from whole blood, we anticipated that trace levels of white blood cells or red blood cells may be present in the sample to be interrogated using conductivity detection due to the high abundance of these cell types compared to the CTCs. For example, in 1 mL of whole blood, the number of white blood cells (WBCs) can be on the order of $>10^6$, and the red blood cell (RBCs) population could be $>10^9$.[13] In this same 1 mL of whole blood, the CTC abundance can be as low as <10 cells. Even if molecular recognition of particular integral membrane proteins specific for the CTCs were used to capture these cell types, residual WBCs or RBCs may be present due to non-specific types of interactions. The presence of these cells could give rise to false positives. Therefore, we investigated the ability of our conductivity detector to transduce WBCs and RBCs.

Measurement of WBC cell suspensions containing 150 cells/µL was carried out with the conductivity detector using a flow rate of 0.05 µL/min. Figure 5.8   shows the resulting conductivity response, clearly indicating that no signal were observed as these cells traversed through the electrode pair. Video microscopy revealed that the cells were traveling through the micro-electrodes, but during their observed travel, no conductivity signal from these cells was observed.

We next evaluated the ability of the conductivity detector to transduce RBCs. Conductivity measurement of RBC sample concentration of 150 cells/µL was generated; the resulting response is shown in Figure 5.8. As can be seen, no visible conductivity
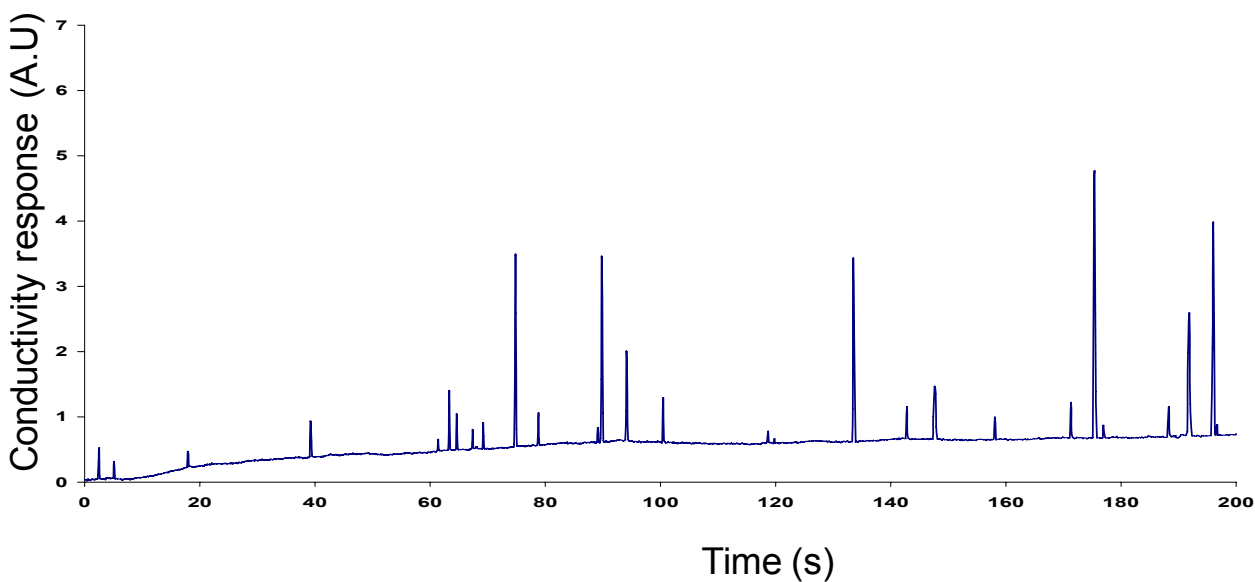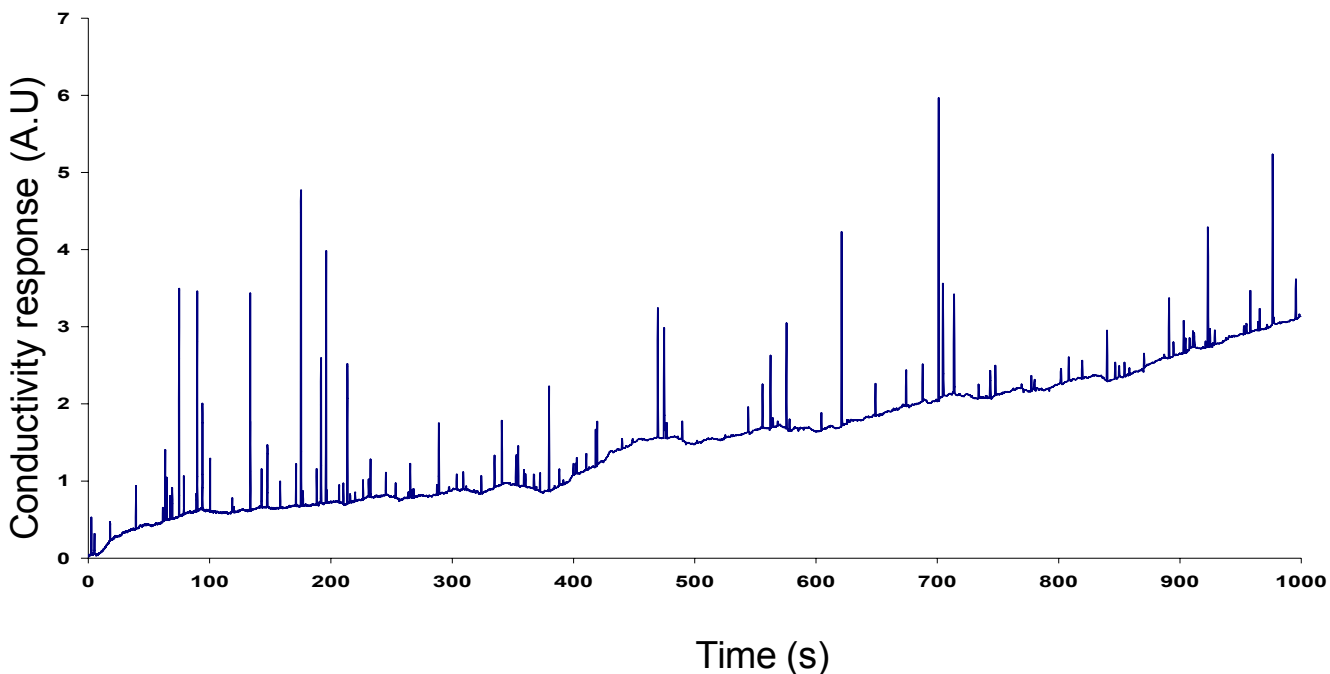
Figure 5.6 Conductivity response from MCF-7 cells ([cell] = 146 cells/ µL using tris-glycine buffer as the suspension medium and at a flow rate of 0.05 µL/min. Upper panel shows signal obtained over 1000s with a total of 122-cells registered from the volume processed (0.83 µL), the lower panel shows the signal over the first 200s. Experiments were run at a sampling time 0.1s using ±5µA AC current, ±0.5 bipolar voltage, and 40KHz frequency.

changes were observed as the RBCs traversed the electrode pair. The travel of single RBCs through the electrode pair was again verified using video microscopy.

The absence of signals produced for the RBCs and WBCs in the present case is due to both the electrical properties of these cells and their morphology (*i.e.*, cell size). In the present case, the conductivity response that is elicited is due to changes in the bulk solution conductance of the volume present between the electrode pair when single cells are resident within this volume. In the case of the tumor cells, their larger sizes compared to the WBCs and RBCs induces a larger perturbation on the measured conductance when they are resident in this interstitial space. For example, the average volume size of a CTC is 14 pL (d = 30 µm), for a RBC it is 0.06 pL (d = 5 µm) and finally the WBC volume is 1.7 pL (d = 15 µm). In our case, the interstitial volume between the electrodes is 226 pL and therefore, a CTC occupies 7% of this interstitial volume, while for RBCs it is only 0.03% and 0.7% for the WBC. Therefore, more buffer and its ionic components are displaced when a CTC is resident between the electrodes as compared to a RBC or WBC. In addition, the high ionic content of tumor cells and their low membrane potentials provides a much higher conductivity compared to RBCs and WBCs. These factors indicate that a much larger perturbation on the bulk solution conductance is affected when a tumor cell is present in the probing volume. While the RBCs and WBCs do produce a difference in the bulk solution conductance when they are resident in the probing volume, the perturbations is below the SNR of the measurement and as such, are not seen. Scaling down the size of the probing volume by reducing the electrode size and spacing would provide better opportunities for transducing these cells (i.e. in cases where their signals is vital, for example in apoptosis study) using conductivity detection.

5.3.3 Calibration Plot

To establish the counting efficiency of our detector with regards to CTCs, different cell densities (10 -250 cells/µL, in tris-glycine buffer) were measured using the same experiment conditions (±0.5 V bipolar voltage, ±5 µA AC current, 40 KHz frequency and 0.05 µL/min flow rate). Five replicate measurements were averaged and a calibration plot was constructed (see Figure 5.9). The obtained slope (0.998) and correlation coefficient (r = 0.9998) clearly indicates the high accuracy and precision of the detector in enumerating CTCs.
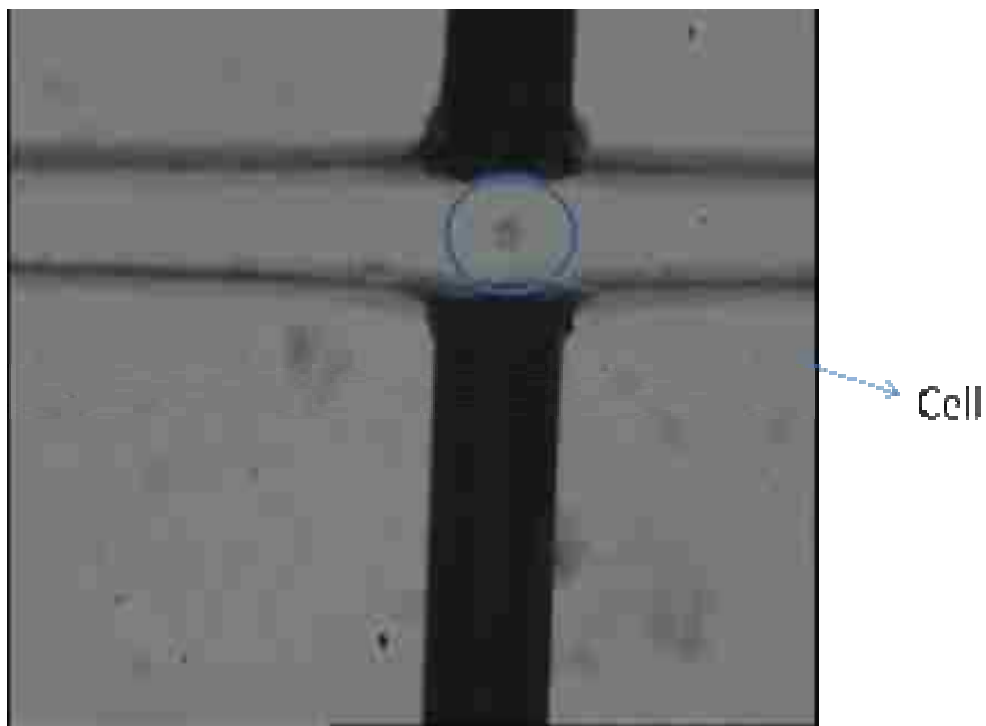
Figure 5.7 Video frame image acquired with video microscope showing a tumor cell as it traversed the electrode pair. This image was acquired in real time with conductivity measurement.
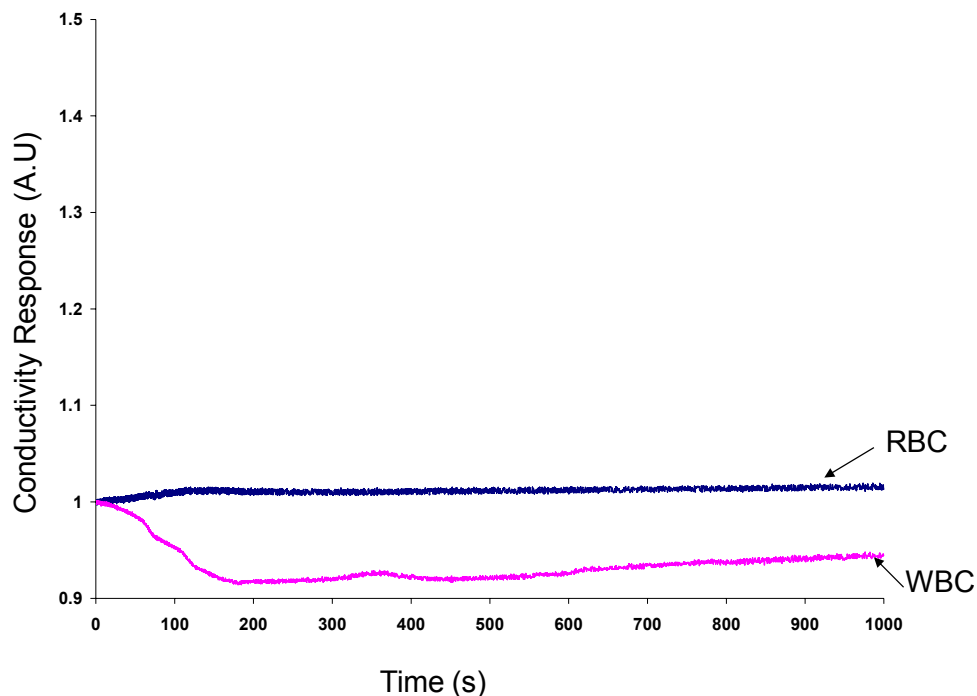
Figure 5.8 Conductivity response from WBCs (cell density =150 cells/µL in tris-glycine buffer) and RBCs (cell density = 150 cells/µL in tris-glycine buffer). Both cell suspensions were run at 0.05 µL/min flow rate using ±0.5V bipolar voltage, ±5 µA AC current and 40 KHz frequency.
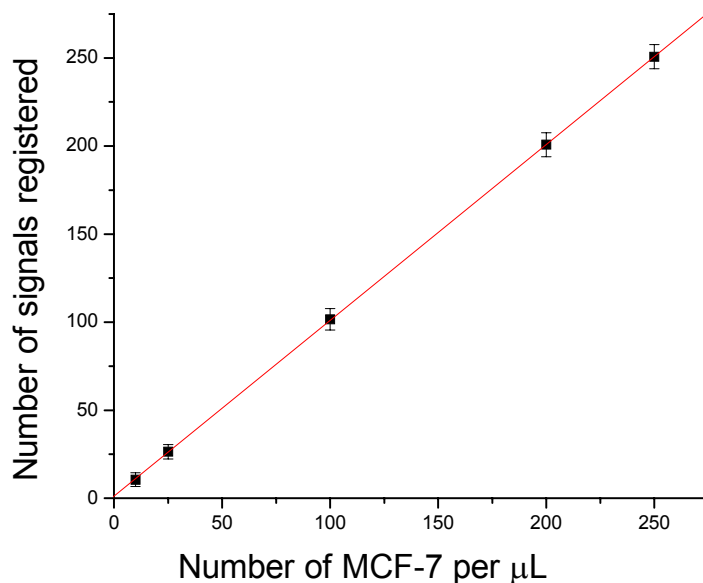
Figure 5.9 Calibration plot of different cell (MCF-7) densities (10 - 250 cells/µL in Tris Glycine bufer). Results were average from five replicate measurements of each sample processed at 0.05 µL/min flow rate using ±0.5V bipolar voltage, ±5µA AC current, and 40 KHz frequency (m = 0.998, r = 0.9998).

154

5.4 Integration of the Conductivity Detection System with a High Throughput Microsampling Unit (HTMSU) for CTCs Detection in Clinical Samples

The detection system herein reported was recently integrated with a high throughput microsampling unit (HTMSU) for label-free enumeration of isolated CTCs from whole blood.[57] The HTMSU contains 51 microsampling units (MSU), which were fabricated in PMMA and decorated with monoclonal antibody to specifically isolate CTCs from whole blood (see Figure 5.10). As a model clinical sample, citrated blood (1 mL) was seeded with 10 CTCs (MCF-7 breast cancer cell line) and processed with the HTMSU. Subsequently, a proteolytic CTC releasing buffer (Trypsin-tris-Glysine Buffer) was used to detach the captured CTCs from the HTMSU for label-free enumeration with the integrated conductivity sensor. In this study, 8 CTCs were successfully counted (see Figure 5.10E), which demonstrated high efficiency detection. In a similar assay, the system has been employed in enumerating prostate cancer cells (LNCaP) from blood samples.

5.5 Conclusion and Future Work

A highly sensitive integrated conductivity detector system consisting of a pair of Pt electrodes was developed for a PMMA-based microfluidic device to identify and enumerate CTCs isolated from clinical samples. The detector was able to detect CTCs, but due to scaling issues and their electrical properties, RBCs and WBCs could not be transduced. This is particularly attractive in this application, since the device is targeted for transducing CTCs and thus, will eliminate false positive signals generated from these interfering species. In addition, the conductivity transduction modality adopted herein will generate precise and accurate quantitative measurements of tumor cells

without the need for cell staining. This has already been demonstrated with high

efficiency via integration with microsystems for label-free enumeration of isolated CTCs
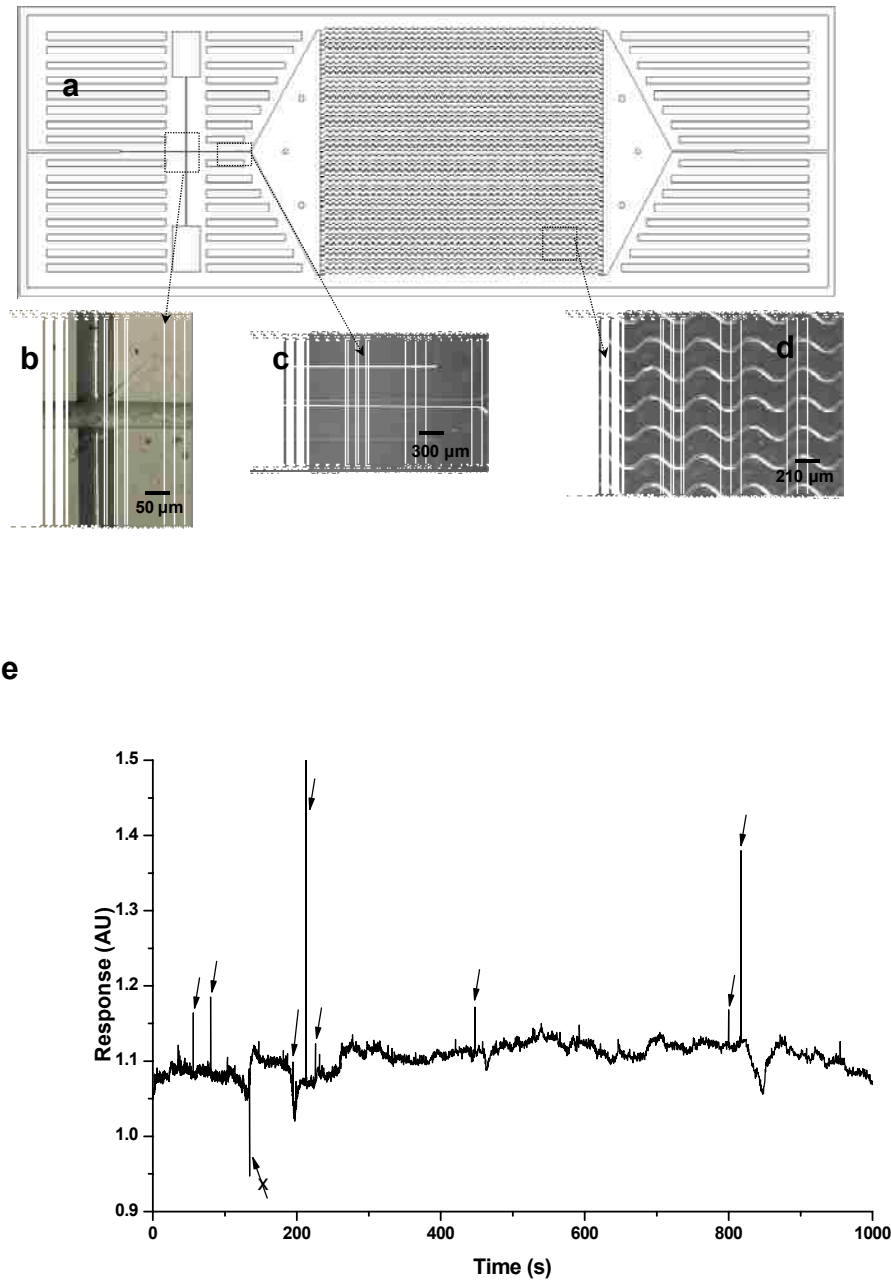
Figure 5.10 Top (labeled a) is the schematics of the HTMSU showing the integrated conductivity sensor (labeled b), a single port exit for detached cells (labeled c) and the sinusoidal cell capture channels (labeled d). Bottom (labeled e) is the conductivity response from a 1.0 mL of whole blood spiked with 10 CTCs and processed in the HTMSU followed by detachment (using a releasing buffer that was hydrodynamically pumped through the device at a flow rate of 0.05 µL/min) and enumeration of the CTCs. 8 CTCs were scored as indicated by the arrow. Adapted with permission.[57]

from whole blood associated with breast cancer,[57] and Prostate cancer (see section 5.4). In the experiment reported herein, tumor cells, RBCs and WBC were only used as examples; the detector can be configured to other application areas as well, such as selecting biopathogens from environmental or clinical samples. Furthermore, the detection system can serve as a tool for investigating the efficacy of therapeutic agents by monitoring CTCs from blood samples of patients under clinical management. This could expand its utility to clinical evaluation of drug candidates in the drug discovery process (e.g. clinical trial).

We are currently working on the detection and quantification of pathogens and bacteria in environmental samples as well as biological samples with a careful manipulation of their electrical properties. Tumor cells of epithelia origin including those of liver, colon, duodenum, bladder, Lung and stomach are currently being cultured for further application of this method. The detection and quantification of these mixed cells will be followed with molecular profiling using a highly sensitive fluorescence detection method for diagnostic information (see Chapter 2).

5.6 References

(1)   Eccles, S. A.; Welch, D. R. *Lancet* **2007**, *369*, 1742-1757.

(2)   Han, K. H.; Han, A.; Frazier, A. B. *Biosens. Bioelectron.* **2006**, *21*, 1907-1914.

(3)   Han Ki-Ho, H. A., Frazier Bruno *Biosens. Bioelectron.* **2006**, *21*, 1907 - 1914.

(4)   Elmore, J. G.; Barton, M. B.; Moceri, V. M.; Polk, S.; Arena, P. J.; Fletcher, S. W. *N. Engl. J. Med.* **1998**, *338*, 1089-1096.

(5)   Husemann, Y.; Geigl, J. B.; Schubert, F.; Musiani, P.; Meyer, M.; Burghart, E.; Forni, G.; Eils, R.; Fehm, T.; RiethmUller, G.; Klein, C. A. *Cancer Cell* **2008**, *13*, 58-68.

(6)   Fehm, T.; Sagalowsky, A.; Clifford, E.; Beitsch, P.; Saboorian, H.; Euhus, D.; Meng, S. D.; Morrison, L.; Tucker, T.; Lane, N.; Ghadimi, B. M.; Heselmeyer-Haddad, K.; Ried, T.; Rao, C.; Uhr, J. *Clin. Canc. Res.* **2002**, *8*, 2073-2084.

(7)   Racila, E.; Euhus, D.; Weiss, A. J.; Rao, C.; McConnell, J.; Terstappen, L.; Uhr, J. W. *Proc. Natl. Acad. Sci. USA* **1998**, *95*, 4589-4594.

(8)   Pantel, K.; Alix-Panabieres, C. *Nature Clin. Pract. Oncology* **2007**, *4*, 62-63.

(9)   Pantel, K.; Brakenhoff, R. H. *Nature Rev. Canc.* **2004**, *4*, 448-456.

(10)   Muller, V.; Stahmann, N.; Riethdorf, S.; Rau, T.; Zabel, T.; Goetz, A.; Janicke, F.; Pantel, K. *Clin. Canc. Res.* **2005**, *11*, 3678-3685.

(11)   Meng, S. D.; Tripathy, D.; Frenkel, E. P.; Shete, S.; Naftalis, E. Z.; Huth, J. F.; Beitsch, P. D.; Leitch, M.; Hoover, S.; Euhus, D.; Haley, B.; Morrison, L.; Fleming, T. P.; Herlyn, D.; Terstappen, L.; Fehm, T.; Tucker, T. F.; Lane, N.; Wang, J. Q.; Uhr, J. W. *Clin. Canc. Res.* **2004**, *10*, 8152-8162.

(12)   Pantel, K.; Brakenhoff, R. H.; Brandt, B. *Nature Rev. Canc.* **2008**, *8*, 329-340.

(13)   Cristofanilli, M.; Budd, G. T.; Ellis, M. J.; Stopeck, A.; Matera, J.; Miller, M. C.; Reuben, J. M.; Doyle, G. V.; Allard, W. J.; Terstappen, L.; Hayes, D. F. *New Engl. J. Med.* **2004**, *351*, 781-791.

(14)   Braun, S.; Marth, C. *New Engl. J. Med.* **2004**, *351*, 824-826.

(15)   Paterlini-Brechot, P.; Benali, N. L. *Canc. Lett.* **2007**, *253*, 180-204.

(16)   Cristofanilli, M.; Mendelsohn, J. *Proc. Natl. Acad. Sci. USA* **2006**, *103*, 17073-17074.

(17)   Wiedswang, G.; Borgen, E.; Schirmer, C.; Karesen, R.; Kvalheim, G.; Nesland, J. M.; Naume, B. *Intl. J. Canc.* **2006**, *118*, 2013-2019.

(18)   Benoy, I. H.; Elst, H.; Philips, M.; Wuyts, H.; Van Dam, P.; Scharpe, S.; Van Marck, E.; Vermeulen, P. B.; Dirix, L. Y. *Brit. J. Canc.* **2006**, *94*, 672-680.

(19)   Ignatiadis, M.; Xenidis, N.; Perraki, M.; Apostolaki, S.; Politaki, E.; Kafousi, M.; Stathopoulos, E. N.; Stathopoulou, A.; Lianidou, E.; Chlouverakis, G.; Sotiriou, C.; Georgoulias, V.; Mavroudis, D. *J. Clin. Oncology* **2007**, *25*, 5194-5202.

(20)   Soeth, E.; Grigoleit, U.; Moellmann, B.; Roder, C.; Schniewind, B.; Kremer, B.; Kalthoff, H.; Vogel, I. *J. Canc. Res. Clin. Oncology* **2005**, *131*, 669-676.

(21)   Ladanyi, A.; Soong, R.; Tabiti, K.; Molnar, B.; Tulassay, Z. *Clin. Chem.* **2001**, *47*, 1860-1863.

(22) Xi, L.; Nicastri, D. G.; El-Hefnawy, T.; Hughes, S. J.; Luketich, J. D.; Godfrey, T. E. *Clin. Chem.* **2007**, *53*, 1206-1215.

(23) Chen, T. F.; Jiang, G. L.; Fu, X. L.; Wang, L. J.; Qian, H.; Wu, K. L.; Zhao, S. *Lung Cancer* **2007**, *56*, 105-114.

(24) Fehm, T.; Solomayer, E. F.; Meng, S.; Tucker, T.; Lane, N.; Wang, J.; Gebauer, G. *Cytotherapy* **2005**, *7*, 171-185.

(25) Weihrauch, M. R.; Skibowski, E.; Koslowsky, T. C.; Voiss, W.; Re, D.; Kuhn-Regnier, F.; Bannwarth, C.; Siedek, M.; Diehl, V.; Bohlen, H. *J. Clin. Oncology* **2002**, *20*, 4338-4343.

(26) Cabioglu, V.; Igci, A.; Yildirim, E. O.; Aktas, E.; Bilgic, S.; Yavuz, E.; Muslumanoglu, M.; Bozfakioglu, Y.; Kecer, M.; Ozmen, V.; Deniz, G. *Amer. J. Surg.* **2002**, *184*, 414-417.

(27) Jung, R.; Petersen, K.; Kruger, W.; Wolf, M.; Wagener, C.; Zander, A.; Neumaier, M. *Brit. J. Cancer* **1999**, *81*, 870-873.

(28) Gascoyne, P. R. C.; Wang, X. B.; Huang, Y.; Becker, F. F. *IEEE Transact. Industry Appl.* **1997**, *33*, 670-678.

(29) Wang, X. B.; Huang, Y.; Gascoyne, P. R. C.; Becker, F. F.; Holzel, R.; Pethig, R. *Biochimica Et Biophys. Acta-Biomembranes* **1994**, *1193*, 330-344.

(30) Foster, K. R.; Schepps, J. L. *J. Microwave Power Electromag. Energy* **1981**, *16*, 107-119.

(31) Yang, J.; Huang, Y.; Wang, X. B.; Becker, F. F.; Gascoyne, P. R. C. *Anal. Chem.* **1999**, *71*, 911-918.

(32) Cheng, J.; Sheldon, E. L.; Wu, L.; Uribe, A.; Gerrue, L. O.; Carrino, J.; Heller, M. J.; O'Connell, J. P. *Nature Biotechnol.* **1998**, *16*, 541-546.

(33) Djamgoz B.A. Mustafa, M. M., Zbigniew Madeja, Fraser P. Scott, Korohoda Wlodzimierz *J. Cell Sci.* **2001**, *114*, 2697 - 2705.

(34) Wang, X. B.; Yang, J.; Huang, Y.; Vykoukal, J.; Becker, F. F.; Gascoyne, P. R. C. *Anal. Chem.* **2000**, *72*, 832-839.

(35) Becker, F. F.; Wang, X. B.; Huang, Y.; Pethig, R.; Vykoukal, J.; Gascoyne, P. R. C. *Proc. Natl. Acad. Sci. USA* **1995**, *92*, 860-864.

(36) Pethig, R.; Kell, D. B. *Phy. Med.Biol.* **1987**, *32*, 933-970.

(37)   Labeed H Fatima, C. M. H., Thomas Hilary, Hughes P Michael *Biophysic. J.* **2003**, *85*, 2028 - 2034.

(38)   Rigaud, B.; Morucci, J. P.; Chauveau, N. *Critic. Rev. Biomed. Eng.* **1996**, *24*, 257-351.

(39)   Gomez R., B. R. *Biomed. Microdev.* **2001**, 201 -209.

(40)   Malich A, B. T., Facius M, Kleinteich I, Fleck M, Sauna D, Anderson R, Kaiser W.A *Nucl. Instrum. Methods Phy. Res. A* **2003**, *497*, 75 - 81.

(41)   Galloway Michelle, S. W., Henry Alysa, Ford M. Sean, Llopis Shawn, McCarley L. Robin, Soper A Steven *Anal. Chem.* **2002**, *74*, 2407 - 2415.

(42)   McWhorter Scott, S. A. S. *J. Chromatogr. A* **2000**, *883*, 1 - 9.

(43)   Cone, C. D. *Ann NY Acad. Sci.* **1975**, *238*, 420 - 435.

(44)   Cone, C. D. *Oncology* **1970**, *24*, 438 - 470.

(45)   Cone, C. D. *Boca Raton, Florida: CRC Press* **1985**.

(46)   Cure, J. C. *Jupiter, Florida* **1995**.

(47)   Revici, E. *Princeton, NJ: D. Van Nostrand Company* **1961**.

(48)   Seeger, P. G., Wolz, S *Gesamtherstellung: Neuwieder Verlagsgesellschaft mbH* **1990**.

(49)   Warren, L., Fuhrer, J. P., Buck C. A. *Proc. Natl. Acad. Sci. USA* **1972**, *69*, 1838 - 1842.

(50)   Hakomori, S. S. *Immunol. Allergy Clin. North Am.* **1990**, *10*, 781 - 802.

(51)   Hazelwood, C. K., Chang, D.C., Nichold B.J., Woesner, D.E. *Biophysic. J.* **1974**, *14*, 583 - 606.

(52)   Brewer, A. K., Passwater, R. *Am Lab 1976* **1976**, *10*, 37 - 45.

(53)   Cure, J. C. *Resonant* **1991**, *1*.

(54)   Shadpour Hamed, S. A. S. *Anal. Chem.* **2006**, *78*, 3519 - 3527.

(55)   Caserta K.J., H. F. J., Crouch S.R., and Enke C.G. *Anal. Chem.* **1978**, *50*, 1534 - 1541.

(56)   Johnson, D. E., Enke C.G. *Anal. Chem.* **1970**, *42*, 329 - 335.

(57)   Adams, A. A.; Okagbare, P. I.; Feng, J.; Hupert, M. L.; Patterson, D.; Gottert, J.; McCarley, R. L.; Nikitopoulos, D.; Murphy, M. C.; Soper, S. A. *J. Am. Chem. Soc.* **2008**, *130*, 8633-8641.

CHAPTER 6

SUMMARY AND FUTURE WORK

6.1 Summary

Microfluidics and single molecule detection (SMD) technologies were integrated with wide-field fluorescence technology to provide the ability to monitor biochemical reactions in a high throughput format with single molecule sensitivity. This integration of unique technologies presents an approach to revolutionize the drug discovery process through massive parallelization of processing units to increase data production rates while at the same time generating assay results with high statistical accuracy. The economic advantage of this integrated technology brought about by the exquisite capability for sample miniaturization to conserve precious biological reagents will undoubtedly minimize the cost of registering a validated drug for therapeutic administration. In addition, the system eliminates several bottlenecks associated with current technology for high throughput screening (HTS), which will greatly reduce automation complexities in drug discovery.

Background information related to SMD with emphasis on single molecule fluorescence was outlined in chapter 1. A thorough explanation of the basic principle of SMD together with the photophysical phenomena that impact fluorescent signal from single molecules was presented. In addition, Advances in single molecule fluorescence technology and its biochemical applications as well as the merger of microfluidics to SMD were discussed and reviewed.

In chapter 2, the design, performance and application of a novel wide-field optical system for high throughput SMD configured in a continuous flow format using microfluidics was presented. The system consisted of a microfabricated polymer-based

multi-channel fluidic network situated within the field-of-view (FoV) of the optical system for parallel sample processing. Photo transduction of molecular fluorescent signal was accomplished using an electron-multiplying CCD (EMCCD) operated in a frame transfer mode that allowed tracking single molecules as they passed through the illumination zone, as well as allowing for high speed data acquisition with 100 % duty cycle. The system was used to monitor biochemical reactions with single molecule sensitivity in a high throughput format.

In chapter 3, a novel cyclic olefin copolymer (COC) core waveguide embedded in PMMA and situated orthogonal to multiple fluidic channels along the width of a PMMA wafer was constructed and described. The waveguide system allowed for fluorescence detection from multiple fluidic channels using evanescent excitation and a CCD camera for parallel readout. Two methods of launching light into the embedded waveguide were evaluated; the use of a monolithic prism for effective laser launch into the waveguide and the use of an optical fiber coupled to the waveguide. The two designs generated a sufficient evanescent field for the wide field excitation of fluorescent dyes traveling above the waveguide in fluidic channels, which enabled reading fluorescent signal from multiple fluidic channels in a parallel format.

In chapter 4, a high density fluidic device with series of individual sample processors (fluidic network), configured in a small footprint suitable for optical imaging, was presented. The polymer microchip possessed multiple fluidic processors with an individual input reservoir for multi-sample analysis. An ultrasensitive fluorescence detection system with a large field-of-view (FoV) was used to transduce fluorescence signal simultaneously from each fluidic processor onto the active area of an electron multiplying charge coupled device (EMCCD). The utility of the multichannel network for

HTS with an optical system for producing the prerequisite sensitivity was demonstrated by parallel detection of fluorescent and non-fluorescent samples in the individual fluidic processors. In the present configuration, the fluidic system was characterized with 50-fold increase in sample throughput and a projected 400-fold increase with slight modification in channel dimensions.

In chapter 5, the construction of a novel microfluidic device with integrated conductivity sensor for quantitative enumeration of circulating tumor cells (CTCs) was described in detail. The system was designed to transduce conductivity signal from the few copies of CTCs present in blood without interference from the vast amount of co-existing erythrocytes and leukocytes. The conductivity transduction modalities generated precise and accurate quantitative measurements of tumor cells without the need for cell staining. The system presents an approach to the design of a viable tool for investigating the efficacy of therapeutic agents by monitoring CTCs in blood samples of patients under clinical management.

6.2 Future Work

6.2.1 HTS with APE1 as Therapeutic Target

As alluded previously in chapter 4 (section 4.4), a combinatorial library of potential drug candidates will be screened against APE1, a target that has been linked to radio- and chemo-resistance in human tumors. An oligonucleotide duplex will be designed to possess the apurinic (AP) site recognized by APE1. The substrate will be labeled with a fluorophore at the 5'-end of the sense strand and a quencher at the 3'-end of the antisense strand (see Figure 3.5). The high density fluidic device presented in chapter 4 and the optical system presented in chapter 2 will be employed in the screening experiments to monitor fluorescence signal from individual reactor channel

resulting from molecular perturbation in the substrate due to the activity of the enzyme in the presence of a small molecule inhibitor.

6.2.2 HTS with L1-Endonuclease (L1-EN) as Therapeutic Target

Similar to the assay described above, a library of small molecule inhibitors will be screened against L1-EN. In this case, the substrate will be designed to possess the consensus site (AATTTT motif) recognized by this enzyme (L1-EN).

6.2.3 Throughput Enhancement via Increased Fluidic Channel Density

A slight modification in the dimensions of the fluidic device presented in chapter 4 will be adopted to increase the number of individual reactor channels (increase the packing density of the channels) that can be probed in parallel using our optical system to further increase throughput in our HTS campaign. The production of a 1 µm wide channel (pitch = 1 µm) has commenced, which will allow interrogation of 100 vias when the system is operated with FoV of 200 µm, and 200 vias when the system is operated with FoV of 400 µm. The channel dimensions will be driven further to 500 nm (pitch = 500 nm), which will double the throughput by allowing interrogation of 200 vias and 400 vias using FoV of 200 µm and 400 µm respectively. These throughputs are higher than anticipated from our proposed microfluidic system for HTS (see Introduction: section 1.5, Figure 1.3).

6.2.4 Integration of the High Density Fluidic Network with Embedded Orthogonal Waveguide

The high density fluidic network described in chapter 4 will be integrated with the embedded orthogonal planar waveguide described in chapter 3. This integration will provide a system that will enhance fluorescence sensitivity in our HTS experiments.

6.2.5 Fluorescence Multiplexing Using Two-color Detection

The next goal of this project will be to modify the optical detection system presented in chapter 2 for two color detection. To achieve this color multiplexing capability, a spectrograph will be incorporated into the optical system for spectral sorting of fluorescence from different molecular species using two excitation sources. The two color excitation sources have already been constructed and shall be built upon to realize this goal.

Permission Request Response

Pimentel, Jada show details 6:14 PM (2 hours ago)

 to me

Thank you for your request for permission to reprint the figure cited in your e-mail below. Permission is granted provided that you obtain the author's permission (whenever possible), and you use the following acknowledgment (preferably on the page(s) where this material appears):

"Reprinted, with permission, from the Annual Review of Biochemistry, Volume 77 © 2008 by Annual Reviews   www.annualreviews.org"

The fee for this usage has been waived. Any subsequent use of this material would require submission of a new permission request. If I can be of further assistance, please do not hesitate to contact me.

Best wishes for success with your dissertation.

Sincerely,
Jada

Jada Pimentel
Human Resources Associate
ANNUAL REVIEWS
A Non-Profit Scientific Publisher
4139 El Camino Real
Palo Alto, CA 94306
tel. 650.843.6679
fax. 650.855.9815

Permissions

AW: Republication/Electronic Request Form

Rights DE show details 10:47 AM (3 minutes ago)

to me

Dear Customer,

Thank you for your email.

We hereby grant permission for the requested use expected that due credit is given to the original source.
For material published before 2007 additionally: Please note that the author's permission is also required.

If material appears within our work with credit to another source, authorisation from that source must be obtained.

Credit must include the following components:
- Books: Author(s)/ Editor(s) Name(s): Title of the Book. Page(s). Publication year. Copyright Wiley-VCH Verlag GmbH & Co. KGaA. Reproduced with permission.

- Journals: Author(s) Name(s): Title of the Article. Name of the Journal. Publication year. Volume. Page(s). Copyright Wiley-VCH Verlag GmbH & Co. KGaA. Reproduced with permission.

With kind regards

Bettina Loycke
****
Bettina Loycke
Copyright & Licensing Manager
Wiley-VCH Verlag GmbH & Co. KGaA
Boschstr. 12
69469 Weinheim
Germany

Phone: +49 (0) 62 01- 606 - 280
Fax: +49 (0) 62 01 - 606 - 332
Email: rights@wiley-vch.de
_____

Wiley-VCH Verlag GmbH & Co. KGaA
Location of the Company: Weinheim
Chairman of the Supervisory Board: Stephen Michael Smith
Trade Register: Mannheim, HRB 432833
General Partner: John Wiley & Sons GmbH, Location: Weinheim
Trade Register Mannheim, HRB 432296
Managing Directors : Christopher J. Dicks, Bijan Ghawami, William Pesce

-----Ursprüngliche Nachricht-----
Von: Johnson, Bradley - Hoboken
Gesendet: Mittwoch, 25. Februar 2009 17:14
An: Rights DE
Betreff: FW: Republication/Electronic Request Form

Brad Johnson, Permissions Assistant - John Wiley & Sons Inc. - 111 River St. - Hoboken, NJ
07030 - Mail Stop 4.02 - Ph: 201.748.6786 - Fax: 201.748.6008 - bjohns@wiley.com

Visit our website <http://www.wiley.com/go/permissions> for permissions information

-----Original Message-----
From: republication@wiley.com on www.wiley.com [mailto:webmaster@wiley.com]
Sent: Wednesday, February 25, 2009 11:13 AM
To: Republication
Subject: Republication/Electronic Request Form

A01_First_Name: Paul
A02_Last_Name: Okagbare
A03_Company_Name: Louisiana State University
A04_Address: 232 Choppin Hall
A05_City: Baton Rouge
A06_State: Louisiana
A07_Zip: 70803
A08_Country: USA
A09_Contact_Phone_Number: 2252523417
A10_Fax: 2255783458
A11_Emails: pokagb1@tigers.lsu.edu
A12_Reference:
A13_Book_Title: Angewandte Chemie: Angew. Chem. Int. Ed.
A40_Book_or_Journal: Journal
A14_Book_Author:
A15_Book_ISBN:

A16_Journal_Month: DOI: 10.1002/anie.200300647
A17_Journal_Year: 2005
A18_Journal_Volume: 44
A19_Journal_Issue_Number: Tinnefeld, P.; Sauer, M. Angew. Chem. Int. Ed. 2005, 44, 2642-2671
A20_Copy_Pages: Figure 3a and Figure 3b (on page 2646)
A21_Maximum_Copies: 1
A22_Your_Publisher: Louisiana State University
A23_Your_Title: Dissertation
A24_Publication_Date: May 2009
A25_Format: print
A41_Ebook_Reader_Type:
A26_If_WWW_URL:
A27_If_WWW_From_Adopted_Book:
A28_If_WWW_Password_Access:
A45_WWW_Users:
A29_If_WWW_Material_Posted_From:
A30_If_WWW_Material_Posted_To:
A42_If_Intranet_URL:
A32_If_Intranet_From_Adopted_Book:
A33_If_Intranet_Password_Access:
A48_Intranet_Users:
A34_If_Intranet_Material_Posted_From:
A35_If_Intranet_Material_Posted_To:
A50_If_Software_Print_Type:
A60_If_Other_Type:
A37_Comments_For_Request:

Permission

Paul
Okagbare

Prof. Markus Sauer show details 11:12 AM (34 minutes ago)

 to me

Permission granted.

All the best,

Markus Sauer

_____

Prof. Dr. Markus Sauer

Applied Laser Physics & Laser Spectroscopy

and

Bielefeld Institute for Biophysics and Nanoscience (BINAS)

Bielefeld University

Universitätsstr. 25

33615 Bielefeld

Germany

Phone: +49-521-106-5450 or 5451

Fax: +49-521-106-2958

http://www.physik.uni-bielefeld.de/experi/d3/

Von: Paul Okagbare [mailto:pokagb1@tigers.lsu.edu]
Gesendet: Mittwoch, 25. Februar 2009 18:09
An: tinnefeld@physik.uni-bielefeld.de; sauer@physik.uni-bielefeld.de
Betreff: Permission

- Show quoted text -

Dear Dr. Tinnefeld and Prof. Sauer,
I sincerely request permission to use Figure 3a and Figure 3b (on page 2646) of your article referenced below in my dissertation.

Tinnefeld, P.; Sauer, M. *Angew. Chem. Int. Ed.* **2005**, *44*, 2642-2671

I have already obtained permission from the publisher and require permission from you also.

Sincerely,
Paul Okagbare

Reply Forward

Philip Tinnefeld show details 11:14 AM (31 minutes ago) Reply

 to me, Markus

Dear Paul,

I have no objection. You may certainly use the figure. Good luck with the dissertation.

Best regards

Philip

Von: Paul Okagbare [mailto:pokagb1@tigers.lsu.edu]

Gesendet: Mittwoch, 25. Februar 2009 18:09
An: tinnefeld@Physik.Uni-Bielefeld.DE;   sauer@Physik.Uni-Bielefeld.DE
Betreff: Permission
- Show quoted text -

Dear Dr. Tinnefeld and Prof. Sauer,
I sincerely request permission to use Figure 3a and Figure 3b (on page 2646) of your article referenced below in my dissertation.

Tinnefeld, P.; Sauer, M. *Angew. Chem. Int. Ed.* **2005**, *44*, 2642-2671

I have already obtained permission from the publisher and require permission from you also.

Sincerely,
Paul Okagbare

Re: Request for permission

 Paul Workman show details 6:59 PM (10 minutes ago)

  to me
Sure fine PW

Professor Paul Workman PhD FMedSci FIBiol
Centre Director
Cancer Research UK Centre for Cancer Therapeutics
The Institute of Cancer Research
15 Cotswold Road
Sutton. Surrey SM2 5NG
UK
Tel: +44 (0) 208 722 4301
Fax: +44 (0) 208 722 4324

>>> Paul Okagbare <pokagb1@tigers.lsu.edu> 02/25/09 12:52 am >>>
Dear Dr. Workman,
The illustration (Figure 1) you presented in the article referenced
below,
that detailed the central role of HTS in the drug screening process,
nicely
represents the overview of the drug discovery process, and it is a nice
fit
for my dissertation. I am wondering if you could permit the use of
that
figure (Figure 1, page 149) in my dissertation.

        Aherne, G. W.; McDonald, E.; Workman, P. *Breast Canc.
Res.* *
2002*, *4*, 148-154.

Sincerely,

Paul Okagbare

The Institute of Cancer Research: Royal Cancer Hospital, a charitable Company Limited by Guarantee,
Registered in England under Company No. 534147 with its Registered Office at 123 Old Brompton Road,
London SW7 3RP.

This e-mail message is confidential and for use by the addressee only. If the message is received by
anyone other than the addressee, please return the message to the sender by replying to it and then delete
the message from your computer and network.

This is a License Agreement between Paul I Okagbare ("You") and The American Association for the Advancement of Science ("The American Association for the Advancement of Science") provided by Copyright Clearance Center ("CCC"). The license consists of your order details, the terms and conditions provided by The American Association for the Advancement of Science, and the payment terms and conditions.

All payments must be made in full to CCC. For payment instructions, please see information listed at the bottom of this form.

License Number 2136701225262
License date Feb 26, 2009
Licensed content publisher The American Association for the Advancement of Science
Licensed content publication Science
Licensed content title Illuminating Single Molecules in Condensed Matter
Licensed content author W. E. Moerner, Michel Orrit
Licensed content date Mar 12, 1999
Type of Use Thesis
Requestor type Other Individual
Format Electronic
Portion Text Excerpt
Order reference number 3000168314
Title of your thesis /
dissertation
Polymer-based microfluidic devices for high throughput single
molecule detection: applications in drug discovery
Expected completion date Apr 2009
Estimated size(pages) 200
Total 0.00 USD
Terms and Conditions

American Association for the Advancement of Science TERMS AND CONDITIONS

Regarding your request, we are pleased to grant you non-exclusive, non-transferable permission, to republish the AAAS material identified above in your work identified above, subject to the terms and conditions herein. We must be contacted for permission for any uses other than those specifically identified in your request above.

The following credit line must be printed along with the AAAS material: "From [Full Reference Citation]. Reprinted with permission from AAAS."

All required credit lines and notices must be visible any time a user accesses any part of the AAAS material and must appear on any printed copies and authorized user might make.

This permission does not apply to figures / photos / artwork or any other content or materials included in your work that are credited to non-AAAS sources. If the requested material is sourced to or references non-AAAS sources, you must obtain authorization from that source as well before using that material. You agree to hold harmless and indemnify AAAS against any claims arising from your use of any content in your work that is credited to non-AAAS sources.

License Number 2136750518776
License Date Feb 26, 2009
Licensed content publisher American Chemical Society
Licensed content publication ACS Chemical Biology
Licensed content title A Survey of Single-Molecule Techniques in Chemical Biology
Licensed content author Cornish Peter V.† and Ha Taekjip‡*
Licensed content date Jan 1, 2007
Volume number 2
Issue number 1
Type of Use Thesis/Dissertation
Requestor type Not specified
Format Electronic
Portion Table/Figure/Chart
Number of
Table/Figure/Charts
1
Author of this ACS article No
Order reference number
Title of the thesis /
dissertation
Polymer-based microfluidic devices for high throughput single
molecule detection: applications in drug discovery
Expected completion date Apr 2009
Estimated size(pages) 200
Billing Type Invoice
Billing Address Louisiana State University
232 Choppin Hall
Baton Rouge, LA 70803
United States
Customer reference info
Total 0.00 USD
Terms and Conditions

AMERICAN CHEMICAL SOCIETY LICENSE
TERMS AND CONDITIONS
Feb 26, 2009

This is a License Agreement between Paul I Okagbare ("You") and American Chemical Society ("American Chemical Society") provided by Copyright Clearance Center ("CCC"). The license consists of your order details, the terms and conditions provided by American Chemical Society, and the payment terms and conditions.

All payments must be made in full to CCC. For payment instructions, please see information listed at the bottom of this form.

License Number 2136751018039
License Date Feb 26, 2009
Licensed content publisher American Chemical Society
Licensed content publication Analytical Chemistry
Licensed content title Imaging Single Fluorescent Molecules at the Interface of an Optical Fiber Probe by Evanescent Wave Excitation
Licensed content author Xiaohong Fang and Weihong Tan*
Licensed content date Aug 1, 1999
Volume number 71
Issue number 15
Type of Use Thesis/Dissertation
Requestor type Not specified
Format Electronic
Portion Table/Figure/Chart
Number of
Table/Figure/Charts
1
Author of this ACS article No
Order reference number
Title of the thesis /
dissertation
Polymer-based microfluidic devices for high throuhput single
molecule detection: applications in drug discovery
Expected completion date Apr 2009
Estimated size(pages) 200
Billing Type Invoice
Billing Address Louisiana State University
232 Choppin Hall
Baton Rouge, LA 70803
United States
Customer reference info
Total 0.00 USD
Terms and Conditions

**SPRINGER LICENSE
TERMS AND CONDITIONS**
Feb 26, 2009

This is a License Agreement between Paul I Okagbare ("You") and Springer ("Springer") provided by Copyright Clearance Center ("CCC"). The license consists of your order details, the terms and conditions provided by Springer, and the payment terms and conditions.

All payments must be made in full to CCC. For payment instructions, please see information listed at the bottom of this form.

License Number 2136730632232
License date Feb 26, 2009
Licensed content publisher Springer
Licensed content publication Analytical and Bioanalytical Chemistry
Licensed content title Polymer microfabrication technologies for microfluidic systems
Licensed content author Holger Becker
Licensed content date Jan 1, 2008
Volume number 390
Issue number 1
Pages 89 - 111
Type of Use Thesis / Dissertation
Details of use University intranet
Requestor Type Individual
Portion of the article Excerpts
Title of your thesis /
dissertation
Polymer-based microfluidic devices for high throughput single
molecule detection: applications in drug discovery
Expected completion date Apr 2009
Billing Type Invoice
Company Paul I Okagbare
Billing Address Louisiana State University
232 Choppin Hall
Baton Rouge, LA 70803
United States
Customer reference info
Total 0.00 USD
Terms and Conditions

Introduction

The publisher for this copyrighted material is Springer Science + Business Media. By clicking "accept" in connection with completing this licensing transaction, you agree that the following terms and conditions apply to this transaction (along with the Billing and Payment

RE: Permission Request Form: Paul Okagbare

CONTRACTS-COPYRIGHT (shared) show details 2:58 AM (11 hours ago) Reply

 to me

Dear Dr Okagbare

The Royal Society of Chemistry (RSC) hereby grants permission for the use of your paper(s) specified below in the printed and microfilm version of your thesis. You may also make available the PDF version of your paper(s) that the RSC sent to the corresponding author(s) of your paper(s) upon publication of the paper(s) in the following ways: in your thesis via any website that your university may have for the deposition of theses, via your university's Intranet or via your own personal website. We are however unable to grant you permission to include the PDF version of the paper(s) on its own in your institutional repository. The Royal Society of Chemistry is a signatory to the STM Guidelines on Permissions (available on request).

Please note that if the material specified below or any part of it appears with credit or acknowledgement to a third party then you must also secure permission from that third party before reproducing that material.

Please ensure that the thesis states the following:

Reproduced by permission of The Royal Society of Chemistry

and include a link to the article on the Royal Society of Chemistry's website.

Regards

Gill Cockhead

Contracts & Copyright Executive

Gill Cockhead (Mrs), Contracts & Copyright Executive

Royal Society of Chemistry, Thomas Graham House

Science Park, Milton Road, Cambridge CB4 0WF, UK

Tel +44 (0) 1223 432134, Fax +44 (0) 1223 423623

http://www.rsc.org

```
-----Original Message-----
From: pokagb1@tigers.lsu.edu [mailto:pokagb1@tigers.lsu.edu]
Sent: 25 February 2009 20:34
To: CONTRACTS-COPYRIGHT (shared)
Subject: Permission Request Form: Paul Okagbare
```

```
Name    : Paul Okagbare
```

```
Address :
```

```
232 Choppin Hall
```

Louisiana State University

```
Baton Rouge,
```

```
LA 70803
```

```
Tel     : 2252523417
```

```
Fax     : 2255783458
```

```
Email   : pokagb1@tigers.lsu.edu
```

```
I am preparing the following work for publication:
```

Article/Chapter Title : Polymer-based microfluidic devices for high
throughput single molecule detection

Journal/Book Title   : Dissertation

Editor/Author(s)   : Paul Okagbare

Publisher   : Louisiana State University

I would very much appreciate your permission to use the following material:

Journal/Book Title   : Analyst

Editor/Author(s)   : Paul I. Okagbare

Volume Number   : 134

Year of Publication   : 2009

Description of Material : Article

Page(s)   : 97-106

Any Additional Comments   :

I sincerely request permission to use this article in my dissertation

License Number 2136760426095
License Date Feb 26, 2009
Licensed content publisher American Chemical Society
Licensed content publication Journal of the American Chemical Society
Licensed content title Highly Efficient Circulating Tumor Cell Isolation from Whole Blood and Label-Free Enumeration Using Polymer-Based Microfluidics with an Integrated Conductivity Sensor
Licensed content author André A. Adams†, Paul I. Okagbare†, Juan Feng⊥, Matuesz L.

Hupert†§, Don Patterson§, Jost Göttert‖, Robin L. McCarley†§,

Dimitris Nikitopoulos‡§, Michael C. Murphy‡§ and Steven A.
Soper†‡§
Licensed content date Jul 1, 2008
Volume number 130
Issue number 27
Type of Use Thesis/Dissertation
Requestor type Not specified
Format Electronic
Portion Table/Figure/Chart
Number of
Table/Figure/Charts
4
Author of this ACS article Yes
Order reference number
Title of the thesis /
dissertation
Polymer-based microfluidic devices for high throughput single
molecule detection: applications in drug discovery
Expected completion date Apr 2009
Estimated size(pages) 200
Billing Type Invoice
Billing Address Louisiana State University
232 Choppin Hall
Baton Rouge, LA 70803
United States
Customer reference info

FW: Republication/Electronic Request Form

Johnson, Bradley - Hoboken show details 10:05 AM (11 minutes ago)   Reply

 to me

Dear Mr. Okagbare:

Please be advise permission is granted to reuse figure 1, pg. 234 and figure 5, pg. 236 from Cytometry 1999, 36:232-238 in your forthcoming Thesis which will be published by Louisiana State University. Credit must appear on every copy using the material and must include the title; the author (s); and/or editor (s); Copyright (year and owner); and the statement "Reprinted with permission of Wiley-Liss, Inc. a subsidiary of John Wiley & Sons, Inc." Please Note: No rights are granted to use content that appears in the work with credit to another source.

Good luck with your thesis

Sincerely,

Brad Johnson, Permissions Assistant - John Wiley & Sons Inc. - 111 River St. - Hoboken, NJ 07030 - Mail Stop 4.02 - Ph: 201.748.6786 - Fax: 201.748.6008 - bjohns@wiley.com

Visit our website <http://www.wiley.com/go/permissions> for permissions information

-----Original Message-----
From: republication@wiley.com on www.wiley.com [mailto:webmaster@wiley.com]
Sent: Wednesday, February 25, 2009 10:56 AM
To: Republication
Subject: Republication/Electronic Request Form

A01_First_Name: Paul
A02_Last_Name: Okagbare
A03_Company_Name: Louisiana State University
A04_Address: 232 Choppin Hall
A05_City: Baton Rouge
A06_State: LA
A07_Zip: 70803
A08_Country: USA
A09_Contact_Phone_Number: 2252523417
A10_Fax: 2255783458
A11_Emails: pokagb1@tigers.lsu.edu

A12_Reference:
A13_Book_Title: Cytometry
A40_Book_or_Journal: Journal
A14_Book_Author:
A15_Book_ISBN:
A16_Journal_Month: 23 February, 1999
A17_Journal_Year: 1999
A18_Journal_Volume: 36
A19_Journal_Issue_Number: Moerner, W. E.; Peterman, E. J. G.; Brasselet, S.; Kummer, S.; Dickson, R. M. Cytometry 1999, 36, 232- 238
A20_Copy_Pages: Figure 1 (on page 234) and Figure 5 (on page 236)
A21_Maximum_Copies: 1
A22_Your_Publisher: Louisiana State University
A23_Your_Title: Dissertation
A24_Publication_Date: May 2009
A25_Format: print
A41_Ebook_Reader_Type:
A26_If_WWW_URL:
A27_If_WWW_From_Adopted_Book:
A28_If_WWW_Password_Access: No
A45_WWW_Users:
A29_If_WWW_Material_Posted_From:
A30_If_WWW_Material_Posted_To:
A42_If_Intranet_URL:
A32_If_Intranet_From_Adopted_Book:
A33_If_Intranet_Password_Access:
A48_Intranet_Users:
A34_If_Intranet_Material_Posted_From:
A35_If_Intranet_Material_Posted_To:
A50_If_Software_Print_Type:
A60_If_Other_Type:
A37_Comments_For_Request:

Brad Johnson - Hoboken.vcf

Re: AIP Corp Correspondence

Dear Dr. Okagbare:

Thank you for requesting permission to reproduce material from American Institute of Physics publications.

Permission is granted – subject to the conditions outlined below – for the following:

Figures 1b and 6a:
Moerner, W.E., Fromm, D.P.
Rev. Sci. Instrum. 74, 3597-3619, 2003,

To be used in the following manner:

Reproduced as part of your dissertation.

1. The American Institute of Physics grants you the right to reproduce the material indicated above on a one-time, non-exclusive basis, solely for the purpose described. Permission must be requested separately for any future or additional use.

2. This permission pertains only to print use and its electronic equivalent, including CD-ROM or DVD.

3. The following copyright notice must appear with the material (please fill in the information indicated by capital letters): "Reprinted with permission from [FULL CITATION]. Copyright [PUBLICATION YEAR], American Institute of Physics."
Full citation format is as follows: Author names, journal title, Vol. #, Issue #, Page #, Year of publication.
For an article, the copyright notice must be printed on the first page of the article or book chapter. For figures, photographs, covers, or tables, the notice may appear with the material, in a footnote, or in the reference list.

4. This permission does not apply to any materials credited to sources other than the copyright holder.

5. If you have not already done so, please attempt to obtain permission from at least one of the authors. The author's address can be obtained from the article.

Please let us know if you have any questions.

Sincerely,

Susann Brailey

~~~~~~~~~~~~
Office of the Publisher, Journals and Technical Publications
Rights & Permissions
American Institute of Physics
Suite 1NO1
2 Huntington Quadrangle
Melville, NY 11747-4502
516-576-2268   TEL
516-576-2450   FAX
rights@aip.org

>>> <pokagb1@tigers.lsu.edu> 2/24/2009 9:00 PM >>>
Name: Paul Okagbare
Email: pokagb1@tigers.lsu.edu

Comments: In the article referenced below:
Moerner, W. E.; Fromm, D. P. Rev. Sci. Intrum. 2003, 74, 3597-3619.

I sincerely request permission to reprint the following figures in my
dissertation:

Figure 1b; page 3598
Figure 6a page 3609
Sincerely,
paul Okagbare

Permission

Dear Dr. Okagbare:

Thank you for requesting permission to reproduce material from American Institute of Physics publications.

Permission is granted – subject to the conditions outlined below – for the following:

Figure 8a, page 3611
Methods of single-molecule fluorescence spectroscopy and microscopy
Moerner, W. E.; Fromm, D. P. Rev. Sci. Instrum. 2003, 74, 3597-3619.

To be used in the following manner:

Reproduced in your dissertation for submission to Louisiana State University.

1. The American Institute of Physics grants you the right to reproduce the material indicated above on a one-time, non-exclusive basis, solely for the purpose described. Permission must be requested separately for any future or additional use.

2. This permission pertains only to print use and its electronic equivalent, including CD-ROM or DVD.

3. The following copyright notice must appear with the material (please fill in the information indicated by capital letters): "Reprinted with permission from [FULL CITATION]. Copyright [PUBLICATION YEAR], American Institute of Physics."
Full citation format is as follows: Author names, journal title, Vol. #, Issue #, Page #, Year of publication.
For an article, the copyright notice must be printed on the first page of the article or book chapter. For figures, photographs, covers, or tables, the notice may appear with the material, in a footnote, or in the reference list.

4. This permission does not apply to any materials credited to sources other than the copyright holder.

5. If you have not already done so, please attempt to obtain permission from at least one of the authors. The author's address can be obtained from the article.

Please let us know if you have any questions.

Sincerely,

Susann Brailey

~~~~~~~~~~~
Office of the Publisher, Journals and Technical Publications
Rights & Permissions
American Institute of Physics
Suite 1NO1
2 Huntington Quadrangle
Melville, NY 11747-4502
516-576-2268   TEL
516-576-2450   FAX
rights@aip.org

>>> Paul Okagbare <pokagb1@tigers.lsu.edu> 4/6/2009 9:53 AM >>>
- Show quoted text -

Grant of Permission
Dear Dr. Okagbare:

Thank you for your interest in our copyrighted material, and for requesting permission for its use.

Permission is granted for the following subject to the conditions outlined below:

Article Title: Experiences in Implementing uHTS - Cutting Edge Technology Meets the Real World Citation: Current Drug Discovery Technologies, 2004, 1, 27-35
Figure 1A (page 28) and Figure 5A (page 32)

To be used in the following manner:

1. Bentham Science Publishers grants you the right to reproduce the material indicated above on a one-time, non-exclusive basis, solely for the purpose described. Permission must be requested separately for any future or additional use.

2. For an article, the copyright notice must be printed on the first page of article or book chapter. For figures, photographs, covers, or tables, the notice may appear with the material, in a footnote, or in the reference list.

Thank you for your patience while your request was being processed. If you wish to contact us further, please use the address below.

Sincerely,

 AMBREEN IRSHAD

Permissions Billing Officer
Bentham Science Publishers Ltd
Email: permission@bentham.org
URL: www.bentham.org

-----Original Message-----
From: pokagb1@lsu.edu [mailto:pokagb1@lsu.edu]
Sent: Tuesday, April 07, 2009 5:58 AM
To: permission@bentham.org
Subject: C-Query: Permission Requests

 ==============[C-Query: Permission Requests]==============

Dear Ms. Ambreen Irshad ,

   Please kindly look at the matter

===

I sincerely request permission to use Figure 1A (page 28) and Figure 5A (page 32) of the article referenced below for illustration in my dissertation;

Article Title: Experiences in Implementing uHTS - Cutting Edge Technology Meets the Real World
Citation: Current Drug Discovery Technologies, 2004, 1, 27-35

Authors: Philip Gribbon, Sabine Schaertl, Malcolm Wickenden, Gareth Williams, Rachel Grimley, Frank
Stuhmeier, Hartwig Preckel, Christian Eggeling, Joachim Kraemer, Jeremy Everett, Wilma W. Keighley, Andreas Sewing

 Paul Okagbare

Supplier Elsevier Limited
The Boulevard,Langford Lane
Kidlington,Oxford,OX5 1GB,UK
Registered Company Number 1982084
Customer name Paul I Okagbare
Customer address Louisiana State University
Baton Rouge, LA 70803
License Number 2136740409708
License date Feb 26, 2009
Licensed content publisher Elsevier
Licensed content publication Biomolecular Engineering
Licensed content title Merging microfluidics with microarray-based bioassays
Licensed content author Catherine Situma, Masahiko Hashimoto and Steven A. Soper
Licensed content date October 2006
Volume number 23
Issue number 5
Pages 19
Type of Use Thesis / Dissertation
Portion Figures/table/illustration/abstracts
Portion Quantity 1
Format Electronic
You are an author of the Elsevier article No
Are you translating? No
Order Reference Number
Expected publication date May 2009
Elsevier VAT number GB 494 6272 12
Permissions price 0.00 USD
Value added tax 0.0% 0.00 USD

VITA

Paul Ichide Okagbare was born to Mr. Jackson Okagbare Ichide and Mrs. Rhoda Esiekpe Okagbare in April of 1973, in Delta State, Nigeria. He has five siblings, two brothers and three sisters. He attended Ugono Mixed Secondary School in Delta State, Nigeria, from 1985 to 1991. Upon graduation, he enrolled at Delta State University, Delta State, Nigeria, in 1992. He obtained his Bachelor of Science in industrial chemistry in December, 1997.

Upon receiving his Bachelor of Science, he immediately accepted employment with General Motors in Lagos, Nigeria, as a Plant Chemist. In December 1998, he entered the graduate school at the University of Ibadan, Ibadan, Nigeria. He obtained his Master of Science (M.Sc.) degree in analytical chemistry in December 2000. He got employed by SmithKline Beecham, Nigeria, in 2000 as a Production Supervisor, and became a Manufacturing Manager in GlaxoSmithKline, Nigeria in 2001. Paul got enrolled in the doctorate program in Chemistry Department, Louisiana Sate University, in the spring of 2005. He is an active member of the American Chemical Society (ACS), and the National Organization for Professional Advancement of Black Chemists and Chemical Engineers (NOBCChE). Paul Ichide Okagbare is currently a candidate for the Doctor of Philosophy in analytical chemistry, which will be awarded at the May 2009 commencement.